CARBON DIOXIDE REMOVAL IN STEAM REFORMING: ADSORPTION OF CO_2 ONTO HYDROTALCITE AND ACTIVATED SODA

A THESIS SUBMITTED TO
THE GRADUATE SCHOOL OF NATURAL AND APPLIED SCIENCES
OF
MIDDLE EAST TECHNICAL UNIVERSITY

BY

BERKER FIÇICILAR

IN PARTIAL FULFILLMENT OF THE REQUIREMENTS
FOR
THE DEGREE OF MASTER OF SCIENCE
IN
THE DEPARTMENT OF CHEMICAL ENGINEERING

AUGUST 2004

Approval of the Graduate School of Natural and Applied Sciences

Prof. Dr. Canan Özgen
Director

I certify that this thesis satisfies all the requirements as a thesis for the degree of Master of Science.

Prof. Dr. Timur Doğu
Head of Department

This is to certify that we have read this thesis and that in our opinion it is fully adequate, in scope and quality, as a thesis and for the degree of Master of Science.

Prof. Dr. Gülşen Doğu
Co-Supervisor

Prof. Dr. Timur Doğu
Supervisor

Examining Committee Members

Prof. Dr. Tunçer Özdamar (Ankara Univ., CHE)

Prof. Dr. Timur Doğu (METU, CHE)

Assoc. Prof. Dr. Naime A. Sezgi (METU, CHE)

Assoc. Prof. Dr. Gürkan Karakaş (METU, CHE)

Asst. Prof Dr. Yusuf Uludağ (METU, CHE)

I hereby declare that all information in this document has been obtained and presented in accordance with academic rules and ethical conduct. I also declare that, as required by these rules and conduct, I have fully cited and referenced all material and results that are not original to this work.

Name, Last name : Berker Fıçıcılar

Signature :

ABSTRACT

CARBON DIOXIDE REMOVAL IN STEAM REFORMING: ADSORPTION OF CO_2 ONTO HYDROTALCITE AND ACTIVATED SODA

Fıçıcılar, Berker
M.S., Department of Chemical Engineering
Supervisor: Prof. Dr. Timur Doğu
Co-Supervisor: Prof. Dr. Gülşen Doğu
August 2004, 151 pages

Conversion of natural gas and other light hydrocarbons via steam reforming is currently the major process for hydrogen production. However, conventional hydrogen production technologies are not cost effective and therefore, cost is the biggest impediment to use hydrogen in fuel cell applications. In order to optimize and overcome cost problems in hydrogen production, sorption and membrane enhanced reaction processes are the two novel technologies for in situ operation of reforming and removal of carbon dioxide.

Adsorption of carbon dioxide onto activated hydrotalcite and activated soda, obtained from either trona or $NaHCO_3$, had been studied using a stainless steel packed bed tubular reactor as a function of temperature. Adsorption of CO_2 in the presence and absence of steam onto activated hydrotalcite was conducted in the temperature range of 400-527 ^oC, whereas sorption studies with activated soda were performed for 80 to 152 ^oC in the presence of steam. Also, two-parameter deactivation model was developed to justify the experimental data and predictions of the breakthrough curves by deactivation

model indicated a good agreement with the experimental results. In order to obtain physical properties of the sorbents, untreated and calcined sorbents were characterized by using TGA, B.E.T (N_2 adsorption), and Hg porosimetry techniques.

When hydrotalcite was used as the sorbent, total adsorption capacity of the material reduced from 1.18 mol/kg to 0.66 mol/kg as the temperature was increased from 400 ^{o}C to 527 ^{o}C. On the other hand, activated soda exhibited a total adsorption capacity 1.15 to 0.68 mol/kg for a temperature change from 80 to 152 ^{o}C.

For high temperature removal of CO_2, hydrotalcite and its promoted forms (using K_2CO_3 or Na_2CO_3) are pretty good sorbents to be used in single step hydrogen production processes, such as SERP. On the other hand, activated soda could also be used for CO_2 abatement of the effluent gas from the reformer only when the temperature is lowered enough to obtain efficient adsorption capacity within the multi-bed adsorbers.

Keywords: Adsorpstion, breakthrough curves, carbon dioxide removal in steam reforming, hydrotalcite, activated soda, trona, sodium bicarbonate, hydrogen production, SMR, SERP

ÖZ

HİDROJEN GAZI ÜRETİMİ SIRASINDA OLUŞAN KARBONDİOKSİT GAZININ ARITILMASI: KARBONDİOKSİTİN HİDROTALSİT VE AKTİF SODA ÜZERİNE ADSORPLANMASI

Fıçıcılar, Berker
Yüksek Lisans, Kimya Mühendisliği Bölümü
Tez Yöneticisi: Prof. Dr. Timur Doğu
Ortak Tez Yöneticisi : Prof. Dr. Gülşen Doğu
Ağustos 2004, 151 sayfa

Günümüzde hidrojen, yaygın olarak, doğal gaz ve hafif hidrokarbonlardan buhar biriktirme yöntemi ile üretilmektedir. Ne var ki, geleneksel hidrojen üretim teknolojileri ekonomik olmamakla beraber hidrojenin yakıt pili uygulamaları için önündeki en büyük engel hidrojenin üretim maliyetidir. Bu yüzden, SERP ve MERP prosesleri (karbondioksit arıtımı ve reforming tepkimesinin birlikte gerçekleştiği) hidrojen üretim maliyetlerini azaltmak ve proses optimizasyonu için geliştirilen iki yeni teknolojidir.

Karbondioksitin trona veya $NaHCO_3$'den elde edilen, aktifleştirilmiş hidrotalsit ve aktifleştirilmiş soda üzerine adsorpsiyonu, paslanmaz çelik sabit yataklı tübüler reaktörde sıcaklığın fonksiyonu olarak çalışılmıştır. Karbondioksitin buharlı ve buharsız ortamlarda aktif hidrotalsit üzerine adsorplanma deneyleri 400-527 ^{o}C sıcaklıkları arasında yapılmıştır. Aktif soda ile yapılan çalışmalar ise buharlı ortamda 80-152 ^{o}C arasında gerçekleştirilmiştir. Bunun dışında, deneysel verinin doğruluğunu ölçmek için 2 parametreli deaktivasyon modeli geliştirilmiş ve bu modelin deneysel veri ile uyumlu olduğu

gözlenmiştir. Sorbentlerin fiziksel özelliklerinin karekterizasyonu TGA, B.E.T (N_2 adsorplanması) ve civa porosimetresi analiz yöntemleri kullanılarak yapılmıştır.

Sorbent olarak hidrotalsit kullanıldığında, malzemenin toplam adsorpsiyon kapasitesi, sıcaklığın 400 ^{o}C'den 527 ^{o}C'ye arttırılmasıyla 1,18 mol/kg'dan 0,66 mol/kg'a düşmüştür. Öte yandan, aktifleştirilmiş soda 80 ^{o}C'den 152 ^{o}C'ye sıcaklık değişimi için 1,15 mol/kg/'dan 0,68 mol/kg'a toplam adsorpsiyon kapasitesi göstermiştir.

Hidrotalsit ve kimyasal olarak geliştirilmiş hidrotalsit (K_2CO_3 ve Na_2CO_3 ile aktifliği arttırılmış), yüksek sıcaklıklarda karbondioksit arıtımı için çok uygun sorbentlerdir ve SERP prosesi gibi tek basamaklı hidrojen üretim proseslerinde bu sorbentlerin kullanılması verimliliği arttırmaktadır. Hidrotalsitten farklı olarak aktif soda da hidrojen üretimi sırasında oluşan karbondioksitin tutulmasında kullanılabilir. Aktif soda düşük sıcaklıklarda daha iyi karbondioksit adsorplayabildiği için reforming reaktörünün çıkışındaki gaz soğutulduktan sonra çok yataklı adsorplayıcılara yollanarak düşük sıcaklıklarda karbondioksit arıtımı yapılmalıdır.

Anahtar sözcükler: Adsorpsiyon, S-eğrileri, hidrojen üretiminde karbondioksit arıtımı , hidrotalsit, aktif soda, trona, sodyum bikarbonat, hidrojen üretimi, SMR, SERP

To My Family,

ACKNOWLEDGEMENTS

I wish to express my deepest gratitude to my supervisors Prof. Dr. Timur Doğu and Prof. Dr. Gülşen Doğu for their supervision and guidance throughout this study.

I also would like to thank my friends Canan, Hakan, Berna, Sinan, Alper, Barış, Umut, Başak Açan, Başak Kurbanoğlu, Onur, Ceylan, Ural, Sezen, Işık, Atilla, Seha, Ela, Ayşe, and shadow warriors for their support and friendship.

I wish to thank my kinetic lab. mates Canan, Gülsün, Zeynep, Nezahat, Dilek Karayılan, Dilek Varışlı, Aslı, and Yeşim. There is a quotation from Albert Einstein; he said, "No problem can be solved from the same level of consciousness that created it". I suppose my lab mates and I experienced this feeling very deeply during the times we had performed our experiments.

Finally, I would like to thank to my mother and father for their patience and endless support throughout this study. After all, I would like to thank to my brother for his outstanding help-without him I am lost.

TABLE OF CONTENTS

LIST OF TABLES

Table

LIST OF FIGURES

Figure

LIST OF SYMBOLS AND ABBREVIATIONS

a	Activity of the solid reactant
C_A	Concentration of reactant in the outlet gas stream, kmol.m^{-3}
C_{Ab}	Bulk phase concentration of reactant gas, kmol.m^{-3}
C_{Ao}	Concentration of reactant in the inlet gas stream, kmol.m^{-3}
c_b	Break point concentration, kmol.m^{-3}
C_i	Concentration of CO_2 within the pores of particles, kmol.m^{-3}
D_e	Effective diffusivity, m^2.s^{-1}
E_{ad}	Activation energy for the deactivation rate constant, kj/mol
E_{as}	Activation energy for the adsorption rate constant, kj/mol
k_d	Deactivation rate constant, min^{-1}
k_m	Film mass transfer coefficient, mol.m^{-2}.s^{-1}
k_o	Initial sorption rate constant, cm^3.g^{-1}.min^{-1}
k_s	Surface reaction rate constant at any time
$k_{s,o}$	Initial surface reaction rate constant
L	Length of the packed bed, cm
L_b	Length of the bed used up to the break point, cm
L_t	Total bed length, cm
L_{unb}	Length of unused bed, cm
M_B	Molecular weight of solid reactant B, g/mol
N	Dimensionless paramter defined in Equation (5.2.2.5)
N_A	Molar flux with respect to stationary coordinates, mol.m^{-2}.s^{-1}
Q	Volumetric flow rate, m^3.min^{-1}
R	Particle radius, cm
R_A	Rate of reaction, mol.g^{-1}.min^{-1}
r_c	Radius of particle at the sharp interface, cm
S_g	Active surface area per gram of particle at any time, m^2.g^{-1}
$S_{g,0}$	Initial active surface area per gram of particle, m^2.g^{-1}
t	Time, min
t_b	Time equivalent to break point concentration, min
t_t	Time equivalent to the total or stoichiometric capacity, min

t_u	Time equivalent to the usable capacity, min
U_o	Superficial velocity, m/s
W	Adsorbent mass, g
z	Axial position in the packed bed, cm
ν	Dimensionless parameter defined in Equation (5.2.2.6)
θ	Dimensionless time
ψ	Normalized reactant gas concentration in the bed outlet
β	Parameter defined in Equation (5.2.2.3), s^{-1}
τ	Time after which no significant conversion occurs, min
ε_b	Void fraction of bed
ρ_B	Solid density of adsorbent, $g.cm^{-3}$
ϕ_o	Initial thiele modulus
ε_p	Particle porosity
ρ_p	Particle density at any time, $g.cm^{-3}$
$\rho_{p,o}$	Initial particle density, $g.cm^{-3}$
HT	Hydrotalcite
HTlc	Hydrotalcite-like compound
LDH	Layered Double Hydroxide
MERP	Membrane Enhanced Reaction Process
PSA	Pressure Swing Adsorption
SERP	Sorption Enhanced Reaction Process
SMR	Steam Methane Reforming
SNG	Substitute Natural Gas
WGS	Water Gas Shift

CHAPTER 1

INTRODUCTION

Being a potential energy carrier and a valuable chemical for many industrial processes, hydrogen production has increased significantly in recent years. Among the hydrogen production methods, Steam Methane Reforming (SMR) process is the dominant conventional technology for hydrogen production. However, hydrogen production cost is still not reduced to use it world wide as an energy carrier such as fuel cell applications. Once hydrogen is produced in a cost effective way, it will probably replace all the fuels in the future.

In conventional hydrogen producing plants, reformer effluent gas contains typically 15-20 mole percent carbon dioxide (dry basis). This large amount of carbon dioxide requires high capacity absorbers or adsorbers to purify outlet stream from the reformer, which means that carbon dioxide removal unit of hydrogen producing plant, in fact, has a large impact on the overall cost of hydrogen production.

It is critical to remove carbon dioxide from the off-gas to purify and optimize the hydrogen production. In today's technology, there are several processes for carbon dioxide abatement. Among these processes, absorbers and multi-bed adsorbers (PSA unit) are widely used for carbon dioxide removal. However, these processes are not cost-efficient and some other alternative processes are sought to enhance hydrogen production. It is possible to carry out reaction and separation together in the reformer to enhance hydrogen production. By doing so, there is no need for further use of an additional CO_2 removal unit such as absorbers or adsorbers.

There are two novel technologies for carbon dioxide removal for hydrogen production, both of which depend on the idea that separation and reaction is coupled to reach higher conversions in a single reformer. These processes depend on the idea that when one of the products (CO_2 or hydrogen) is removed from the reaction zone continuously, according to Le Chatelier's principle, hydrogen production is enhanced. In other words, the more you remove one of the products the more yield of hydrogen is achieved. 99+ % hydrogen streams can be obtained with the use of either sorption enhanced reaction process (SERP) or membrane enhanced reaction process. SERP is used for the adsorption of carbon dioxide and regeneration for cyclic processes. On the other hand, membrane enhanced reaction process focuses on selectively removing hydrogen from the reaction zone.

Basic advantage of these two processes is that the reformer temperature is significantly reduced so that the reactor costs are lowered tremendously. Moreover, hydrogen conversions are so high that in many cases the desired conversions are reached in the reformer. If off-gas composition is below the design value, very low capacity adsorbers or absorbers are required for further purification. This study mainly focuses on the use of SERP process to remove carbon dioxide efficiently. For this purpose, some adsorbents are selected and investigated for the removal of carbon dioxide at high temperatures.

The goal of this study was to perform adsorption experiments with carbon dioxide on several adsorbents such as hydrotalcite, sodium bicarbonate, and trona. Applicability of these adsorbents for the removal of carbon dioxide in the production of hydrogen was investigated. Reaction compositions were adjusted such that it simulated the effluent from a typical Steam Methane Reformer (SMR). Having obtained the experimental data, calcination and breakthrough curves were derived for carbon dioxide.

Among several alternative models (deactivation, shrinking core, pore, and grain models) for breakthrough data, deactivation model was selected regarding to its wide use and simplicity. In order not to introduce too much parameter, deactivation model was used with its two-parameter form, which takes into account activity changes.

Considering breakthrough and total capacities for some temperature range and some other properties of adsorbents, use of Sorption Enhanced Reaction Process (SERP) or Pressure Swing Adsorption (PSA) process for the removal of carbon dioxide in hydrogen production was discussed and some further studies were recommended to reach a better conclusion for the selection of best adsorbent for carbon dioxide removal in steam reforming process.

CHAPTER 2

HYDROGEN PRODUCTION

2.1 Wonder Chemical: Hydrogen

Hydrogen is not an energy source but a carrier that must be manufactured. Today, hydrogen is produced by "decarbonizing" fossil fuels (reforming reactions). In the future, it will be produced from water, solar energy, and perhaps from "cleaner" forms of nuclear energy. Cost is the major problem to be overcome for using hydrogen more widely as a fuel. For instance, electricity is required by many hydrogen production technologies, which makes hydrogen more expensive than the fuels it would replace. Hydrogen is a clean and sustainable form of energy that could be used in mobile and stationary applications. Once it has been separated and purified, hydrogen is the ultimate clean energy carrier. Hydrogen is an obvious alternative to hydrocarbon fuels, such as gasoline. It has many potential uses, it is safe to manufacture, and is environmentally friendly. Today, many technologies exist that can use hydrogen to power cars, electrical plants, and buildings. Absence of an infrastructure for producing, transporting and storing large quantities of hydrogen prevents its practical use [1].

2.1.1 Hydrogen in Use

Hydrogen is an important industrial chemical in petroleum refining and in the synthesis of ammonia and methanol. These three areas account for more than 90% of worldwide hydrogen consumption. Remaining hydrogen is consumed in the production of various chemicals, e.g., cyclohexane, benzene by toluene dealkylation, oxo-alcohols, and aniline. To illustrate the wide use of hydrogen, several hydrogen consuming technologies are listed below:

- Commercial fixation of nitrogen from the air to produce ammonia for fertilizer production (ca. 2/3 of commercial hydrogen is used for this purpose)
- Hydrogenation of oils, in which vegetable oils are changed from liquids to solids; shortening is an example of a hydrogenated oil
- Methanol production, in hydrodealkylation, hydrocracking
- Welding
- Hydrochloric acid production
- Metallic ore reduction
- Cryogenics and the study of superconductivity (liquid hydrogen)
- Hydrogen's main use as a fuel is in the space program. Today, hydrogen fuels both the main engine of the space shuttle and the onboard fuel cells that provide the shuttle's electric power [2, 3].

2.1.2 Hydrogen as a Fuel

Potentially, hydrogen could provide electricity and fuel for the residential, commercial, industrial, and transportation sectors. When properly stored, hydrogen as a fuel burns in either gaseous or liquid state. Motor vehicles and furnaces can easily be converted to use hydrogen as a fuel. Hydrogen burns 50% more efficiently than gasoline, and burning hydrogen creates less air pollution. Hydrogen has a higher flame speed; wider flammability limits, higher detonation temperature, burns hotter, and takes less energy to ignite than gasoline. This means that hydrogen burns faster, but carries the danger of pre-ignition and flashback. While hydrogen has its advantages as a vehicle fuel it still has to be investigated before it can be used as a substitute for gasoline.

Fuel cells use hydrogen to produce useful energy. Fuel cells capable of powering automobiles and buses are being developed to use in the near future. Hydrogen could be considered as an alternative way to store energy produced from renewable resources such as solar, wind, biomass, hydro, and geothermal. Hydrogen could then be stored and burned as fuel or to function as a fuel in a cell to generate electricity [3].

Table 2.1.1 Mass energy densities for various fuels [4]

Fuel	Hydrogen Weight Fraction	Ambient State	Mass Energy Density (MJ/kg)
Hydrogen	1.00	Gas	120
Methane	0.25	Gas	50 (43)[2]
Ethane	0.20	Gas	47.5
Propane	0.18	Gas (Liquid)[1]	46.4
Gasoline	0.16	Liquid	44.4
Ethanol	0.13	Liquid	26.8
Methanol	0.12	Liquid	19.9

(1) A gas at room temperature, but normally stored as liquid at moderate pressure

(2) The larger values are for pure methane. The values in parentheses are for a "typical" Natural Gas.

In order to visualize the importance of hydrogen as a fuel, it is best to compare energy contents of common fuels with hydrogen. Mass energy densities of some common fuels are listed in Table 2.1.1. Hydrogen mass energy density is around 120 MJ/kg and this value is very large with respect to other fuels such as gasoline. Relatively high energy content of hydrogen points out one of the reasons for using hydrogen as a fuel.

After all, fossil fuels, renewables yield hydrogen. This flexibility would make countries less dependent upon oil from foreign countries. If hydrogen is used in very high efficiency fuel cells for transportation and to generate power, green house gas emissions could be reduced significantly- especially if the hydrogen is produced using renewable resources, or clean fossil technologies. Hydrogen will be produced cost-effectively from a variety of energy sources and

made readily available for wide spread use as a clean energy carrier and fuel. It is essential to develop advanced technologies to produce, deliver, store, and detect hydrogen for its safe handling and use [5].

2.2 Production of Hydrogen

Simple structure of hydrogen provides many routes for efficiently producing hydrogen. Today, the vast majority of hydrogen is produced from fossil fuel sources as a by-product or reforming. Table 2.2.1 shows main sources for hydrogen production and it is clear that significant amount of hydrogen is produced from natural gas.

Table 2.2.1 Worldwide hydrogen production [3]

Origin	Amount in billions (Nm^3/year)	Percent (%)
Natural Gas	240	48
Oil	150	30
Coal	90	18
Electrolysis	20	4

Although hydrogen production technologies are very wide depending on the origin, reforming and water splitting technologies are well established and commonly used for hydrogen production. Commonly used technologies for hydrogen production are as follows:

- Steam reforming converts methane (and other hydrocarbons in natural gas) into hydrogen and carbon monoxide by reaction with steam over a nickel catalyst supported by alumina

- Electrolysis uses electrical current to split water into hydrogen at the cathode (+) and the oxygen at the anode (-). Steam electrolysis (a variation of conventional electrolysis) uses heat, instead of electricity, to provide some of the energy needed to split water, making the process more energy efficient
- Thermochemical water splitting uses chemicals and heat in multiple steps to split water into its component parts to produce hydrogen at the end
- Photoelectrochemical systems use semi-conducting materials (like photovoltaics) to split water using only sunlight
- Photobiological systems use microorganisms to split water using sunlight.
- Biological systems use microbes to break down a variety of biomass feedstocks into hydrogen
- Thermal water splitting uses very high temperature (approximately 1000 ^{o}C) to split water
- Gasification uses heat to break down biomass or coal into a gas from which pure hydrogen can be generated [3]

There is a significant renewed interest in the use of electrolyzers to produce hydrogen as a fuel for automotive applications with a number of refueling stations around the world. In addition, some research continues in the integration of renewable resources (PV and wind) with electrolyzers, for producing hydrogen to be used as a fuel or for energy storage.

2.3 Steam Methane Reforming

Natural gas will probably remain as the major feedstock for the production of hydrogen via syngas ($CO+H_2$). Although coal remains available at lower prices than hydrocarbons and coal reserves are large, initial investment in a coal-based syngas plant is around three times that required for a natural gas plant [6]. Steam methane reforming (SMR) is a well-established process for the conversion of natural gas and other hydrocarbons into syngas. When essentially methane is considered as the feed for hydrogen production, the following two reactions are considered to be the basic reactions that are taking place in the reformer and shift reactors.

(1) $CH_4(g) + H_2O(g) \leftrightarrow CO(g) + 3H_2(g)$ (SMR) ΔH= 206.36 kJ/mol

(2) $CO(g) + H_2O(g) \leftrightarrow CO_2(g) + H_2(g)$ (WGS) ΔH= -41.16 kJ/mol

First reaction, named steam methane reforming reaction, is an endothermic reaction and second reaction, so called water gas shift reaction, is an exothermic reaction. Besides these reforming and shift reactions, there are four more reactions to be avoided in the course of production. The product spectrum from all these reactions is controlled predominantly by thermodynamics. Methane is the favored product at lowered temperatures, while hydrogen being preferred at 700-800 ^oC. Several potential problems are introduced due to the necessity to operate reformers at these high temperatures. One of these problems is the thermal stability of the catalyst (steam tends to favor catalyst and support sintering). However, the major problem lies in the formation of coke [9].

Conversion of carbon monoxide into carbon and carbon dioxide is known as Boudouard reaction, (3), and this reaction might poison the catalyst depending on the operating conditions. Another possibility of soot formation might be due to the direct cracking of methane, (4), and this reaction will also lower the conversion from the reformer process [8]. In addition, reactions (5) and (6) will coke the catalyst and design of reformers should carefully be done considering these reactions to prevent soot formation.

(3) $2CO(g) \leftrightarrow C(s) + CO_2(g)$ (Boudouard Reaction) ΔH= -172.54 kJ/mol

(4) $CH_4(g) \leftrightarrow C(s) + 2H_2(g)$ (Methane cracking) ΔH= 74.9 kJ/mol

(5) $CO(g) + H_2 \leftrightarrow C(s) + H_2O(g)$ ΔH= -131.3 kJ/mol

(6) $C_nH_{2n+2}(g) \leftrightarrow nC(s) + (n+1)H_2(g)$ ΔH= 74.9-166.9 kJ/mol (for n=1-6)

2.3.1 Description of SMR Process

SMR reaction is generally carried out in a catalytic (usually Ni/Al_2O_3) multi-tubular bed reactor placed into a gas-fired furnace at a pressure of 3-40 atm (depending on the purpose) and a temperature of 750-900 ^oC (temperature in the tubes evolves from 675 to 1000 K, necessitating very high heat fluxes).

Figure 2.3.1 shows a conventional steam methane reforming process for hydrogen production.

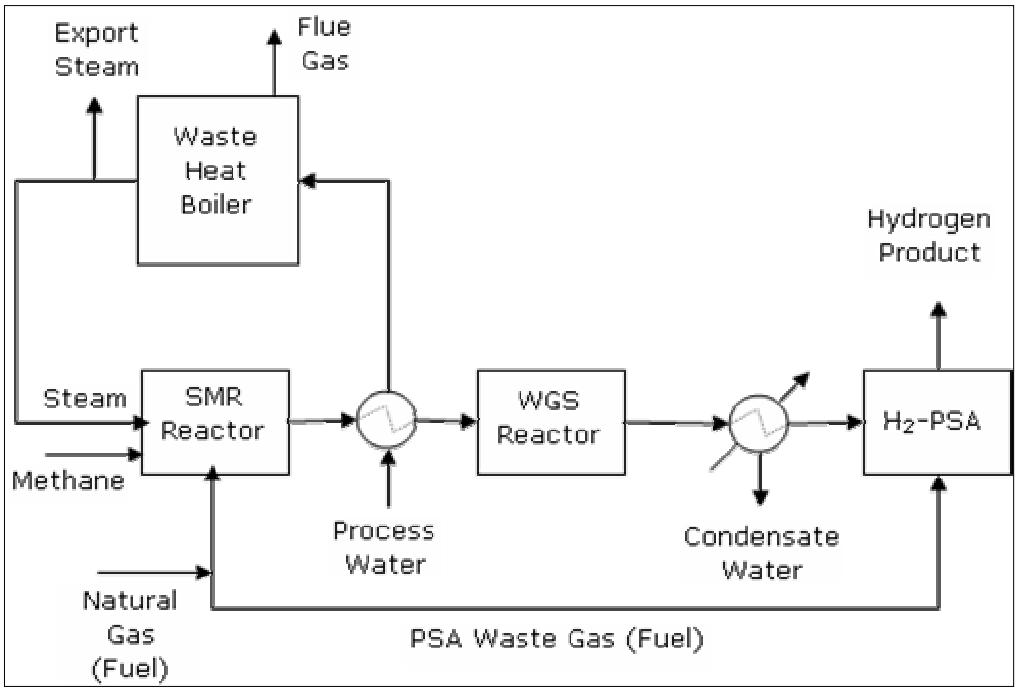

Figure 2.3.1 Steam methane reforming process for hydrogen production [7]

The reactor feed gas is a mixture of methane (natural gas) and steam in the ratio of 2.5-6.0. The reactor effluent gas typically contains 70-72% H_2, 6-8% CH_4, 8-10% CO, 10-14% CO_2 on a dry basis. This gas is cooled in a waste heat boiler (steam produced) and fed to another catalytic (Fe or Cu on alumina) reactor for the exothermic water-gas shift (WGS) reaction. The high temperature WGS reactor is generally functioned at a temperature of 300-400 ^{o}C. The effluent gas from the reactor typically contains 71-75% H_2, 4-7% CH_4, 1-4% CO and 15-20% CO_2 on a dry basis. The effluent is further cooled down to a temperature of 20-50 ^{o}C (more steam is produced and water is condensed) and fed to a multi-column pressure swing adsorption (PSA) process at a pressure of 3-40 atm (PSA feed gas is saturated with water). A multi-column PSA process containing 4-12 adsorption beds is generally used for carbon dioxide removal [7].

The net H_2 recovery from the PSA process and its sorbent inventory depend on many variables like feed gas pressure, composition, operating conditions and cycle times of the PSA process because bulk CO_2 is hard to desorb and dilute CO is difficult to adsorb. Removal of carbon dioxide is an essential part of steam methane reforming process. In older technologies, carbon dioxide abatement is completed in scrubbers or in absorption units. In today's technology, PSA units are well-established adsorber units for hydrogen purification. In hydrogen purification, PSA process produces a hydrogen product stream containing dry 98-99.999+ $\%H_2$ at the feed gas pressure.

2.3.2 Steam Methane Reforming Catalysts

Reformer tubes contain catalyst normally dispersed nickel on an alumina or magnesium spinel carrier in the shape of cylinders or raschig rings. In conventional tubular reforming the catalyst is usually a metal from group VIII, the most commonly used being nickel. Cobalt and the noble metals are active catalysts but are more expensive [8]. The formation of coke, also favored under these conditions, is a major problem. Although carbon formation is not a serious problem over noble metals, the economic advantages of the use of nickel still favor the use of this metal. The catalyst should be mechanically strong and it must be stable in a steam atmosphere at high temperatures (750-850 ^{o}C). For these reasons, the most common support materials are based on ceramic oxides, such as α-alumina or magnesia, or on stabilized oxides. The inclusion of silica is avoided as it may be volatilized under steam reforming conditions [10]. Potassium and/or calcium alkali ions are good additives to catalyst, which basically serve to squeeze excessive carbon deposition on the catalyst. These catalysts could be used in excess of five years of continuous operation.

Many materials are capable of catalyzing the water-gas shift reaction. Two classes of materials are used very frequently in industry as shift catalysts: the iron-based catalysts and the copper-based catalysts. The iron-based catalysts are so called high temperature shift catalysts, operating from about 320 to 450 ^{o}C and iron oxide catalysts can tolerate small quantities of sulfur. On the other hand, copper-based catalysts are a more recent development and these catalysts are so called low temperature shift catalysts, operating from about 200 to 250 ^{o}C. These catalysts have good activity (high yield) at low temperatures and are therefore attractive since equilibrium is more favorable at lower

temperatures. Another material as an industrial water gas shift catalyst is sulfided cobalt oxide-molybdenum oxide on alumina. This type of catalyst is completely insensitive to sulfur, and certain variations are claimed to possess good activities at both high and low temperatures [11].

2.3.3 Hydrogen Production: Need for a New Technology

The high-temperature of the SMR reactor, the catalyst deactivation due to coking, the use of high temperature metallurgy for construction of the steam methane reforming reactor, the requirement of large interstage heat recovery systems, and the complex design of the multicolumn H_2-PSA system significantly raises the cost of hydrogen production. Nevertheless, the process described in Figure 2.3.1 remains the most cost-effective method for production of pure hydrogen in the commercial scale (1-100 MM SCFD H_2). In addition, the technology has been improved in the areas of natural gas desulphurization, SMR and WGS catalysis, reactor design, heat supply and removal systems, PSA process design and adsorbents, process control, heat generation and management [24].

Considering hydrogen as a promising fuel has increased the demand for this chemical in the recent years. Therefore, it will be extremely desirable if novel technologies for production of hydrogen by SMR can be developed which in turn will lower the capital cost compared to conventional technology.

2.4 Membrane Enhanced Steam Reforming

Industrial fixed bed steam reformers suffer from several problems, which seriously affect their performance. For this reason, a membrane-included technology for the production of hydrogen is a good choice for minimizing problems within the reactor. Inclusion of a high temperature hydrogen permeable membrane moderately increases the conversion of methane in the hydrogen production [13]. Moreover, reaction and separation are carried out in a single reactor. In other words, excluding carbon dioxide removal unit and shift reactors, it is possible to obtain high conversions in a membrane reactor. In terms of optimizing hydrogen production costs, membrane enhanced reaction

process is a very promising alternative to conventional steam methane reforming process.

Jarosch and De Lasa et al. reported a novel membrane reformer [12], so called catformer, for hydrogen production. Simplified process for catformer is shown in Figure 2.4.1. The reaction is usually carried out in a fixed bed reactor using nickel deposited on a monolithic support such as α-alumina. The catforming process differs from conventional tubular steam reforming in that FCC style catalyst is used and a high temperature membrane for hydrogen removal is placed into the reactor. In the catformer reactor concept, the reactant gas is mixed with regenerated catalyst and the resulting gas solid suspension is sent to the downflow section of the catformer. As the suspension falls down the reactor tube, the reforming and water gas shift reactions take place and hydrogen is continuously removed from the mixture via diffusion through a membrane. Hydrogen removal shifts the conversion of methane to values above those attainable at equilibrium as well as favorably affecting the selectivity. For low steam to methane ratios, coke formation is expected and the catalyst should be regenerated and recirculated to the reaction zone [12].

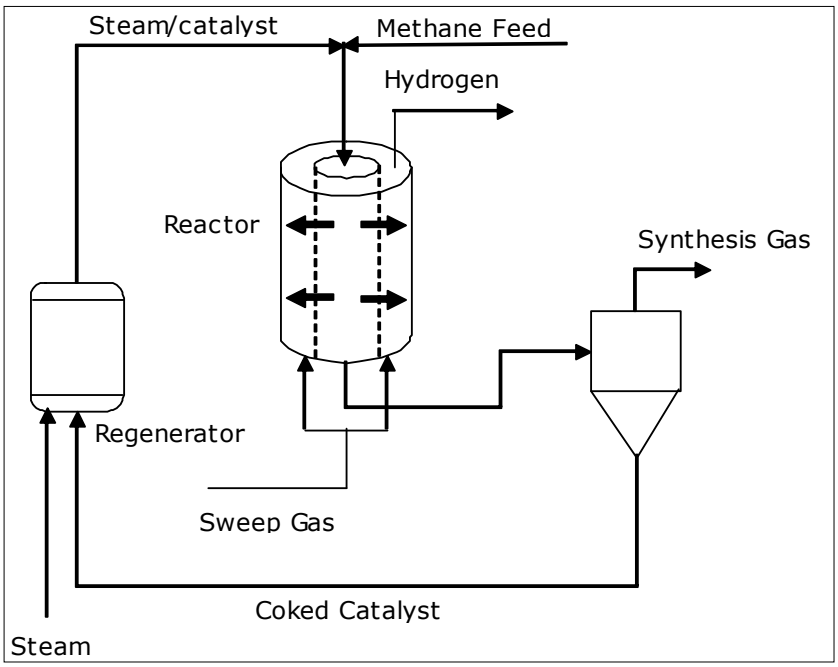

Figure 2.4.1 Membrane enhanced reaction process for hydrogen production [12]

Barbieri et al. [14] studied with a palladium-based catalytic membrane reactor for hydrogen production (utilizing membranes of Pd and Pd/Ag supported on Al_2O_3). The possibility of overcoming the limitation imposed by the thermodynamic equilibrium could be considered as an important advantage of these kind of reactors. To remove hydrogen from the reaction volume, it is possible to use palladium and its alloys, permeable only by hydrogen. Recently, many techniques have been developed aimed at depositing a small amount of Pd over porous supports (chemical vapor deposition, electroless plating, sputtering, and solvated metal atom deposition). In this way, it is possible to reduce the thickness of the membrane with the advantages of lower costs and of higher permeability. The durability of the Pd membranes, which are highly fragile after thermal excursions in the presence of hydrogen, is, however, a significant problem. In order to overcome this drawback, Barbieri et al. [14] have used Pd/Ag and other alloys.

In literature, Adris et al. [13] reported a fluidized bed membrane reactor for steam methane reforming process. Problems with conventional reformers can be alleviated by using a fluidized bed membrane reactor (FBMR) system for steam methane reforming. This novel reactor combines several advantages of fluidized beds as chemical reactors, in particular catalyst bed temperature uniformity, improved heat transfer and elimination of intracatalyst diffusional limitations. Moreover, shifting the conventional thermodynamic equilibrium in situ separation and removal of a desirable reaction product in a very pure state are the particular advantages of this technology.

Barbieri et al. [15] suggested another membrane reactor to achieve high conversions in a single unit. The idea is simply lies on the fact that one or more products are continuously removed from the reaction zone, which in turn shifts the reaction toward the products. Packed bed inert membrane reactor (incorporating the reaction zone and the separation system in a single unit) is generally used to obtain higher conversions in the reactor.

To sum up, using membranes in a single reactor efficiently yields high methane conversions at a lower temperature with respect to SMR process. However, particular attention should be given to thermal durability of the membranes. Once the membrane (developing new membranes) technology is improved for selectively removing products and the design of these membrane-

enhanced systems become well established, it could be possible to use membrane reactors in place of conventional reformers. This replacement will considerably lower the initial cost for hydrogen production.

2.5 Sorption Enhanced Reaction Process

In the last decade, combining reaction and separation to simplify chemical processes, conserve energy and/or to improve product quality and yield has received increased attention to optimize production cost of hydrogen. Modification of the conventional steam methane reforming (SMR) process to incorporate an adsorbent in the reformer to remove carbon dioxide from the product stream may offer a number of advantages over conventional processes. Upsetting the reaction equilibrium in this way drives the reaction to produce additional hydrogen at lower temperatures than conventional SMR reactors (Le Chatelier's Principle). Although still in the research stage, the cost of hydrogen from this modified process is expected to be 25-30% lower, primarily because of reduced capital (no shift reactors or PSA units) and operating costs. In addition, the sorption of the carbon dioxide in the reforming stage results in a high-purity carbon dioxide stream from the adsorbent regeneration step [17].

For gas-phase catalytic reactions, the separation can be based on adsorption, selective permeation through a membrane, or through simultaneous reaction of the molecule (reaction inhibitor) with a chemical acceptor. Adsorption or chemical acceptor-based separation processes have distinct advantages to the membrane-based systems in terms of the material tolerance to high temperatures and pressures, and the wide choice and availability of sorbents for achieving the desired separations under reaction conditions.

SERP is a process for carrying out simultaneous reaction and separation of desired products in a single unit operation. Although performing reaction and separation simultaneously is not a new concept, Sircar et al. [17] has introduced sorption enhanced reaction process (SERP) concept for the production of hydrogen. In SERP, a fixed packed column of an admixture of a catalyst and a sorbent is used that selectively removes (physisorption or chemisorption) a reaction by-product from the reaction zone. Using the principles of pressure swing adsorption periodically regenerates the sorbent. The process steps allow

direct production of the desired product at high purity and at the reaction pressure. High conversion of reactants to products in an endothermic, equilibrium controlled reaction can be performed while operating the reaction at a substantially lower temperature than would be necessary by steam methane reformer packed with the catalyst alone.

The process for combining chemical reaction and adsorptive separation of reaction products in a single unit operation in conjunction with sorbent regeneration using the principles of pressure-swing adsorption is generally called Periodic Separating Reactors [18]. The same idea is used in SERP technology to regenerate adsorbent for a new efficient cycle.

A simplistic approach to SERP concept is shown in Figure 2.5.1. Essentially two major units included in the production route; one being the reformer (admixture of catalyst and sorbent) and the other unit is the sorbent regeneration unit.

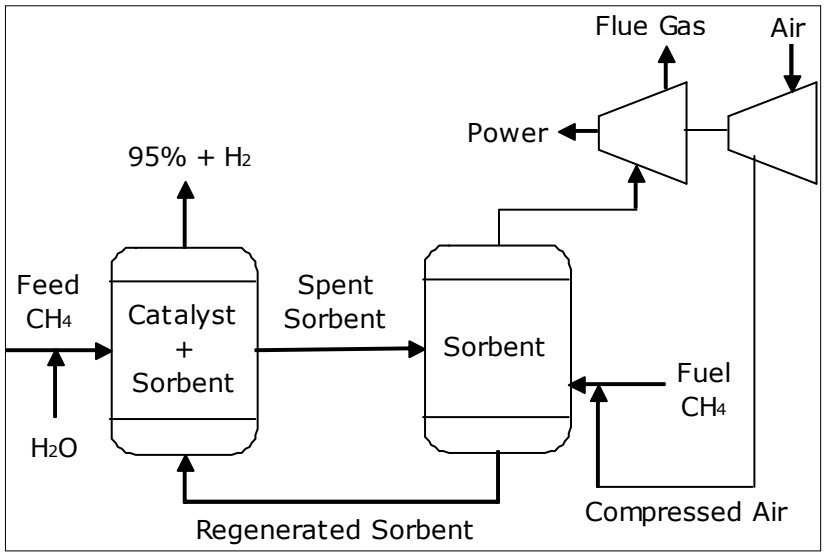

Figure 2.5.1 Simplified flow diagram of the sorption enhanced reaction process [16]

Harrison et al. [16] performed a set of experiment to produce hydrogen in a single step process. In their work, calcium-based CO_2 acceptor was added to commercial steam methane reforming catalyst, which permitted the production of 95+% H_2 in a single-step process. Higher temperatures resulted in increased

CH_4 conversion but decreased carbon oxide removal, leaving CO_2 as the primary impurities. Potential advantages of the single step process, in addition to reducing the number of processing steps, include improved energy efficiency, elimination of the need for shift catalysts, and reduction in the temperature of the primary reactor by 150-200 ^oC. Continuous separation of catalyst and acceptor and the durability of the acceptor for multiple cycle operation are seemed to be the basic problems to be overcome to replace the older technologies with this cyclic operation.

The advantageous of coupling reaction systems with some form of in situ separation have been widely reported in the literature. Such configurations may substantially improve reactant conversion or product selectivity and, for reversible reactions, establish a more favorable reaction equilibrium than that which could be achieved under conventional reactor operation. Reaction enhancement may enable a lower temperature of operation, which in turn may solve the problems associated with catalyst fouling, high process energy requirements and poor energy transfer within the plant environment. The reforming reactions will also be favored at low pressures, whereas the water-gas shift reaction is largely unaffected by changes in pressure. For a reaction which is not kinetically limited, the use of a sorbent will thus enable a lower operating temperature for a desired conversion. Two major process vessels (Figure 2.5.1) -the primary reactor and regenerator– replace five vessels (the reformer, two shift reactors and the CO_2 scrubber and stripper, or PSA unit) in the conventional process.

Hufton et al., [21] used a fixed packed column of an admixture of an SMR catalyst and a chemisorbent to remove carbon dioxide selectively from the reaction zone. The chemisorbent (promoted hydrotalcite) used in packed column is periodically regenerated by using the principles of pressure swing adsorption. They reported a novel chemisorbent, which reversibly sorbs carbon dioxide in the presence of excess steam at a temperature of 300-550 ^oC that was developed for application in the SERP. SERP reactor was operated at 450 ^oC, about 300 ^oC lower than the conventional reformer.

Potential advantages over the current shift process, which requires multiple catalytic reactors (high and low temperature shift reactors), an extensive network of heat exchangers, and separate processing for CO_2 removal

involving wet scrubbing or pressure swing adsorption are the two important factors to use sorption based approach to minimize initial and operating costs. Heat exchanger requirements are reduced because the entire process occurs at elevated temperature. No separate absorber or stripper required (or a PSA unit). Besides these, eliminating the sulfur-sensitive shift catalyst may become increasingly important in the future as heavier, higher-sulfur feedstocks are used for synthesis gas production.

Harrison et al. [22] combined reaction and separation by carrying out the water-gas shift reaction in the presence of calcium based CO_2 acceptor (dolomite). The continuous removal of CO_2 from the gas phase alters the shift reaction equilibrium and permits almost complete CO conversion and CO_2 removal. The reaction temperature is significantly higher than employed in the traditional shift process, that is, no shift catalyst is required. In other words, magnesium-based sorbent also acted as if it were shift catalyst (as a CO_2 acceptor). Hence, overall conversion of methane into products together separation was achieved in a single reactor. For the process to be economical, it is necessary that the CO_2 acceptor retain its activity and capacity through a number of carbonation-calcination cycles. As a result, attention should be given to investigate the effects of temperature, gas composition, and space velocity on multicycle performance.

Han et al. [20] studied selective removal of a product of a reversible reaction (shift reaction). This selective product removal upsets the "normal" equilibrium and permits effectively complete conversion of the limiting reactant and reaction was carried out at a temperature equal to or greater than 500 ^{o}C (no catalyst). In their work, total carbon oxide concentrations in the range of 400 ppm or less and fractional removal of carbon oxides (using dolomite type material) in excess of 0.995 were obtained during the prebreakthrough period of multi-cycle fixed bed reactor tests over a range of shift-carbonation reaction temperatures, feed gas compositions, and space velocities.

2.6 Alternative to Steam Methane Reforming Process

Hydrogen has always been an important chemical in the processes as either a reactant or a product. However, in the last years the real need for

hydrogen is due to its use as a fuel. Many companies have already built fuel cells that are using hydrogen or some fuel cells have their own reformers inside. That is, first hydrogen is produced than it is consumed in the cells to generate electricity.

Conventional SMR process is still the basic process for hydrogen production on a large scale. In order to compete with gasoline and other fuels, some modifications in the older technology should be done. Although pure hydrogen is obtained from the CO_2 abatement, carbon dioxide removal step is a very costly way of purifying the off-gas from the shift reactor. Membrane and sorption based technologies will replace SMR technology in the near future. When membrane based technologies and sorption-based technologies are compared, SERP [19, 23] seems to be a better candidate for hydrogen production. This is because of the fact that there is a wide range of adsorbents that are capable of adsorbing carbon dioxide at a wide range of temperature. On the other hand, thermal durability of membranes is still a big problem for membrane technologies due to high temperature nature of reforming reactions. After all, sorbents that are tolerable to cyclic processes and capable of adsorbing carbon dioxide at relatively high temperatures could be used in the reformer to produce hydrogen. Developing technologies for MERP and SERP might give the chance to use both processes in a single production unit in the near future.

CHAPTER 3

CARBON DIOXIDE REMOVAL

Among the separation processes, separation of carbon dioxide from mixtures with other gases is a process of substantial industrial importance. In the manufacture of ammonia and hydrogen from hydrocarbons or coal feeds, the removal of CO_2 from the synthesis gas is an important process step.

Table 3.1 Reasons for carbon dioxide removal [25]

Reasons for CO_2 Removal	**CO_2 Leakage**
1. Poison to catalysts	
a. NH_3 synthesis	5-10 ppm (vol.)
b. Hydrocracker	50-100 ppm (vol.)
c. Hydrodesulfurization	
2. Recovery of CO_2 for subsequent process	
a. Urea manufacture	98-99%
b. Liquid CO_2 and Dry ice	83-99%
c. Secondary oil recovery	
3. Fuel gas heating value	
a. High CO_2 natural gas	1-3%
b. SNG from liquid hydrocarbons or coal	0.1-2%
4. Adjustment of gas composition	
a. Methanol synthesis	1%
b. Oxo synthesis	0.1-0.6%
c. Iron ore reduction	1%
d. Fischer-Tropsch	1-2%
5. Avoid solid CO_2 plugging cryogenic plants	
a. Nitrogen wash of NH_3 synthesis gas	1 ppm
b. Air separation plants	
c. Liquefied natural gas	50-150 ppm (vol.)
d. Expander hydrocarbon recovery plants	
6. CO_2 removal incidental to sour gas sweetening	1-3%

The reasons for and the degree of carbon dioxide removal are varied and depend on the final use of the separated gases. Most common reasons for carbon dioxide removal are shown in Table 3.1.

3.1 Classification of CO_2 Removal Units

Abatement systems could be classified according to the chemical characteristics of carbon dioxide. Properties of carbon dioxide, which permit it to be separated from other gases, are as follows:

1. It is weakly acidic, forming H_2CO_3 when dissolved in water. This permits the use of liquid alkaline solutions, either regenerable or nonregenerable, for absorption of CO_2.

2. It is soluble in water and in many organic liquids. Therefore, processes based on solubility as opposed to chemical affinity are also used.

3. Its molecular size and structure permit it to be selectively adsorbed on solid adsorbents, particularly molecular sieves (low temperature application). However, the amount of carbon dioxide removed in this way is small compared to that removed with liquid absorbent systems.

4. Its acidic nature or its size and structure in some mixtures would permit to be separated by use of permeable membranes.

Typical gases from which CO_2 could be separated using one of the above properties include hydrocarbons, H_2, CO, N_2, and air (Where H_2S, mercaptan, COS, and CS_2 are present, the requirement for their removal tends to dominate the problem). Stronger acids such as SO_2, HCN, and HCOOH, and also ammonia, oils, phenols present special problems and tend to affect the choice of process used or, if present in sufficient amounts, they may need to be removed prior to the carbon dioxide removal system [25].

Most of the modern large CO_2 removal plants employ a weakly alkaline steam-regenerable aqueous solution in an absorber or contactor. The CO_2-laden "rich" solution is regenerated to lean solution by countercurrent stripping of the solution in another tower commonly known as a regenerator, stripper, desorber or reactivator.

In the case of CO_2 removal in ammonia, hydrogen, substitute natural gas (SNG), sour gas, oil, and coal gasification, and similar plants, low pressure stripping, steam, having little or no other use, is generally sufficiently available or recoverable from low level waste heat sources in the associated process for use as stripping steam. Examples of waste heat sources are:

- Steam-gas mixture leaving the low temperature shift converter
- Back pressure steam turbine drivers
- Ammonia synthesis converter
- Low pressure steam from waste heat boilers
- Sulfur plant by-product stream
- SNG methanator effluent or recycle steam-gas mixtures

The steam utility balance usually dictates the selection of the CO_2 removal process, since this system is considered the "heat sink" of the process plant. In some cases, credit is due to CO_2 removal system for eliminating at least a portion of the plant cooling system. Also credit may be due for boiler feed water preheating achieved by cooling a hot process stream.

3.2 Critical Characteristics of CO_2 Removal Processes

The most critical characteristics of a CO_2 removal process are its energy requirements and the concentration level to which CO_2 can be lowered in the exit gas. These two characteristics are somewhat interrelated and in turn are related to other parameters of the system.

Energy requirement is related primarily to solution circulation rate and, with the alkaline systems, the solution strength. In solvent systems, circulation rate is dependent on the available inlet partial pressure of CO_2, on the absorption coefficient, and on the temperature at which the absorption is carried out. In some cases, use of a small amount of refrigeration to cool the solvent results in minimum overall energy requirement.

Each of the various processes available has advantages and disadvantages. The selection of a process for a given situation involves weighing of many factors, and in some cases a number of processes could be found applicable with little or no technical advantage favoring one or another. There are, however, some broad criteria, which may directionally indicate the likeliest choice [26].

3.3 Carbon dioxide Removal in Hydrogen Production

In many cases it is necessary to purify hydrogen by using a variety of processes. These must be chosen in accordance with the final use of the hydrogen to give an economically efficient result.

Frequently in industrial-scale plants combinations of the various processes (absorber, adsorber) are used. In addition, several alternative processes may be available and may be used depending on the economic situation.

3.3.1 Low Temperature Process

The large temperature difference between the boiling point of hydrogen and that of the most frequent impurities is the basis of the low temperature process (LT process) for the purification of hydrogen. Low temperature rectification processes are used, if the impurities are also to be separated from one another. The use of scrubbing and adsorption processes at low temperatures leads to both high purities and high yields.

Because of the only slightly interaction of hydrogen with the usual adsorbing agents in technically important pressure and temperature ranges,

adsorption processes are particularly suitable not only for the separation from other gases but also for the separation of impurity traces from hydrogen.

The adsorbents for hydrogen purification are chosen according to the impurities to be removed. Various effects separate the gas mixtures. For instance, steric effects prevail if the adsorbent has a uniform and narrow micropore distribution, as is found particularly with the zeolites. Equilibrium effects result from different adsorption forces of the gases on the solids, and kinetic effects are caused by the different diffusion mobilities of the gases into the pores of the adsorbing agents.

3.3.2 Pressure Swing Adsorption

The combustion of fossil fuels, such as coal or natural gas, releases of large volumes of carbon dioxide to the environment (e.g. Natural gas treatment, production of hydrogen gas and in the aerospace industry). A number of techniques can be used for separation of carbon dioxide from fuel gas streams. The large scale separation of carbon dioxide by absorption is a commercial operation used throughout the world. Other techniques exist that could be considered for energy related applications, such as cryogenic separation, membrane separation and adsorption processes, such as pressure swing adsorption (PSA), vacuum swing adsorption and temperature swing adsorption. PSA is well suited for the removal and recovery of carbon dioxide from any fuel gas stream which contains carbon dioxide. PSA process could be operated at elevated temperatures [21].

Hydrogen purification takes place in adsorption vessels with fixed beds of adsorbents. Other types, such as trickle beds, adsorption columns with solid circulation, moving beds, or adsorption in ebullating beds, are not suitable to use for hydrogen purification on a technical scale.

Contrary to adsorption with thermal regeneration, pressure-swing adsorption operates at almost constant temperature using partial pressure differences. However, the small temperature gradients occurring with adsorption and desorption contribute considerably to the mechanism of the process. The components to be adsorbed at high system pressure and high partial pressure and are desorbed at low system pressure in accordance with the appropriate

equilibrium isotherms of the various impurities. Figure 3.3.1 shows a typical carbon dioxide removal unit. Multi-bed adsorbers, using molecular sieve (commonly used) as sorbent, are processed to yield high purity hydrogen. Depending on the desired end-use more adsorbers could be placed in the PSA unit.

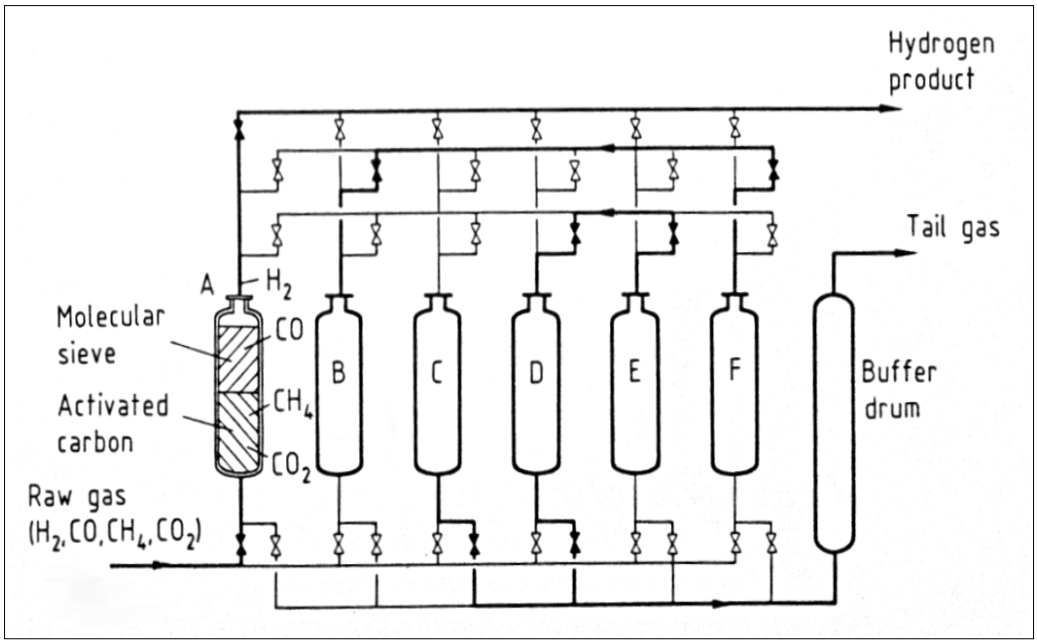

Figure 3.3.1 Six-bed pressure swing adsorption unit for hydrogen production [25]

PSA process is cyclic, however, contrary to temperature swings, pressure changes can be carried out more rapidly and allow a shorter adsorption time. Typical cycle times are in the range of 3 to 10 min. thus, removal of impurities present in high concentrations can be accomplished using moderately sized adsorber vessels. Each adsorber is performing a different task, depending on which phase of the complete PSA cycle is regarded. The chronological sequence of all steps constitutes the cycle of an adsorber:

1. Adsorption at the pressure of the raw gas (highest system pressure), hydrogen production (adsorber A, Figure 3.3.1);

2. Cocurrent depressurization, provision of gas for pressure equalization and purging (adsorbers F and E);

3. Countercurrent depressurization, production of part of the tail gas (adsorber C);

4. Countercurrent purging (lowest system pressure), production of another part of the tail gas (adsorber D);

5. Countercurrent repressurization (adsorber B)

This latter mode of operation is indicated for the enrichment and recovery of the adsorbed component. However, production of concentrated byproducts during the production of pure hydrogen is usually carried out by low temperature processes and not by the adsorption process.

The mode of operation of a PSA can be summarized as follows:

1. Pure hydrogen is produced continuously at adsorption pressure.

2. Tail gas is produced continuously, the pressure, composition, and amount of which fluctuate periodically. These fluctuations are smoothed out by buffer vessels.

3. The efficiency of a PSA is defined by the amount of pure hydrogen produced in relation to the total hydrogen amount present in the crude gas. Depending on the crude gas composition and the degree of technical sophistication utilized, the PSA efficiency ranges between 70 and 90% at least.

The major cost for pressure swing adsorption is in the compressor costs. If the mixture is available at elevated pressure, the costs for separation are substantially reduced. The gas throughput and product purities are also important considerations. The costs for adsorption separation are generally are lower than distillation for small to medium throughputs, and when high purity products are not required. After all, a novel process should be replaced with the older PSA technology to overcome cost-dependent problems in hydrogen production.

CHAPTER 4

ADSORBENTS FOR CARBON DIOXIDE REMOVAL

In search for a good adsorbent for carbon dioxide removal in hydrogen production, it is critical to know certain characteristics of the sorbents to decide on which adsorbent is more suitable for the abatement process via pressure swing adsorption or SERP processes.

When certain characteristics of the adsorbents are considered, a large specific surface area is preferable for providing large adsorption capacity, but the creation of a large internal surface area in a limited volume inevitably gives rise to large numbers of small sized pores between adsorption surfaces. The size of the micropores determines the accessibility of adsorbate molecules to the internal adsorption surface, so the pore size distribution of micropores is another important property for characterizing adsorptivity of adsorbents. Especially, materials such as zeolite and carbon molecular sieves can be specifically engineered with precise pore size distributions and hence tuned for a particular separation.

Another criterion for a typical adsorbent is its surface polarity. Surface polarity corresponds to affinity with polar substances such as water or alcohols. Polar adsorbents are thus called "hydrophilic" and aluminosilicates such as zeolites, porous alumina, silica gel or silica-alumina are examples of adsorbents of this type. On the other hand, nonpolar adsorbents are generally "hydrophobic". Carbonaceous adsorbents, polymer adsorbents and silicalite are typical nonpolar adsorbents. These adsorbents have more affinity with oil or hydrocarbons than water [27].

4.1 Selection of an Adsorbent

The surface of a solid represents a discontinuity of its structure. The forces acting at the surface are unsaturated. Hence, when the solid is exposed to a gas, the gas molecules will form bonds with it and become attached (adsorption). The process had to be regenerative; that is, the adsorbent could be regenerated to permit reuse in further cycles as well as allowing recovery of the adsorbed gas. In early times, sorbent regeneration was achieved by heating (thermal treatment), but regenerating by heating was not an efficient way because a heating-cooling cycle was necessarily time-consuming (efficient pressure swing cycles were invented).

Regarding to the nature of process, the most important characteristic of a sorbent is its high porosity. Thus, physical characterization is generally more important than chemical characterization. The most important physical characteristics include pore volume, pore size distribution, and surface area. Besides these, bulk density, crush strength, and erosion resistance are also critical parameters to be considered in the selection of an adsorbent for a particular process. However, the predominant scientific basis for sorbent selection is the equilibrium isotherm. The equilibrium isotherms of all constituents in the gas mixture, in the pressure and temperature range of operation, must be considered for the sorbent of interest [28]. In order to highlight the most important properties of adsorbents, some features of good adsorbents are listed below.

The adsorbent must have;

- high selectivity and adsorption capacity for carbon dioxide at high temperature
- adequate adsorption/desorption kinetics for carbon dioxide at operating conditions
- stable adsorption capacity of carbon dioxide after repeated adsorption/desorption cycles

- adequate mechanical strength of adsorbent particles after cyclic exposure to high pressure streams

Based on the nature of the bonding between the adsorbate molecule and the solid surface, adsorption can be categorized as either physical adsorption or chemical adsorption (chemisorption). Chemisorption involves electron transfer and is essentially a two-dimensional chemical reaction, whereas the bonds formed in physical adsorption are held by van der waals and coulombic forces. Surfaces of all commercial sorbents possess some degree of polarity. The capacity of a sorbent depends on two complementary factors: surface area and porosity. The driving force for all adsorptive gas separation processes lies in the departure from equilibrium.

4.2 Overview of Adsorbents for Carbon dioxide Removal

The most important adsorbents are activated carbon, zeolites, silica gel, and aluminum oxide. Zeolites preferentially adsorb polar (e.g. water) or polarizable (e.g. carbon dioxide) materials. Activated carbon has a hydrophobic character and is especially suitable for the removal of organic substances contained in liquids (aqueous solutions) and gases. Sometimes, it is desired to adsorb only molecules below a certain diameter. For this reason, molecular sieves of zeolites or carbon are ideal (they have a very narrow distribution of micropores) [46]. In fact, zeolites are widely used in pressure swing adsorption units to purify hydrogen at low temperatures (ca. 50 ^{o}C). Also, metal oxides are pretty good adsorbents for carbon dioxide removal at lowered temperatures. Table 4.2.1 shows some adsorption characteristics of certain metal oxides.

In this study, two adsorbents were used for the adsorption of carbon dioxide. One of these sorbents was activated soda and it was obtained by calcination of either trona or sodium bicarbonate. The other sorbent used for CO_2 abatement was hydrotalcite, which belongs to a large class of clays that exhibit particular sorption characteristics.

Table 4.2.1 Adsorption properties for metal oxides for carbon dioxide removal [29]

Metal Oxide	Density (g/cm^3)	CO_2 Capacity (g CO_2/g oxide)	Regenaration Energy (kj/g CO_2)
Li_2O	2.01	1.471	5.146
Na_2O	2.27	0.709	7.309
K_2O	2.32	0.468	8.895
Rb_2O	3.72	0.235	9.172
Cs_2O	4.36	0.156	9.279
MgO	3.65	1.092	2.681
CaO	2.62	0.785	4.042
SrO	4.70	0.425	5.249
BaO	5.72	0.287	6.081
ZnO	5.47	0.540	1.616
Ag_2O	7.14	0.189	1.865

4.3 Clays

Clays are very versatile materials and hundred of millions of tons currently find applications not only in ceramics and building materials, paper coating and fillings, drilling muds, foundry moulds, pharmaceuticals, etc., but also as adsorbents, catalysts or catalyst supports, ion exchangers, etc., depending on their specific properties. Two broad classes of clays may be identified: cationic clays (or clay minerals), widespread in nature, and anionic clays (or layered double hydroxides (LDHs)), more rare in nature but relatively simple and inexpensive to synthesize on laboratory and industrial scales. The cationic clays have negatively charged alumina-silicate layers, with small cations in the interlayer space to balance the charge, while the anionic clays have positively charged brucite-type metal hydroxide layers with balancing anions and water molecules located intersititially. Cationic clays are mainly prepared starting from the minerals, whereas anionic clays are usually synthesized [32].

4.3.1 Layered Double Hydroxides (Anionic Clays)

Layered double hydroxides (LDHs), one of the few families of layered materials with positive layers and negative species in the interlayers are deserving increasing interest in recent years, due to the wide scope of applications which are continuously emerging for these and derived materials: catalysis, adsorption, anionic exchange, electroactive materials, water

purification etc. The reason for wide application areas probably lies in the rich chemistry which they show related to their peculiar structure: isomorphous, partial substitution of M^{2+} cation brucite like layers by trivalent cations and simultaneous intercalation of anions in the interlayer space to balance the electric charge. The most outstanding properties of these materials can be summarized as follows [33]:

- Metal ratio in the layers is similar to that in the starting solution
- Easily oxidazible cations are, however, stabilized in the layers
- Solids can be prepared with a given cation in different oxidation states and different environmental geometry
- Solids with many different metal cations, well dispersed in the anion matrix can be obtained

Although there are many anionic clays in use, some of these materials are widely used due to their particular attractive properties. In Table 4.3.1 composition and some other parameters are shown for anionic clays [32].

Table 4.3.1 Composition, crystallographic parameters and symmetry for some HT anionic clays [32]

Mineral	**Chemical composition**	**a(nm)**	**c(nm)**	**Symmetry**
Hydrotalcite	$Mg_6Al_2(OH)_{16}CO_3.4H_2O$	0.3054	2.281	3R
Manesseite	$Mg_6Al_2(OH)_{16}CO_3.4H_2O$	0.3100	1.560	2H
Pyroaurite	$Mg_6Fe_2(OH)_{16}CO_3.4H_2O$	0.3109	2.341	3R
Sjögrenite	$Mg_6Fe_2(OH)_{16}CO_3.4H_2O$	0.3113	1.561	2H
Stichtite	$Mg_6Cr_2(OH)_{16}CO_3.4H_2O$	0.3100	2.340	3R
Barbertonite	$Mg_6Cr_2(OH)_{16}CO_3.4H_2O$	0.3100	1.560	2H
Takovite	$Ni_6Al_2(OH)_{16}CO_3.4H_2O$	0.3025	2.259	3R
Reevesite	$Ni_6Fe_2(OH)_{16}CO_3.4H_2O$	0.3081	2.305	3R
Meixnerite	$Mg_6Al_2(OH)_{16}(OH)_2.4H_2O$	0.3046	2.292	3R
Coalingite	$Mg_{10}Fe_2(OH)_{24}CO_3.2H_2O$	0.3120	3.750	3R

Upon calcination these solids lead to formation of mixed oxides whose chemical composition can be easily tuned when preparing the parent LDH, and depending on the decomposition process and even on the precise composition of the starting material, different crystalline species can be obtained. However,

LDHs calcined at intermediate temperatures are usually amorphous. Furthermore, the specific surface area increases with the calcination temperature (if the volatile anions exist in the interlayer space), then reaching a maximum and decreasing at higher temperatures, when crystallization also occurs; the change in the strength of surface acid/base sites, and the modification in the hydrothermal stability with respect to similar compounds (e.g. MgO) have been also reported in the literature [32]. Although many studies have been reported on the thermal evolution of LDHs containing nonoxidazible cations in the layers, many studies refer to the particular case of hydrotalcite (containing Mg^{2+} and Al^{3+}, with carbonate in the interlayer, Table 4.3.1).

4.3.1.1 Hydrotalcite

Hydrotalcite-like compound (HTlc) is a layered double hydroxide, with the general formula $[Mg_{1-x}\ Al_x(OH)_2]\cdot[A^{n-}_{x/n}\cdot zH_2O]$. Ratio of Mg:Al varies from 4:1 to 2:1 ($0.20 \leq x \leq 0.33$). There is no limitation to nature of interlayer anions, and derivatives of HTlcs with various anions have been synthesized and their physicochemical properties were studied from the viewpoint of catalysis, microporous material, and host of electroactive and photoactive anions [32, 39]. Primarily these derivatives have been synthesized with coprecipitation method and have been obtained by anion exchange in appropriate aqueous solution.

Hydrotalcite (Magnesium aluminum hydroxy carbonate) has a molecular weight of ca. 603.98 g/mol. Depending on the chemical modification in the structure, typical composition might differ. However, usually, hydrotalcite type material has the properties shown in Table 4.3.2.

Table 4.3.2 Typical composition of hydrotalcite ($Mg_6Al_2(CO_3)(OH)_{16}.4H_2O$) [34]

Element	Weight Percent (%)	Compound (%)
Magnesium	24.14	MgO, 40.04
Aluminum	8.93	Al_2O_3, 16.88
Hydrogen	4.01	H_2O, 35.79
Carbon	1.99	CO_2, 7.29
Oxygen	60.93	

4.3.1.1.1 Hydrotalcite Definition

Hydrotalcite like compounds belong to a large class of anionic and basic clays, also known as mixed-metal layered hydroxides and layered double hydroxides. In Figure 4.3.1, schematic representation of hydrotalcite like materials shown with their typical structural arrangement.

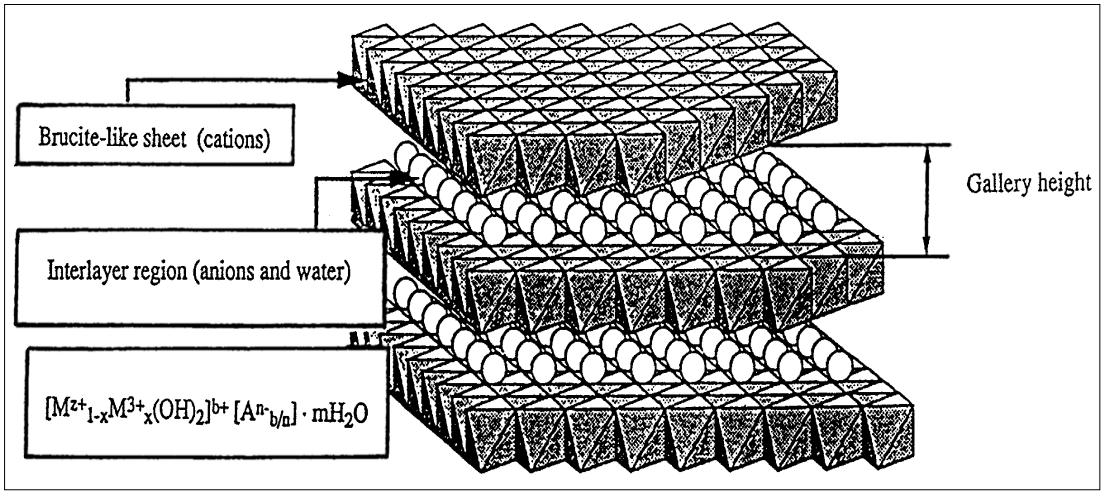

Figure 4.3.1 Schematic representation of the hydrotalcite-type anionic clay structure [36]

Hydrotalcites are composed of positively charged brucite-like, $\left[M^{2+}_{1-x}M^{3+}_{x}(OH)_2\right]^{x+}$, layers (e.g. $Mg(OH)_2$) with trivalent cations substituting for divalent cations at the centers of octahedral sites of the hydroxide sheet, whose vertex contain hydroxide ions, and each –OH group is shared by three octahedral cations and points to the interlayer regions [35]. The anions and water molecules present in the interstitial position compensate the excess positive charge of the HTlcs. Hydrotalcite like compounds possess exchange capabilities for organic and inorganic anions, due to their structural positive charge. Hydrotalcite like material's structure could be shown as follows:

$$\left[(M^{2+}_{1-x}M^{3+}_{x}(OH)_2)^{x+}.(A^{n-}_{x/n}.mH_2O)^{x-}\right] \qquad (4.3.1)$$

Where M^{2+}= Mg, Mn, Fe, Co, Ni, Cu, Zn, Ga etc., M^{3+}= Al, Cr, Mn, Fe, Co, Ni, and La, A^{n-} represents n-valence inorganic (CO_3^{2-}, OH^-, NO^{3-}, SO_4^{2-}, ClO_4^-),

heteropolyacid ($PMo_{12}O_{40}^{3-}$, $PW_{12}O_{40}^{3-}$) or even organic acid anions. The most often studied LDH is $[Mg_{1-x}Al_x(OH)_2][(CO_3)_{x/2}n.H_2O]$. In Figure 4.3.2, arrangement of molecules within the sheet structure is visualized. Almost 40-45% of the structure is desorbed when calcined and material becomes a very porous material.

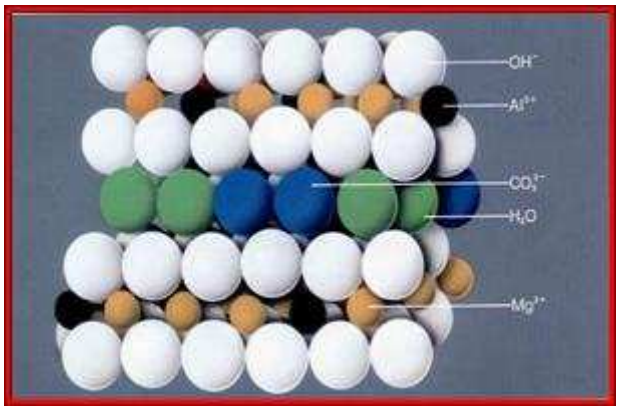

Figure 4.3.2 Schematic representation of hydrotalcite [42]

Although hydrotalcite shows anion exchange properties, it can not readily be used for this purpose. The carbonate is preferentially sorbed and prevents significant anion exchange. Only the thermally treated hydrotalcite can readsorb water and anions as it return to its original structure.

Hydrotalcite (containing carbonates or the interlayer anion is desorbed), decomposed into magnesium and aluminum oxide solution, when heated at 550 °C. The calcined product $Mg_{1-x}Al_xO_{1+x/2}$ can rehydrate and incorporate anions to rebuild the initial hydrotalcite structure as expressed by the following equations:

$$[Mg_{1-x}Al_x(OH)_2](CO_3)_{x/2} \rightarrow Mg_{1-x}Al_xO_{1+x/2} + (x/2)CO_2 + H_2O \qquad (4.3.2)$$

$$Mg_{1-x}Al_xO_{1+x/2} + (x/n)A^{n-} + (1+(x/2)+y)H_2O \rightarrow [Mg_{1-x}Al_x(OH)_2](A^{n-})_{x/n} + xOH^- \qquad (4.3.3)$$

Further reduction of HT compounds or mixed oxides, containing reducible cations yields supported metal catalysts. In these materials, the metallic function and acid-basic properties can both be tailored through several parameters, such as the nature and the amount of cations in the layers, and the activation conditions [38].

HTs could be promising materials as they lead, after calcination at high temperatures, to mixed oxides of small crystallite size, high thermal stability and a large surface area. Since these materials have a well-defined layered structure with nanometer (0.3-3 nm) interlayer distances and contain important functional groups. Very high number of variables has been reported for synthetic clays, which make it possible to produce tailor-made materials able to fulfill specific requirements. Water molecules and anions are located in the interlayer space, and structural and physical properties indicate the strongly disordered nature of these regions, for which a quasi liquid state has been claimed. The interlayer space can also be used to increase the total amount of metals, which may be introduced in anionic form (chromates, ferro or ferricyanides, etc.) or to introduce cations which are not compatible with the octahedral sites of the brucite-type sheets (for example Mo^{4+}, or Ir^{4+}), thus preparing new materials with unusual properties [40].

The most interesting properties of these mixed oxides are;

- High surface area (100-300 m^2/g)
- Homogenous interdispersion of the elements thermally stable also in reducing conditions, with formation of very small stable metal crystallites.
- Synergetic effects between the elements, due to the intimate interdispersion, which favors, for example, the development of unusual basic or hydrogenating properties. Basic properties depend significantly on composition and calcination temperature.
- Memory effect, which allows reconstruction under mild conditions of the original structure by contact with solutions containing various anions.

Each element or compound has certain effects to the behavior of hydrotalcite like materials. Some of these effects has vital importance and

require a careful understanding and study to improve the catalytic or sorption characteristics of these materials.

Effect of the Type of M^{2+} (Mg^{2+})

Yong et al. studied hydrotalcite materials for carbon dioxide removal and they concluded that the higher heat treatment temperature is favorable for adsorption of carbon dioxide [28]. Mg-Al (Mg also acts as a shift catalyst) one among these hydrotalcites exhibited the best sorption characteristics for the pressure swing adsorption process. Other possible hydrotalcites, for purification purposes, are Ni-Al, Co-Al, Cu-Al, Zn-Al.

Effect of M^{3+} (Al^{3+}) Content

Aluminum content in HTlcs strongly affects the adsorption capacity of carbon dioxide, and there is an optimum aluminum content for adsorption of carbon dioxide, both for 25 ^{o}C and 300 ^{o}C. The incorporated aluminum has two functions: one being that the density of the layer charge in HTlcs increased with increasing the aluminum content, which is favorable for adsorption of carbon dioxide and the other leading to a decrease in the interlayer spacing of HTlcs and reducing the number of high strength carbon dioxide adsorption sites of HTlcs with increasing the aluminum content [28].

Effect of Water (Steam)

Steam can increase the adsorption capacity of carbon dioxide on HTlcs, particularly at low pressure (0.05 bar). The adsorption capacity of carbon dioxide at wet condition will be constant above a pressure (such as >0.3 bar) or a period of time. The major reasons of water or steam being favorable for the adsorption capacity of carbon dioxide may be that it can increase potential energy and it is able to further activate adsorption sites, possibly by maintaining the hydroxyl concentration of the surface and/or preventing site poisoning through carbonate or coke deposition.

Effect of Temperature

Hydrotalcite has interesting response to temperature changes. For instance, adsorption capacity of carbon dioxide is at 300 ^{o}C is greater than the adsorption capacity at 20 ^{o}C. Moreover, sorption capacity at 200 ^{o}C is smaller than the one at 20 ^{o}C. Main reason for this unexpected response to different sorption temperatures is that HTlcs have different thermal decomposition behaviors at the different stages of calcination.

Effect of the Cycle Number

The adsorption capacity of carbon dioxide onto hydrotalcites decreases during about the first 10 cycles as a certain portion of the carbon dioxide is irreversibly chemisorbed on the HTlcs. In addition, material's attitude towards cyclic operation is still under investigation.

Effect of the Chemical Modification

The effect of K_2CO_3 (or Na_2CO_3) loading on the adsorption capacity of CO_2 for the promoted HTlcs was studied [28] by Yong et al. and results indicated that K_2CO_3 modification of the HTlcs could greatly improve its adsorption capacity of carbon dioxide, and there was an optimum K_2CO_3 content loading for carbon dioxide.

To sum up, there is an optimum aluminum content and heat treatment temperature for the adsorption capacity; the larger and/or higher is the charge of the anion, the more is the adsorption capacity of carbon dioxide; a low content of water/steam can improve the adsorption capacity; the adsorption capacity of carbon dioxide onto HTlcs is greatly enhanced by chemical modification (such as K_2CO_3), and there is an optimum K_2CO_3 content loading; and the adsorption capacity of carbon dioxide onto HTlcs will remain constant after about 10 cycles adsorption/desorption under dry and wet conditions [28].

Understanding the adsorption mechanism of carbon dioxide, finding the best HTlc for adsorption of carbon dioxide, finding the best chemical reagent to modify HTlcs for enhancing their adsorption capacity of carbon dioxide, studying the adsorption and desorption kinetics of carbon dioxide onto HTlcs, and

choosing the optimum technological conditions for industrialization are the challenge research subjects related to hydrotalcite like compounds.

4.3.1.1.2 Hydrotalcite Preparation

In this study, adsorbent was purchased (Sigma-Aldrich) as hydrotalcite in powder form ($Mg_6Al_2(CO_3)(OH)_{16}.4H_2O$). However, the adsorbent (HT) could be prepared by co-precipitating mixed metal solutions of magnesium and aluminum nitrates as follows:

- 700 ml of an aqueous solution of 1 mol $Mg(NO_3)_2.6H_2O$ and 0.5 mol $Al(NO_3)_3.9H_2O$ is added dropwise to 1 L of an aqueous solution of 3.5 mol/L NaOH and 0.94 mol/L Na_2CO_3 under intense mixing for 4h. The temperature is maintained at 35 ^oC.

- The resulting precipitate is heated at approximately 65 ^oC for 18h to crystallize.

- The slurry is filtered and washed with water to remove the sodium to below the 0.1 % level on a dry weight basis. After drying, the filter cake is pulverized in a ball mill and sieved to obtain -500 +250 μm particle size. Thermally activated product could be obtained by calcination in a tubular furnace at 550 ^oC [37].

Table 4.3.3 Factors influencing the synthesis of HT anionic clays [32]

Structural Variables	**Preparation Variables**
Cation size	pH
Value of x [i.e the $M^{3+}/(M^{3+}+M^{z+})$ ratio]	Precipitation method
Cation stereochemistry	Precipitation Temperature
Cation mixture (nature and ratio)	Reagent concentration
Nature of balancing anions	Aging
Amount of interlayer water	Washing and drying
Crystal morphology and size	Presence of impurities

The properties of Mg-Al mixed oxides obtained from hydrotalcite were affected by the preparation conditions of hydrotalcites. B.E.T surface areas increase with the raising of stirring rate. The Mg-Al mixed oxides show the biggest surface area when the hydrotalcite was calcined at around 550 ^oC, while

it has the greater average pore size at 500 ^{o}C [43]. Table 4.3.3 shows the factors (preparation variables) that influence the synthesis of anionic clays.

4.3.1.1.3 Application Areas of Hydrotalcite

Hydrotalcite like compounds are used as anion-exchange and adsorption materials, carriers for drugs, antacids in medicine, electrode modifiers, catalysts, precursors and supports of catalysts, decolorizing agents, polymer stabilizers, optical hosts and ceramic precursors.

HTs may also be used as components in new nano-materials such as nano-composites. These hydrotalcites are readily synthesized by a co-precipitation method [41].

Many of their most important applications are due to their permanent anion-exchange and adsorption capacity, the mobility of their interlayer anions and water molecules, their large surface areas and the stability and homogeneity of the materials formed by their thermal decomposition.

HT-like compounds as prepared or after calcination at high temperatures have found many practical applications. For instance, hydrotalcites are important in the removal of environmental hazards in acid mine drainage. In addition, hydrotalcite formation also offers a mechanism for the disposal of radioactive wastes. Besides these, hydrotalcite formation may also serve as a means of heavy metal removal from heavy metal contaminated wastes.

They are widely used as adsorbents for liquid ions and gas molecules. They also find use as catalysts for oxidation, reduction, and other catalytic reactions. Recently, LDH materials also found use in novel reactive separation applications in order to increase the conversion of catalytic reactions by removing one of the products from the reactor. These materials find applications in a broad range of temperatures from room temperature adsorption to high temperature catalytic reactions (ca. 500 ^{o}C).

Catalytic Applications

Interest in the study of hydrotalcites results from their potential use as catalysts. The reason for the potential application of hydrotalcites as catalysts rests with the ability to make mixed metal oxides at the atomic level, rather than at a particle level. Such mixed metal oxides are formed through the thermal decomposition of the hydrotalcite.

Many catalysts based on mixed oxides can be obtained by a controlled decomposition of the HT-like compounds. These catalysts show a large surface area, basic properties, high metal dispersion, and stability against sintering. Anionic clays are the most promising precursors of multicomponent catalysts for many catalytic reactions of industrial interest. Catalytic applications of the mixed oxides obtained by their controlled calcination include polymerization of alkene oxides, aldol condensation of aldehydes and ketones, methane or hydrocarbon steam reforming, methanation, methanol synthesis, higher-alcohols or hydrocarbon (Fischer-Tropsch) synthesis, etc [41].

4.3.1.1.4 Thermal Evolution of Hydrotalcite

In general, the layer structure of HTlc collapses at 350°C. MgO phase begins to form above 400°C. Al ions, which have a smaller ionic radius than Mg ions, enter into MgO phase between 400 and 800°C, and Mg-Al double oxide whose lattice constant is smaller than pure MgO then is formed. Migration of Al ions from the double oxide into spinel ($MgAl_2O_4$) is occurred, and the double oxide decomposes to spinel and MgO at 900°C.

Historically, decarbonation of Mg-Al-CO_3 HTlc has been thought to occur between 400 and 500°C, together with dehydroxylation. The evolution of the remaining carbonates was observed as two maxima, at 600 and 900°C. At these temperatures, Al ions go into MgO, and spinel forms. Therefore, the carbonates are released as the Al ions migrate. At a lower Al content, x=0.25, CO_2 evolution is almost complete at 500°C. There is no maximum of CO_2 evolution above 500°C. Consequently we speculate that positive charge in the local area around Al ions could capture carbonates and that amount of remaining

carbonates in calcined material increases suddenly when Al content becomes maximum in the structure.

In Figure 4.3.3 [44], desorption of carbon dioxide from hydrotalcite structure is shown for different structural loadings. In addition, to understand structural effects due to calcination (or thermal evolution), it is necessary to know structure when it is heated uniformly.

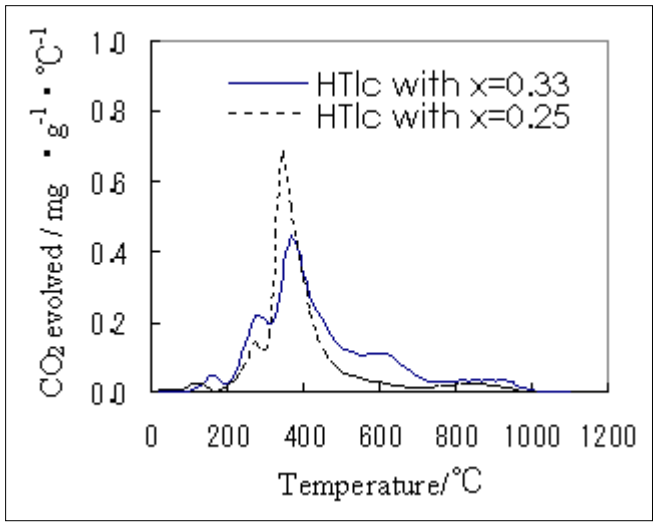

Figure 4.3.3 Desorption of carbon dioxide from hydrotalcite as a function of temperature for different x values in the structure [44]

In Figure 4.3.4 [40] thermal evolution of the hydrotalcite material is shown. Evolution phases that hydrotalcite like compound face is as follows:

1. In the temperature range 70-190 °C, loosely held interlayer water is lost, and there are two different co-existing crystal phases of Mg-Al-CO_3 LDH present, i.e., Phase I with a basal spacing ranging from 7.5 to 7.3 A°, and Phase II with basal spacing of ~ 6.6 A°; the LDH structure, itself, still remain intact.

2. In the temperature range 190-280 °C, the OH^- group bonded with Al^{3+} begins to disappear at 190 °C, and is completely lost at 280 °C. In this temperature region, Phase I is transformed into Phase II.

3. In the temperature range 280-405°C, the OH^- group bonded with Mg^{2+} begins to disappear at 280 °C and is completely lost at 405 °C; a degradation of the LDH structure is also observed in the same region.

4. Finally, in the temperature range 405-580 °C, CO_3^{2-} loss begins and is completed at 580 °C. In this temperature range, the material becomes an amorphous metastable mixed solid oxide solution.

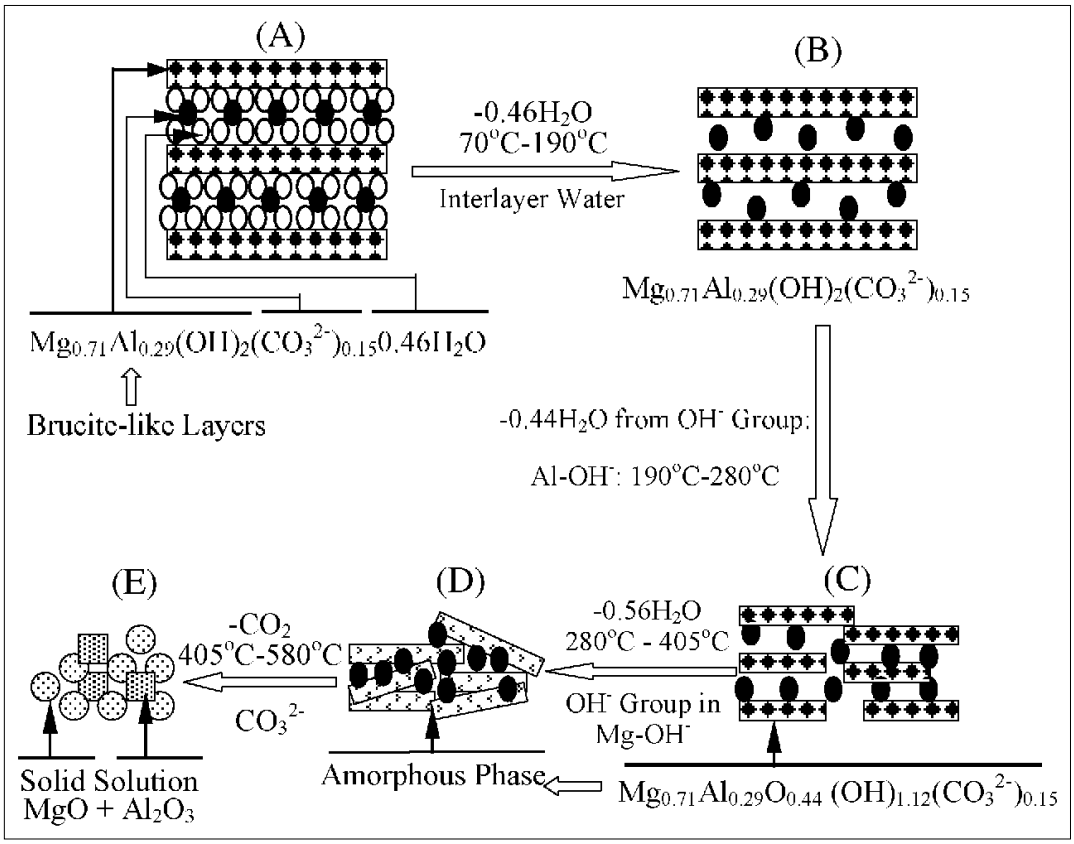

Figure 4.3.4 Thermal evolution of hydrotalcite as a function of temperature [40]

4.4 Activated Soda

Activated soda is a widely used chemical that has already many application areas. Soda ash (Na_2CO_3) is one of the alkalis, which has a major commercial importance. In addition to the two well-known processes, namely the Le Blanc process and the Solvay process, soda ash is also produced from natural sodium

carbonate deposits. Trona is one of the major sodium carbonate-bearing minerals and is used as a source of sodium carbonate.

Soda ash produced by the calcination of $NaHCO_3$ is highly porous and very reactive. The manufacture of glass accounts for approximately 50% of domestic soda ash consumption, with the bottle and container sector comprising 35% of this end use; flat, 8%, fiber, 3%, and specialty, 4%. Soda ash is the second largest tonnage commodity used in glass manufacture, comprising about 19% by weight of the raw materials in a glass container batch. The production of the sodium based inorganic chemicals is the second largest end use of soda ash, representing about 20% of domestic demand. Furthermore, soda ash mixed with lime is used to permanently remove the hardness of industrial water supplies. The miscellaneous end uses of soda ash include agriculture, marine treatment, corn syrup, drilling mud additives, dyes, enamels, flue gas desulfurization, food processing, metal refining, and in the preparation of other chemicals [63].

4.4.1 Trona

In the production of soda ash from trona, generally two processes are used. In one process, dissolved trona ore is first clarified by the removal of solids and organic matter. The solution is then cooled and trona crystals are precipitated. The precipitate is then calcined to produce soda ash. In the second process, trona ore is first calcined and the crude soda ash is dissolved to produce monohydrate crystals. Then, these crystals are heated and calcined to produce soda ash.

Gancy et al. [64] studied the thermal decomposition of solid sodium sesquicarbonate at temperatures between 350 and 487 K in nitrogen and carbon dioxide atmospheres. In this study, equilibrium vapor pressures were measured and they suggested the following two-stage decomposition scheme:

$$3(Na_2CO_3.NaHCO_3.2H_2O) \rightarrow 3NaHCO_3.Na_2CO_3 + 2Na_2CO_3 + 6H_2O \qquad (4.4.1)$$

$$2(3NaHCO_3.Na_2CO_3) \rightarrow 5Na_2CO_3 + 3CO_2 + 3H_2O \qquad (4.4.2)$$

The intermediate, wegscheiderite ($3NaHCO_3.Na_2CO_3$), is naturally occurring. Gancy et al. [64] suggested that it could be formed when carbon dioxide reacts with sesquicarbonate. The thermal decomposition of sodium sesquicarbonate produces two reaction intermediates, sodium carbonate monohydrate and wegscheiderite. Hence, they proposed that the thermal decomposition of these intermediates were the rate-controlling step across a wide range of temperatures and atmospheric composition. Only at low temperatures, the decomposition of sesquicarbonate was rate controlling in carbon dioxide atmosphere.

In Table 4.4.1 [30], chemical analysis of trona samples (Beypazarı), used in this study, are shown. Particles having an average size of 0.0236 cm were used in the preparation of activated soda. Calcination of trona, according to reaction (4.4.3), was carried out at 200 ^oC. Trona contains about 70.4% Na_2CO_3 in an overall base and this structural soda content allows a high adsorption capacity with respect to sodium bicarbonate [31].

Table 4.4.1 Chemical analysis of trona sample [30]

Composition	**Weight Percent (%)**
$NaHCO_3$	30.1
Na_2CO_3	48.8
H_2O	17.9
Impurities	3.2

As a result of thermal decomposition of trona, highly porous structures are obtained. In fact, sorption characteristics for carbon dioxide are slightly better than activated soda obtained from sodium bicarbonate (Chapter 7).

$$2[Na_2CO_3.NaHCO_3.2H_2O] \rightarrow 3Na_2CO_3 + CO_2 + 5H_2O \qquad (4.4.3)$$

4.4.2 Sodium bicarbonate ($NaHCO_3$)

Kinetics of thermal decomposition of sodium bicarbonate [65] is widely studied in the literature. However, Na_2CO_3 sorption characteristics for carbon dioxide capture are rarely studied. Activated sodium bicarbonate (activated

soda) acts as an adsorbent or sometimes a promoter and it readily adsorbs carbon dioxide at low temperatures due to its thermodynamic limitations (App. G). Following reaction occurs in the course of calcination.

$$2NaHCO_3 \leftrightarrow Na_2CO_3 + CO_2 + H_2O \quad \Delta H = -125.2 \text{ kJ/mol} \qquad (4.4.4)$$

Reaction (4.4.1) is a reversible reaction with an exothermic heat of reaction around 125 kj/mol. In experimental studies, sodium bicarbonate, in powder form, is first activated to give off the carbon dioxide and steam and then the rest of adsorption studies were performed with carbon dioxide for different temperatures in the presence of steam.

As a first step in experiments, both sodium bicarbonate and trona were used to obtain activated soda. Different structures of these materials yielded different porous Na_2CO_3 structures at the end. Besides these, temperature of calcination also effects the porosity and pore size distributions of the material [54].

Regarding to the TGA results and data available from literature, calcination temperature of both trona and sodium bicarbonate was kept constant at 200 ^{o}C. Certain features of these sorbents (cost-effective, high porosity, low temperature processes, and ease of regeneration) indicate that activated soda could be used as an adsorbent for carbon dioxide capture. However, activated soda could not be used directly within the reformer for in situ removal of carbon dioxide in the hydrogen production plant due to high heat fluxes. On the other hand, this sorbent could be used in hydrogen purification when effluent gas from the reformer is cooled down to reasonable temperatures so as to carry out adsorption efficiently.

CHAPTER 5

THEORY

There are several fluid-solid reactions in which the solid is reactant. These noncatalytic reactions find applications in very important fields such as gas purification, pollutant (NO_x, CO_2, H_2S, etc.) abatement, water treatment, and metal preparation. During the course of noncatalytic reactions, solid reactant properties change. That is, in noncatalytic reactions rate of reaction is a function of time [45].

Removal of carbon dioxide in hydrogen production is generally performed by either absorption or adsorption. This study focuses onto adsorption of carbon dioxide onto several sorbents. These adsorption reactions are typical examples of fluid-solid noncatalytic reactions. In other words, carbon dioxide (fluid) is adsorbed onto sorbent (solid) and form another solid product around the reactant solid as the reaction proceeds. There are many factors that can affect the reaction rate such as equilibrium, diffusional limitations or pore mouth closure.

5.1 Adsorption

The use of solids for removing substances from either gaseous or liquid solutions has been widely used. This process, known as adsorption, involves nothing more than the preferential partitioning of substances from the gaseous or liquid phase onto the surface of a solid substrate. Adsorption phenomena are operative in most natural, physical, biological, and chemical systems, and adsorption operations employing solids such as activated carbon and synthetic resins are used widely in industrial applications and for purification of waters

and wastewaters. The process of adsorption involves separation of a substance from one phase accompanied by its accumulation or concentration at the surface of another. The adsorbing phase is the adsorbent, and the material concentrated or adsorbed at the surface of that phase is the adsorbate. Adsorption is thus different from absorption; a process in which material transferred from one phase to another (e.g. liquid) interpenetrates the second phase to form a "solution".

Adsorbents are characterized first by surface properties such as surface area and polarity. Adsorption onto solids is classified into physical adsorption (physisorption) and chemical adsorption (chemisorption). In physical adsorption, the gas molecules are held to the solid's surface by relatively weak intermolecular van der waals forces. In chemisorption, a chemical reaction occurs at the solid's surface, and the gas is held to the surface by relatively strong chemical bonds [47]. Distinctions between physical and chemical adsorption could be summarized as follows:

- The heat of physical adsorption is the same order of magnitude as the heat of liquefication, while the heat of chemisorption is of the same order as of the corresponding chemical reaction. In addition, heat of adsorption varies with surface coverage because of lateral interaction effects. Therefore, the heat of adsorption has to be compared on corresponding levels.

- Physical adsorption will occur under suitable temperature pressure conditions in any gas-solid system, while chemisorption takes place only if the gas is capable of forming a chemical bond with the surface.

- A physically adsorbed molecule can be removed unchanged at a reduced pressure at the same temperature where the adsorption took place. The removal of the chemisorbed layer would be far more difficult.

- Physical adsorption can involve the formation of multimolecular layers, while chemisorption is always completed by the formation of a monolayer (in some cases physical adsorption may take place on the top of a chemisorbed monolayer).

- Physical adsorption is instantaneous (the diffusion into porous adsorbent is time consuming), whereas chemisorption may be instantaneous, but generally requires activation energy [27].

5.1.1 Breakthrough Curves

Breakthrough curves refer to the response of an initially clean bed (free of adsorbate) to a feed of constant (time-independent) composition. A broader definition of the term includes a uniformly presaturated bed as well as feed with changing concentration. The shape or width of the breakthrough curve is critically important in the design of adsorbers and cyclic separation processes. A sharp concentration front is desirable for efficient separation. The shape of the breakthrough curve is determined by the nature or the type of the adsorption isotherm.

The concentrations of the solute in the fluid phase and of the solid adsorbent phase change with time and also with position in the fixed bed as adsorption proceeds. Figure 5.1.1 [62] shows the concentration profiles for adsorption in fixed bed for both various positions in the bed and time. At the inlet to the bed the solid is assumed to contain no adsorbate at the start of the process. As the fluid first contacts the inlet of the bed, most of the mass transfer (diffusion of gas through solid reactant) and adsorption takes place in this region. As the fluid passes through the bed, the concentration in this fluid drops very rapidly with distance in the bed to zero way before the end of the bed is reached [62]. In a very short time, the solid near the entrance is almost saturated with adsorbate, and most of the mass transfer and adsorption now takes place at a point slightly farther from the inlet. At a later time t_2 (Figure 5.1.1), the profile or mass-transfer zone, where most of the concentration change takes place, has moved farther down the bed. The concentration profiles shown in Figure 5.1.1 are for the fluid phase. Concentration profiles for the concentration of adsorbates on the solid particle would be similar. The solid at the entrance would be nearly saturated and this concentration would remain almost constant down the mass transfer zone, where it would drop off rapidly to almost zero.

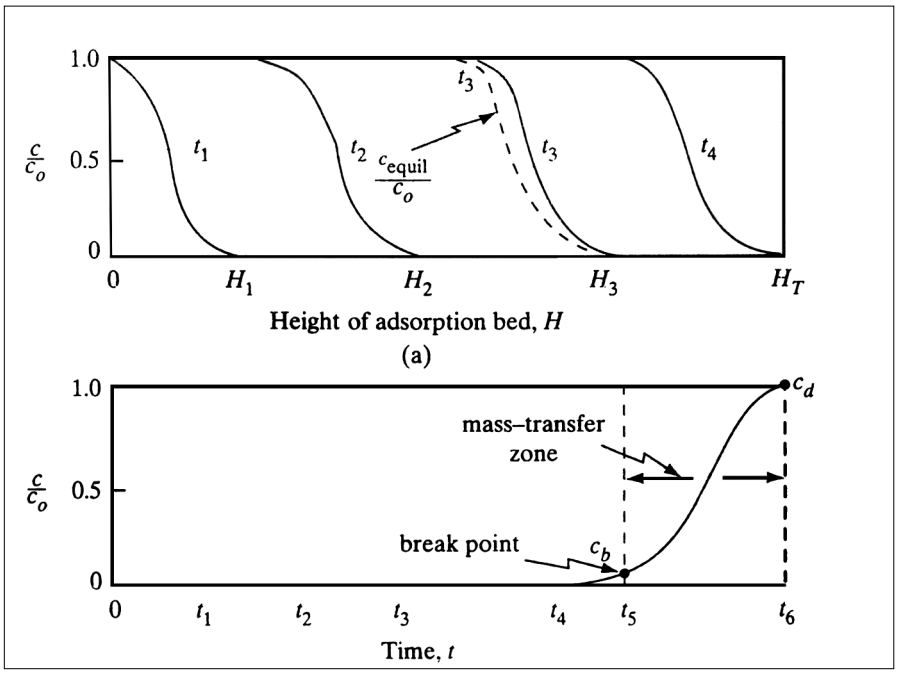

Figure 5.1.1 Concentration profiles for adsorption in a fixed bed: (a) profiles at various positions and times in the bed, (b) breakthrough concentration profile in the fluid at outlet of bed [62]

The outlet concentration starts to rise and at t_5 the outlet concentration has risen to c_b, which is called the break point. After the break-point time is reached, the concentration c rises very rapidly up to point c_d, which is the end of the breakthrough curve where the bed is judged ineffective (usable capacity reached). The break-point concentration indicates the maximum that can be discarded and is often taken as 0.01 to 0.05 for c_b/c_o. The value c_d/c_o is taken as the point where c_d is approximately equal to c_o [62].

For a narrow mass-transfer zone, the breakthrough curve is very steep and most of the bed capacity is used at the break point. This makes efficient use of the adsorbent and lowers energy costs for regeneration. For this reason, diffusional effects should be minimized for design purposes.

The mass-transfer zone width and shape depends on the adsorption isotherm, flow rate, mass-transfer rate to the particles, and diffusion in the pores. The total capacity of the sorbent bed (If the entire bed comes to

equilibrium with the feed) could be shown to be proportional to the area between the curve and a line at c/c_o=1.0 (Figure 5.1.2, [62]).

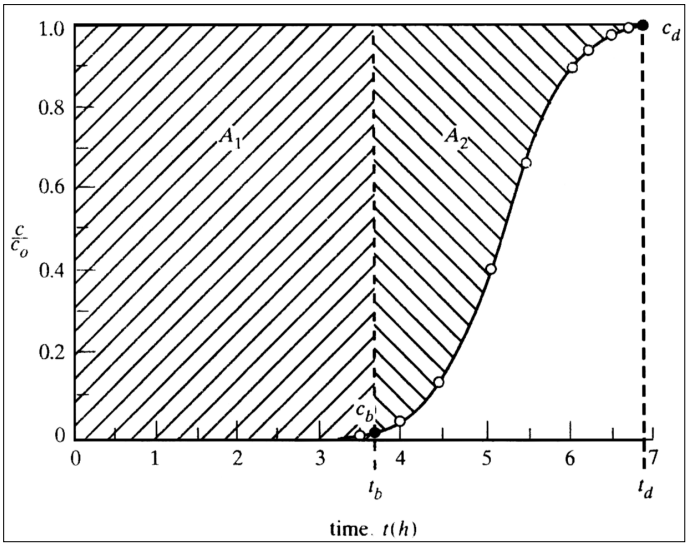

Figure 5.1.2 Typical breakthrough curve obtained from the adsorption of gases onto sorbents [62]

The total shaded area represents the total or stoichiometric capacity of the sorbent bed. This is expressed in terms of sorption time as follows:

$$t_t = \int_0^{\infty} \left(1 - \frac{c}{c_o}\right) dt \qquad (5.1.1.1)$$

In equation (5.1.1.1) t_t is the time equivalent to the total or stoichiometric capacity. The usable capacity of the bed up to the break-point time t_b is the crosshatched area shown in Figure 5.1.3 [62]. The value of usable capacity could be found by integration of elution profile up to break point.

$$t_u = \int_0^{t_b} \left(1 - \frac{c}{c_o}\right) dt \qquad (5.1.1.2)$$

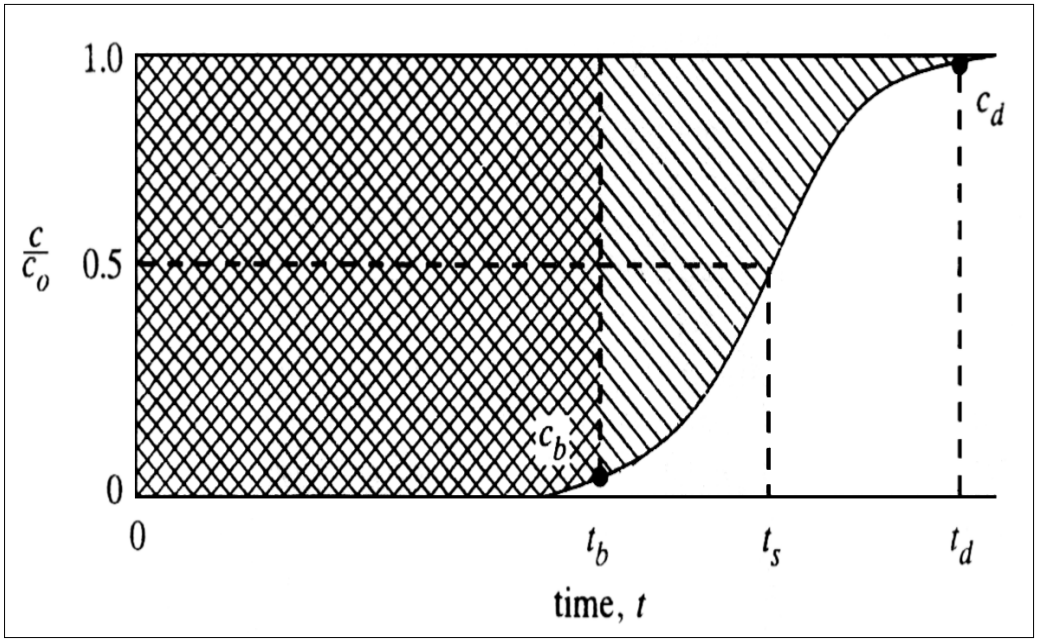

Figure 5.1.3 Determination of capacity of column from breakthrough curve [62]

Where t_u is the time equivalent to the usable capacity or the time at which the effluent concentration reaches its maximum permissible level. The value of t_u is usually very close to that of t_b.

The ratio t_u/t_t is the fraction of the total bed capacity or length utilized up to the break point. Hence, for a total bed length of L_t, L_b is the length of the bed used up to the break point.

$$L_b = \frac{t_u}{t_t} L_t \qquad (5.1.1.3)$$

The length of unused bed L_{unb} is expressed as the unused fraction times the total length:

$$L_{unb} = \left(1 - \frac{t_u}{t_t}\right) L_t \qquad (5.1.1.4)$$

The L_{unb} represents the mass-transfer section or zone. It depends on the fluid velocity and is essentially independent of total length of the sorbent bed. Total bed length is then the summation of unused and usable bed lengths.

$$L_t = L_{unb} + L_b \qquad (5.1.1.5)$$

Another way is to assume breakthrough curve is symmetrical at $c/c_o=0.5$ and t_s. Then the value of t_t is simply t_s. This assumes that the area below the curve between t_b and t_s is equal to the area above the curve between t_s and t_d. This is another simplistic approach for breakthrough capacity determination [62].

5.2 Models for Gas-Solid Noncatalytic Reactions

Gas-solid noncatalytic reactions have great industrial importance and widely encountered in many areas. Hence, there have been many studies conducted up to date to understand the mechanisms of this type of reactions. In order to justify experimental data obtained from these reactions, a number of models were proposed from several researchers. Some of these models could be considered quite complex and require tedious deal of mathematical representations of the governing equations.

Shrinking (unreacted) core and deactivation (activity change is considered) models are rather simple with respect to others. However, for deactivation model, increasing the dependence order of activity term dumped in the equation, it is possible to optimize the accuracy of the model. Besides these models there are other models, which take into account diffusion through gas film (around the solid) and product layer. During the course of most gas–solid noncatalytic reactions the solid undergoes structural changes caused primarily by swelling or shrinkage, due to chemical reaction or by sintering. Therefore,

effects of such structural changes on the conversion-time relationship and on temperature profiles in the pellet should be considered [50, 51, and 52]. For this purpose, structural models for gas-solid reactions with fixed or moving boundaries were developed to express the behavior of experimental data.

Together with pore and grain models [55] proposed in the literature, models considering structural changes would be more realistic in terms of the chemistry involved in these reactions. In recent years, it is easier to handle numerical equations and therefore it is possible to have almost exact solutions to these reactions, but the question is to express the meanings of too many introduced parameters arising from these models and to convert those parameters to useful information in further design of the reactors.

5.2.1 Shrinking (Unreacted) Core Model

Among the several applicable models for breakthrough data, shrinking core model is the simplest one. Reaction is considered to take place at the sharp interface in the solid that assumes the following conditions:

- Pellet retains its spherical shape during reaction
- The densities of the porous product and the reactant are the same so that the total radius of the pellet does not change with time and there is no gaseous region between the pellet and product layer
- dr_c/dt is small enough to assume pseudo steady state for the reaction (only valid if density of the gas in the pores of the product layer is small with respect to density of the solid reactant) [45]

Considering external diffusion, diffusion through product, and reaction at r_c (interface between the solid reactant and product layer), rate of movement of the reaction interface at r_c could be expressed as follows:

$$-\frac{dr_c}{dt} = \frac{bM_B k(C_A)_b / \rho_B}{1+(r_c^2/r_s^2)(k/k_m)+(kr_c/D_e)(1-r_c/r_s)} \qquad (5.2.1.1)$$

In this model, concentration of gas is represented as a function of time considering diffusion through gas film and product layer together with the chemical reaction.

Equation (5.2.1.1) could be integrated to give r_c as a function of concentration of gas in the bulk phase and time. Substituting (5.2.1.1) for r_c into (5.2.1.2) yields the global rate in terms of bulk concentration of gas and time [45]. Depending on the controlling regime for reaction, the derivation of this model could vary. For such cases, determination of which condition controls the reaction is critical.

$$-\frac{dN_A}{dt} = \frac{4\pi r_c^2 (C_A)_b k}{1+(r_c^2/r_s^2)(k/k_m)+(kr_c/D_e)(1-r_c/r_s)} \qquad (5.2.1.2)$$

There some limitations of shrinking core model, in particular, reaction may occur along a diffuse front rather than along a sharp interface between ash and fresh solid, thus giving behavior intermediate between the shrinking core and the continuous reaction models. Furthermore, for fast reaction the rate of heat release may be high enough to cause significant temperature gradients within the particles or between particle and the bulk fluid [48].

5.2.2 Empirical Expression Dumped Diffusion Model

In gas-solid noncatalytic reactions pore structure variation should be taking into account to approximate the relative kinetics of such reactions. In other words, as the reaction proceeds the product layer forming around the reactant solid inevitably changes the structure of the formed solid. That is, product layer, which builds upon the pore walls, causes not only decrease of active surface area but also tends to form an additional diffusion resistance through which the gaseous reactant should diffuse to reach the active surface. Moreover, product layer will also cause the stopping of the reaction due to pore mouth closure [52, 53]. As a result of this fact, effective decrease in the point reaction rate constant is expected. Basic assumptions made in the derivation of such models are as follows:

- Spherical solid reactant particles are assumed

- In place of an equation for diffusion of reactant gas through the product layer, an empirical expression is suggested

- Surface reaction is assumed to be first order with respect to gas concentration

- Pseudo-steady state condition holds

For a packed bed reactor, transient plug flow conservation equation (5.2.2.1) could be written assuming spherical particles with cylindrical coordinates [61]:

$$\varepsilon_b \frac{\partial C_A}{\partial t} = -U_o \frac{\partial C_A}{\partial Z} - \frac{3(1-\varepsilon_b)}{R} D_e \frac{\partial C_i}{\partial r}\bigg|_{r=R} \qquad (5.2.2.1)$$

Equation (5.2.2.1) relates the concentration of gas, C_A, (e.g. CO_2) in the gas phase in the bed with the concentration of gas, C_i, within the pores of the particles. In this equation, diffusional ressistance within the particles are expressed in terms effective diffusivity, D_e, and flow of gas defined with a superficial velocity, U_o. In order to express concentration in the gas phase as a function of time, an additional expression is required for the particle. In other words, a quasi-steady state conservation equation is written for the particle and rate expression is also included in the following equation:

$$0 = \frac{1}{r^2} \frac{\partial}{\partial r}\left(r^2 D_e \frac{\partial C_i}{\partial r} \right) - \rho_p S_g k_s C_i \qquad (5.2.2.2)$$

Rate term is defined in terms of active surface area and particle density. For a gas-solid noncatalytic reaction, both active surface area per unit mass, Sg, and the density any point is expected to vary with time during the reaction. For this reason, one can propose different models for diffusion of reactant gas through the product layer (e.g. single pore and grain models). Another alternative to relate the changes in the particle with respect to time is to propose an empirical equation by intution. This rather reasonable approach has great advantage in terms of simplifying the model and expressing the curve

behavior with reduced parameters. Following empirical expression [54] gives reasonable results for the variation of point reaction rate.

$$\rho_p S_g k_s = \rho_{p,o} S_{g,o} k_{s,o} \exp(-\beta t) \qquad (5.2.2.3)$$

Equation (5.2.2.1), (5.2.2.2), and (5.2.2.3) should be simultaneously solved to express the reactant gas concentration as a function of time. This derivation was shown in detail by Doğu et al. [53]. It is convenient to express gas concentration in the bed outlet in a normalized form. As a result, equation (5.2.2.4) is the final form empirical expression dumped diffusional model.

$$\psi_L = \left[e^{N\upsilon} \frac{\sinh(\phi_0 \exp(-N\theta))}{\sinh(\phi_0 \exp N(\upsilon - \theta))} \right]^{\frac{\partial}{N}} \qquad (5.2.2.4)$$

Equation (5.2.2.4) relates normalized concentration of gas in the bed outlet, ψ_L, to system parameters such as initial thiele modulus, ϕ_o, system parameters N (5.2.2.5), and ν (5.2.2.6), and dimensionless time, θ.

$$N = \frac{\beta\tau}{2} \qquad (5.2.2.5)$$

$$\upsilon = \frac{L\varepsilon_b}{tU_o} \qquad (5.2.2.6)$$

System parameters (N, ν, ϕ_o, θ) could be found from nonlinear regression analysis and these parameters are further used to calculate effective diffusivity, D_e, point reaction rate constant, $\rho_p S_g k_s$, and the constant for empirical expression, β.

After all, empirical expression dumped model is an effective model to justify breakthrough data. This is due to the fact that the model accounts for the effective diffusion through the particle and reduces the system parameters by introducing an empirical expression.

5.2.3 Deactivation Model

In gas-solid reactions (e.g. reaction of carbon dioxide with activated hydrotalcite and soda), formation of a dense product layer over the solid reactant causes an additional diffusion resistance and this would lead to a drop in the reaction rate. Also, this would cause significant changes in the pore structure, active surface area, and the activity of solid reactant. Deactivation model, basically, accounts for the activity changes within the reactant. Depending on the order of dependence of activity with respect to time, modified forms of deactivation model could be obtained. In general, zeroth solution of deactivation model does not fit well to experimental data, whereas higher order solutions exhibit a well-fit to breakthrough data. For this reason, analysis of breakthrough data was achieved by using a two-parameter deactivation model [56, 57].

Basic assumptions made in the derivation of deactivation model are as follows:

- Isothermal conditions exist throughout the reactor
- Diffusional terms are neglected and variation of concentration only along the reactor is (flux in z direction) considered.
- Pseudo steady state conditions hold (i.e. rate of concentration with respect to time is small compared to rate of concentration with respect to position)

Considering above assumptions isothermal species conservation equation is written as follows [61]:

$$\frac{\partial C_A}{\partial t} + (\nabla \cdot N_A) = R_A \qquad (5.2.3.1)$$

Where C_A is the concentration of gaseous reactant (carbon dioxide). Rate term, including sorption rate and activity, is written for the gaseous reactant;

$$R_A = k_O C_A a \rho_p \qquad (5.2.3.2)$$

Neglecting diffusional terms and dividing each side by particle density (to express equation as a function of loading amount);

$$-Q\frac{dC_A}{dw} - k_o a C_A = 0 \qquad (5.2.3.3)$$

Equation (5.2.3.3) is known as isothermal species conservation equation for the reactant gas (CO_2) in the flow reactor. In writing this equation, axial dispersion in the packed bed column and any mass transfer resistances were assumed to be negligible. For deactivation model, the rate of change of the activity of the solid reactant, a, is expressed as;

$$-\frac{da}{dt} = k_d C_A^n a^m \qquad (5.2.3.4)$$

where k_d is the deactivation rate constant. Simplest solution of this model is obtained by taking n=0 and m=1 in equation (5.2.3.4). Solving (5.2.3.4) for a and substituting solution into (5.2.3.3) will give a C_A dependent equation and further solution of equation will yield the elution profile of gaseous reactant from the bed;

$$C_A = C_{Ao} \exp\left[-\frac{k_o W}{Q}\exp(-k_d t)\right] \qquad (5.2.3.5)$$

Equation (5.2.3.5) is the zeroth solution of deactivation model, which predicts the behavior of breakthrough curves for a gas-solid noncatalytic system. This solution assumes a fluid phase concentration that is independent of deactivation process along the reactor. It would be more reasonable to expect the deactivation rate to be concentration dependent and axial position dependent in the flow reactor.

Zeroth solution is substituted into the model equation and first corrected predictions for the activity is obtained by the integration. Excluding higher order

terms in the series solutions of the integrals, following corrected solution for breakthrough curve is derived [56, 58, 59, 60];

$$\frac{C_A}{C_{Ao}} = \exp\left\{\frac{\left[1-\exp(k_o W / Q((1-\exp(-k_d t)))\right]\exp(-k_d t)}{\left[1-\exp(-k_d t)\right]}\right\} \qquad (5.2.3.6)$$

It is also possible to improve this solution by substituting into original equation but equation (5.2.3.6) gives pretty good fit with the experimental data and it is convenient to explain the nature of model with reduced parameters. Equation (5.2.3.6) is known as the solution of two-parameter deactivation model. Sorption rate constant (k_o) and deactivation rate constant (k_d) should be calculated by using a nonlinear regression technique.

5.2.3.1 Deactivation Model by Using Mathematica 4.2

Modeling of breakthrough curve with deactivation model is nothing but the evaluation of the two parameters that appear from the model. In other words, nonlinear regression analysis of model equation should be used together with the experimental data to find out the sorption rate constant (k_o) and deactivation rate constant (k_d). In some cases, it is crucial to supply initial guesses for rate parameters to obtain reasonable rate constants for the model. For this reason, an error minimization technique should be applied to end up with the best results. A similar approach to "R^2" analysis was achieved throughout the modeling of data.

In an experimental context, almost all measured quantities have an error because a perfect experimental apparatus does not exist. Nevertheless, all too often real experimental data do not have explicit errors associated with the values of dependent or independent variables. If there are assigned errors in the experimental data, say erry, then these errors are used to weigh each term in the sum of the squares. Mathematica is used to find the estimates of the standard deviation or a weighted sum called chi-squared [49] of the fit defined by the following equation:

$$ChiSquared = \sum_{i=1}^{N}\left(\frac{residual[i]}{erry[i]}\right)^2 \qquad (5.2.3.7)$$

For a better analysis of data, chi-square analysis technique together with "NonlinearRegress" and "NonlinearFit" commands were used in Mathematica and details of this approach was shown in sample calculations of the Appendices (App E.4).

CHAPTER 6

EXPERIMENTAL

In this study, adsorption of carbon dioxide onto several adsorbents was investigated. Sensitivity of adsorption on temperature changes was observed for activated hydrotalcite, sodium bicarbonate, and trona. As a result of a series of calcination and adsorption experiments, experimental breakthrough curves were obtained for each sorbent for the selected temperature range.

6.1 Experimental Setup

Carbon dioxide adsorption experiments were performed in a tubular flow reactor shown in Figure 6.1.1. Experimental setup used for experiments was designed in such a way that both calcination and adsorption experiments could be performed consequently. Experiments could be carried out for both dry (only carbon dioxide adsorbed) and wet (in the presence of steam) conditions.

During the calcination and adsorption experiments, head pressures of carbon dioxide (Air Products) and helium (Oksan) were set to 40 psi. Flow of gaseous mixture (helium+carbon dioxide) was adjusted by two rotameters (Suitable for flow ranges) and needle valves. Calibration of these rotameters was achieved by using soapmeters connected to exit of rotameters.

In order to obtain steam at a certain flow rate, a water tank in a constant temperature water bath was used (Figure 6.1.1). The idea was to bubble Helium (carrier gas) and carbon dioxide into the water tank and obtain steam at the

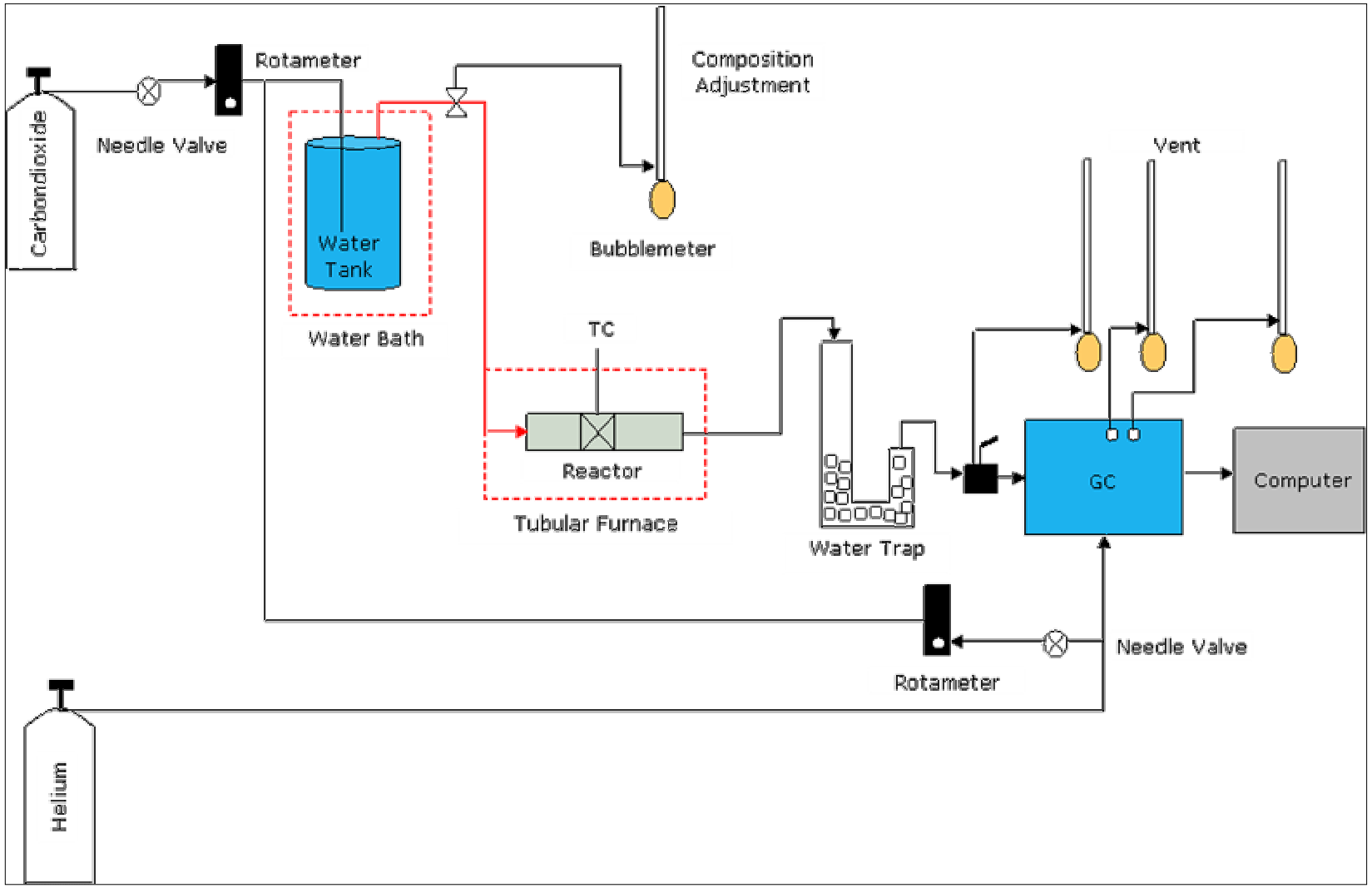

Figure 6.1.1 Experimental setup for adsorption of carbon dioxide

temperature of interest. By varying the temperature of the water bath, it is possible to adjust steam flow rate at the inlet to the tubular reactor. Since adjusting of steam flow rate was not easy, it was preferred to obtain steam in excess with respect to carbon dioxide.

To prevent condensation before the reactor, steam line was heated by means of heating tapes. Temperature controllers of heating tapes were adjusted to 120 ^{o}C to hinder condensation both at the steam lines and at the inlet to the reactor.

Hydrotalcite, sodium bicarbonate, and trona (chemical properties listed in App. B) were used as sorbents for carbon dioxide removal. Adsorbent was placed in a tubular reactor (stainless steel 304) and it was supported by means of quartz wool at both ends (for low temperature applications glass wool was used). There was also a preheating zone (i.e. gas mixture circulated along the tubular furnace) before the reactor to ensure that the gaseous mixture was heated up to reaction temperature. In order to obtain a uniform temperature within the reactor, both ends of the tubular furnace (Carbolite) was insulated with ytong stone and this insulating material was further insulated with glass wool and aluminum folio. Moreover, sorbent was placed in the middle of the furnace to minimize heat loss and to be more precise in terms of reaction temperature.

Adsorption and calcination temperatures were measured by means of a thermocouple placed on top of the loaded section of the tubular reactor. Type K (Cr/Al, with wide range application) thermocouple was used with a controller to follow the reaction temperature during the course of reaction.

Outlet composition from the tubular reactor was sent to a steam trap (U shaped equipment in setup, Figure 6.1.2) to ensure that only CO_2 was analyzed in the gas chromatograph. Molecular sieve 3A was used as steam trap and loading of zeolite particles should be at an optimum value for safely passage of gas through the trap. Since steam trap was also capable of adsorbing carbon dioxide, trap was saturated with CO_2 before each run. When zeolite particles were saturated with steam, regeneration of molecular sieve 3A was achieved in a furnace under vacuum at 250 ^{o}C for 3 hours.

Figure 6.1.2 View of adsorption setup used in experiments

6.2 Experimental Procedure

Experiments were carried out in two steps. At each run adsorbent was first calcined at a selected temperature and than adsorbent was used for the adsorption of carbon dioxide at several temperatures. After calcination was achieved at the desired temperature, tubular reactor was cooled to reaction temperature. As soon as the uniform temperature was obtained in the system, adjusted inlet composition (feed, usually $He+CO_2+H_2O$) was sent to flow reactor.

6.2.1 Calcination of Adsorbents

Calcination of materials was performed under the flow of inert gas Helium. Calcination temperatures were different for each adsorbent. Using TGA results (Chapter7) and information from the literature optimum calcination temperatures were selected and shown in Table 6.2.1.

Table 6.2.1 Calcination temperatures of adsorbents

Adsorbent	**Calcination Temperature (°C)**
Hydrotalcite ($Mg_6Al_2(OH)_{16}CO_3.4H_2O$)	550
Sodium bicarbonate ($NaHCO_3$)	200
Trona ($Na_2CO_3NaHCO_3.2H_2O$)	200

Predetermined amounts of adsorbent (2 g) were placed in a tubular flow reactor and calcination of adsorbents was performed under the flow of Helium at a flow rate of 30 cm^3/min. It was possible to observe desorption of CO_2 online with the use of gas chromatograph (Varian 1400) connected to system. Whenever the carbon dioxide peaks became undetectable from the gas chromatograph, it was concluded that the calcination process was completed. Temperature of tubular furnace was altered and set to adsorption temperature. Hence, temperature dependent desorption peaks were recorded so as to obtain calcination curves.

6.2.2 Adsorption of Carbon dioxide onto Adsorbents

All adsorption experiments were performed in the presence of steam with the feed composition as excess with respect to carbon dioxide. However, it was also possible to adsorp carbon dioxide efficiently onto hydrotalcite without using steam. Therefore, some dry experiments were performed with hydrotalcite so as to compare its adsorption behavior under same conditions.

Trona and $NaHCO_3$ were used in powder form during the experiments. Using hydrotalcite in powder form hindered the flow of gaseous mixture. Thus, increasing particle size lowered pressure drop and continuous flow of gaseous mixture was obtained within the tubular reactor. For this purpose, hydrotalcite was pelletized, crushed, and sieved to obtain a uniform particle size (1.4 mm, ASTM 14 sieves were used).

In order to simulate reformer effluent gas from a hydrogen producing plant, typical 10-20 mole% CO_2 (dry basis) was selected in the feed and steam was sent in excess (around 10 cm^3/min) with respect to carbon dioxide. Remaining part of the gas composition was helium, which was used as a carrier gas for both reaction and gas chromatograph. Keeping total flow rate (around 50 cm^3/min), particle size (powder for trona and sodium bicarbonate and particles having 1.4 mm diameters for hydrotalcite), loading (2 g), and composition (10-20 mole% of CO_2) constant throughout the experiments, only reaction temperature was varied in a range and this range was different for each adsorbent to observe the behavior of adsorption at relatively high temperatures.

After calcination of adsorbents was accomplished, tubular reactor cooled to adsorption temperature and feed composition was adjusted at the inlet of the reactor by using bubblemeter and rotameters. Since the inlet content of carbon dioxide was high, it was necessary to analyze carbon dioxide in short time intervals to observe total breakthrough curve (fast adsorption). For this reason, analysis of carbon dioxide was achieved in every 10 to 30 seconds by using auto injection valve of gas chromatograph (monitoring program was detecting signals 10 times in a second).

Following up reformer off-gas conditions and possible carbon dioxide removal processes, experiments (tabulated in Table 6.2.2) was scheduled and

performed. Due to equilibrium conditions and nature of reaction, it was not possible to use activated soda as a sorbent at high temperatures. For this purpose, trona and sodium bicarbonate reaction temperatures were chosen in a reasonable adsorption range.

Table 6.2.2 Adsorption experiments performed in this study

Adsorbent	**Temperature ^oC**					
Hydrotalcite (Dry)	400	424	452	475	500	527
Hydrotalcite (Wet)	400	424	452	475	500	527
Activated $NaHCO_3$	80	101	125	152		
Activated Trona	80	101	125	152		

6.3 Analysis of Carbon dioxide

In all experiments, analysis of carbon dioxide was achieved by a Varian 1400 gas chromatograph (Figure 6.1.2). Helium was used as the carrier gas for gas chromatograph. It was also possible to use nitrogen as carrier gas but the thermal conductivities of carbon dioxide and nitrogen were so close that it was not easy to detect and separate carbon dioxide when nitrogen was used as the carrier gas (App. A).

Gas chromatograph was equipped with a Thermal Conductivity Detector (TCD) and TCD (thermal conductivities of some gases listed in App. A) temperature of the chromatograph kept constant at 170 ^oC during the experiments. In order to analyze carbon dioxide peaks precisely, Porapak Q 80/100 (porous polymer safe under 250 ^oC) packing material was used and the column temperature of gas chromatograph was set to 120 ^oC (App A). Column temperature was adjusted such that carbon dioxide peaks were monitored at about every 30 seconds. In order to separate peaks from noises, it was necessary to adjust column and reference flow rate to an optimum value to see sharper and detectable peaks. These values were set at 32 cm^3/min for column flow rate and 67.5 cm^3/min for reference flow rate. Current of detection was set to 200 mA to observe rather sharpened peaks. Increasing current was important to discriminate peaks from noises. Since the linearity of chromatograph output voltage was not very sensitive to sudden changes in detection, chromatograph attenuation was first set to 32 and than it was lowered to 1 to enlarge peaks to visible region in the monitor.

Data acquisition card (PCL-711B) was plugged into computer to convert analog data to digital data (AD/DA converter). In order to monitor peaks and obtain time milivolt arrays, a program (gcpeak3d.bas, App. F) was written in QuickBasic language. Output of this program (time-milivolt arrays, App. F) was processed in Mathematica 4.2 to calculate peak areas and convert them into useful information required for the rest of the calculations. Two-parameter deactivation model was applied to experimental breakthrough data to express and discuss the reliability of the results.

For physical characterization of adsorbents, Thermal Gravimetric Analysis (TGA), B.E.T, and Mercury Intrusion Porosimetry techniques were used for uncalcined and calcined samples of trona, sodium bicarbonate, and hydrotalcite. Properties like surface area, porosity, and pore size distribution are reported in Chp. 7.

CHAPTER 7

RESULTS AND DISCUSSION

Adsorption of carbon dioxide onto activated hydrotalcite, trona and sodium bicarbonate was investigated. Adsorption studies with hydrotalcite adsorbent were performed for dry and wet conditions. That is, in one set of experiments no steam was sent to tubular reactor to see dry adsorption capacity of hydrotalcite and in the second set of experiments steam was in excess with respect to carbon dioxide. For adsorption of carbon dioxide onto activated soda, two different Na_2CO_3 sources were used, namely, trona and sodium bicarbonate. Activated soda sorption reactions were performed in the presence of excess steam with respect to carbon dioxide.

Adsorbents were characterized by three methods to investigate physical sorption properties of the sorbents. Thermal Gravimetric analysis (TGA, Du Pont 2000) was used to observe the desorption profiles (e.g. desorption temperature of crystalline water or carbon dioxide) from the adsorbents. This analysis technique was useful to determine the calcination temperature of the sorbent to be used in experimental runs. It was also possible to detect the material's decomposition temperature and this was helpful in experiments to perform experiments on the safe side. Another analysis technique used in the experiments was mercury intrusion porosimetry (Micrometrics Pore Sizer 9310) and by using this method pore size distributions and cumulative pore volumes of untreated and calcined sorbents were derived. Further analysis of data from Hg porosimetry gave the porosities for hydrotalcite, trona, and sodium bicarbonate. B.E.T (Micrometrics ASAP 2000) was the third method applied for sorbent analysis and nitrogen was used as the adsorbate to investigate the surface area and average pore sizes of the adsorbents.

Reactor effluent gas was connected to a gas chromatograph (Varian 1400) to observe the elution profiles of carbon dioxide during the course of reaction. Signals from the chromatograph were converted (AD/DA converter, PCL-711) to time-milivolt arrays and these experimental data were further processed in Mathematica 4.2 to obtain calcination and breakthrough curves for the adsorbents. Having obtained the experimental data, two-parameter deactivation model was used to express the related sorption kinetics of the sorbents at different temperatures.

7.1 Hydrotalcite

Physical properties of hydrotalcite samples were investigated for hydrotalcite (HT) and activated HT by using B.E.T and Hg porosimetry. Table 7.1.1 shows some physical properties obtained from the sorbent characterization techniques.

Table 7.1.1 Physical properties of hydrotalcite samples

Physical Property	**Hydrotalcite**	**Activated Hydrotalcite**
Porosity	0.64	0.70
Surface Area (Hg porosimeter) (m^2/g)	12.56	23.53
B.E.T Surface Area (N_2 adsorption) (m^2/g)	8.10	172.90
Solid Density (g/cm^3)	2.38	1.67
Apparent Density (g/cm^3)	0.86	0.50
Average Pore Diameter (by B.E.T) (A^o)	100.58	40.02

It is interesting to note that surface area of hydrotalcite increased from 8.1 m^2/g to 172.9 m^2/g as the sample was calcined at 550 ^oC. However, for same conditions Hg porosimetry analysis showed that surface area of the sorbent increased from 12.56 m^2/g to 23.53 m^2/g. The difference between two analysis techniques is probably due to the formation of micropores. As a result, when mercury porosimeter was used for analysis, only pores having diameters greater than 60 A^o could be measured and when B.E.T technique was used one could measure pores with diameter 20 A^o for nitrogen adsorption ($\cong$10 A^o for CO_2 sorption).

Hydrotalcite includes crystalline water and carbonate molecule within the structure. For this reason, one would expect a huge change in the porosity of the sample when it is activated. However, porosity of the sample slightly

increased from 0.64 to 0.70 as the sample was activated. Since porosity of the material was calculated from the mercury porosimeter data, these porosity values do not include micropores within the hydrotalcite. Having considered the micropores, an increased porosity could be observed as the sample was activated, however, this change could not be observed clearly from porosimeter data. In addition, activated hydrotalcite samples have an average pore diameter of ca. 40 A^{o}.

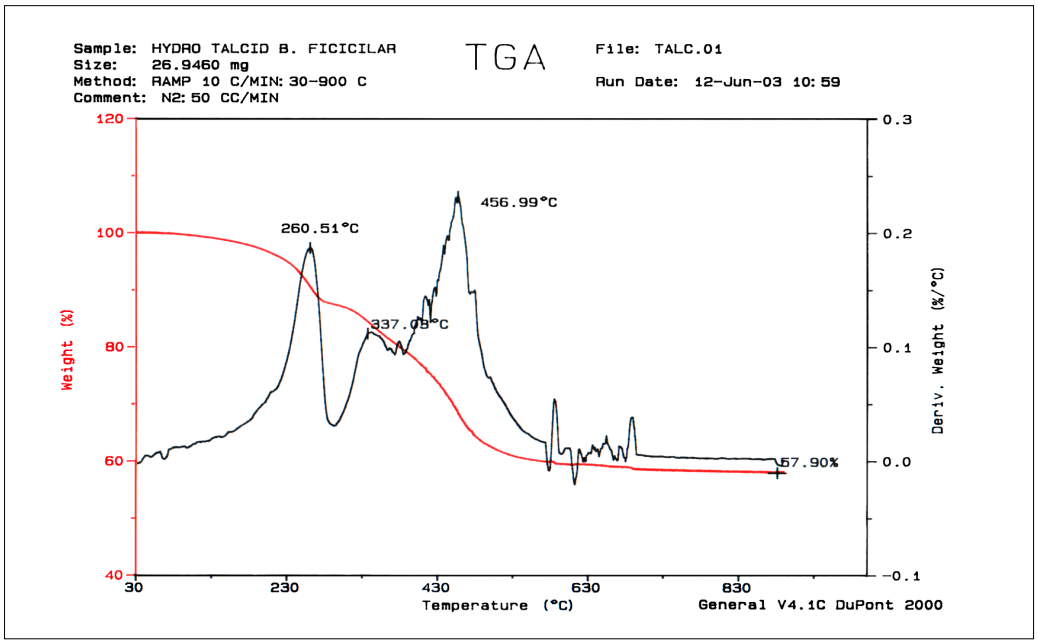

Figure 7.1.1 Thermal Gravimetric Analysis (TGA) results for hydrotalcite sample

Figure 7.1.1 shows Thermal Gravimetric Analysis results for hydrotalcite sample. It could be seen from the figure that crystalline water of hydrotalcite sample was started to desorb at around 260 ^{o}C and carbon dioxide desorption was started at ca. 337 ^{o}C and after this temperature desorption was continued till 550 ^{o}C. After 570 ^{o}C hydrotalcite decomposed to its constituents and became inactive.

Pore size distributions and cumulative pore volume distributions of hydrotalcite samples are shown in Figure 7.1.2 and 7.1.3. According to Figure 7.1.2, it is seen that pore size distribution curve shifts to the larger pore sizes for the calcined sample.

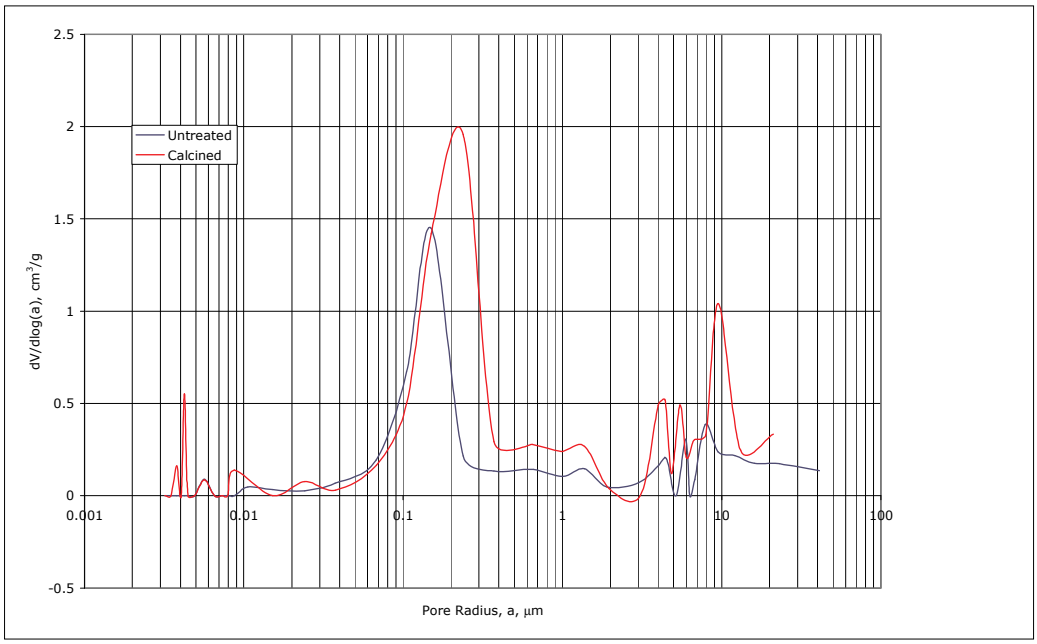

Figure 7.1.2 Pore size distributions of untreated and calcined hydrotalcite samples

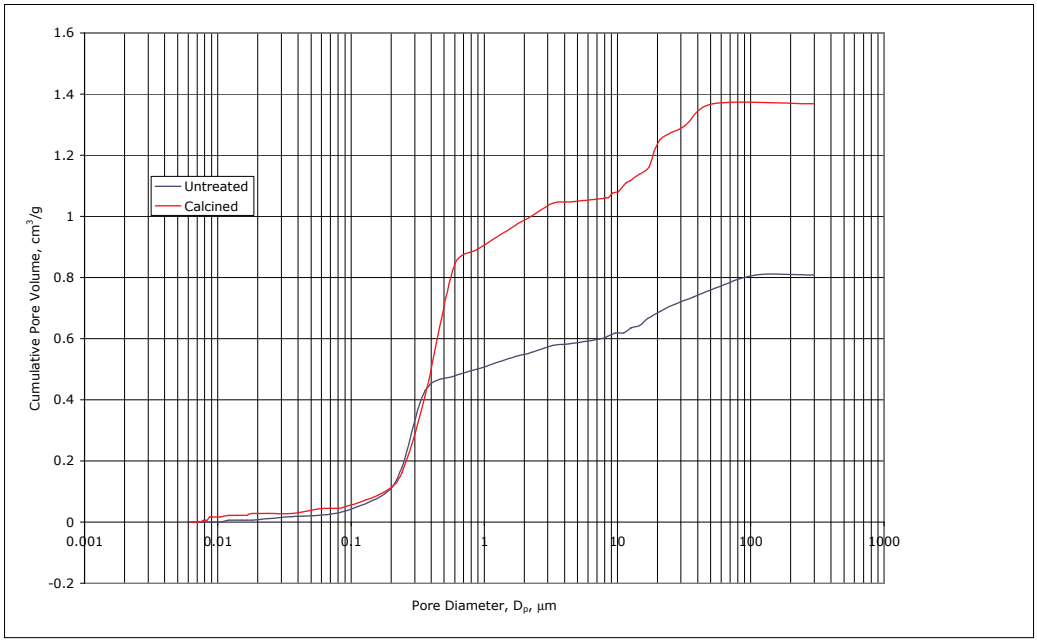

Figure 7.1.3 Cumulative pore volume distributions of untreated and calcined hydrotalcite samples

Calcination of hydrotalcite was achieved at 550 ^{o}C and this temperature could be considered as an upper limit for the calcination of hydrotalcite. Calcined samples of hydrotalcite have an average pore radius of 20 A^{o}. Figure 7.1.3 shows cumulative pore volume distributions of hydrotalcite and this figure

indicates that after a pore diameter of 0.5 μm calcined sample's pore volume distributions shifted upwards for some region and similarities of the structures could be seen from the figure.

In each experimental run performed with hydrotalcite, 2g of sorbent was placed in a tubular reactor and calcined at 550 °C under the flow of helium (30 cm^3/min). Following calcination, adsorption of carbon dioxide onto hydrotalcite was carried out in a temperature range from 400 °C to 527 °C.

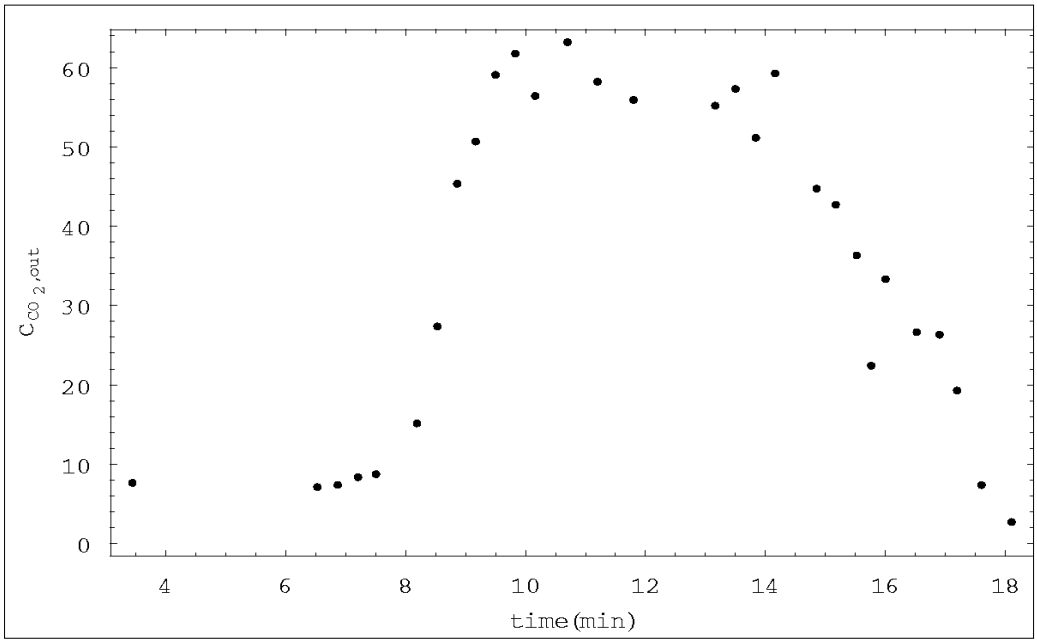

Figure 7.1.4 Temperature variant CO_2 desorption curve for hydrotalcite sample calcined at 550 °C (He flow at 30 ml/min, 2g sorbent)

Figure 7.1.4 shows a typical calcination (maximum heating rate was used in furnace, ca. 70 °C/min) curve for hydrotalcite at 550 °C. Since temperature was varying until it reached its set point (550 °C for hydrotalcite), some of carbon dioxide within the structure was desorbed in this region. Carbon dioxide desorption was observed after 350 °C and calcination was completed at 550 °C. Although CO_2 desorption peaks were monitored via gas chromatograph, for complete calcination reactor temperature was maintained at 550 °C for some time.

7.1.1 Hydrotalcite (dry)

Adsorption of carbon dioxide onto hydrotalcite was performed in the presence and absence of steam. Breakthrough curves for hydrotalcite in the absence of steam were shown in Figure 7.1.5.

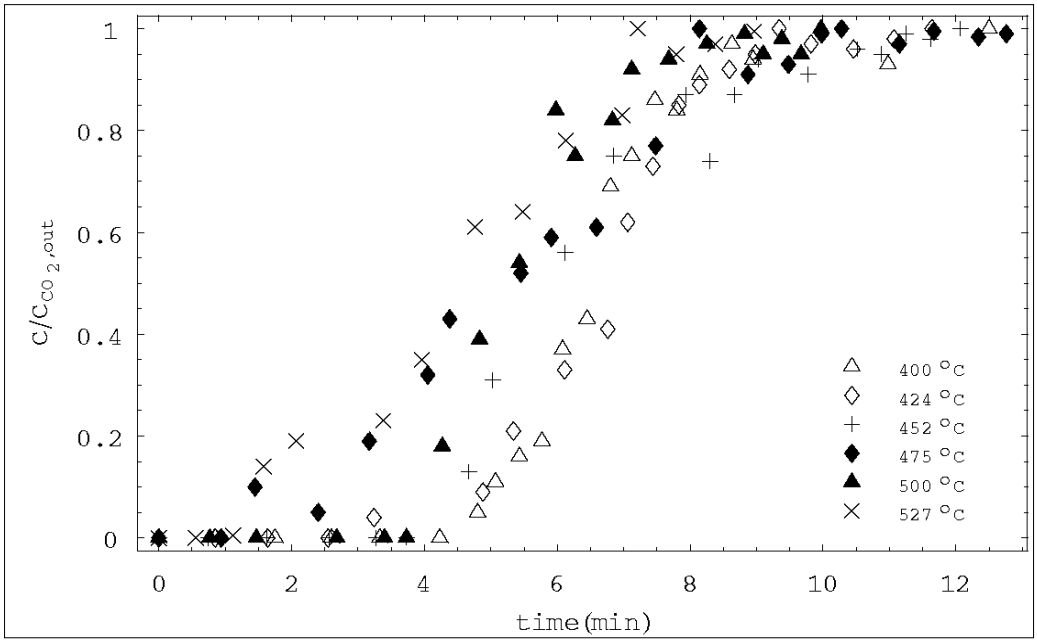

Figure 7.1.5 Experimental CO_2 breakthrough curves obtained with hydrotalcite sorbent in the absence of steam for different temperatures (App C.2.1-C.2.6)

Following temperature in the breakthrough curve, a little shift of breakthrough for different inlet concentrations was observed. Slight sharpening of curves and shift of breakthrough to left was observed for a temperature increase from 400 to 527 °C. Thus, as the temperature was increased from 400 to 527 °C, adsorption capacity of the material decreased considerably as expected. However, general tendency of the curves have rather slow response with respect to time after breakthrough points for different temperatures. That is, one could judge that mass transfer within the particles may play an important role in the sorption of adsorbate to the particle. For this reason, diffusional effects within hydrotalcite pellets should not be ignored in the analysis to find out or estimate the predictions of the breakthrough curves.

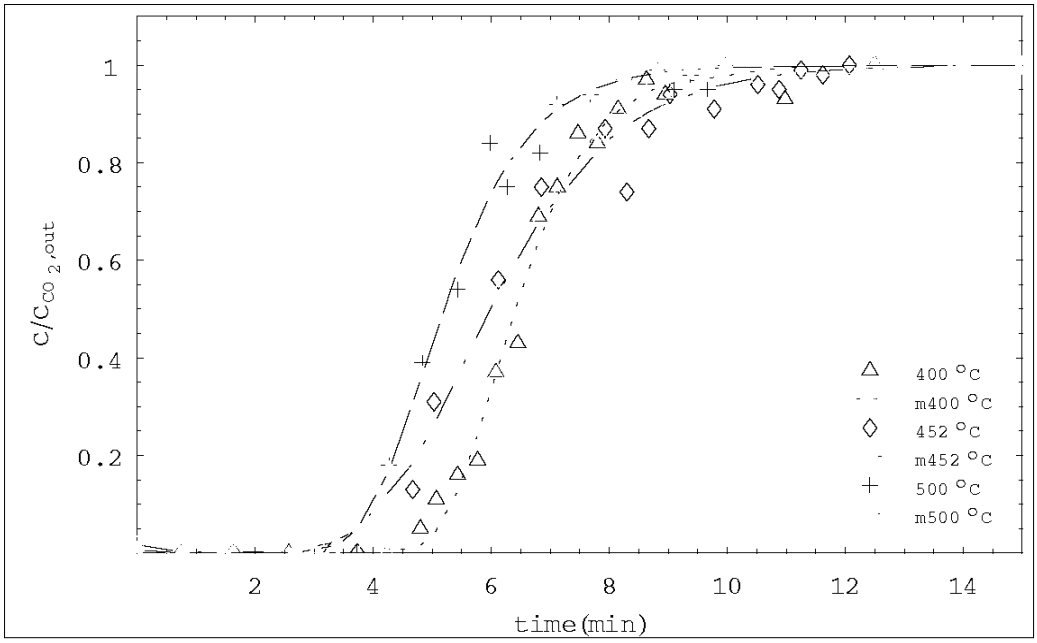

Figure 7.1.6 Comparison of experimental breakthrough curves obtained with hydrotalcite sorbent in the absence of steam with the two-parameter deactivation model for different temperatures (400 °C, 452 °C, 500 °C)

A two-parameter deactivation model was used for the predictions of experimental data. Considering the sluggish response curve for carbon dioxide (Figure 7.1.5), it would be useful to compare the behavior of a diffusional model with the one used in this study. Figure 7.1.6 compares the deactivation model with the experimental breakthrough curves for hydrotalcite in the absence of steam for different temperatures. Best fit of deactivation model can only be obtained when the chi-squares (follows the residual minimization) of the model approaches to zero (Table 7.1.2). Although experimental data obtained from the chromatograph exhibited a scattered profile due to insensitive response of signals, fit of deactivation model to experimental results showed a reasonable prediction. Since two-parameter deactivation model predicts exact breakthrough curves with two parameters, model fit can only be qualified as long as the shape of breakthrough becomes a S-shape curve. In other words, one could obtain a better fit only if more experimental data were measured during the adsorption of carbon dioxide. In addition, adsorbing large amounts of carbon dioxide caused system to become instabilized and manual control of chromatograph was insufficient to collect more data due to fast adsorption in nature.

Table 7.1.2 lists sorption (k_o) and deactivation rate constants (k_d) for the reaction temperatures (equation 5.2.3.6 was used for nonlinear regression

analysis). Observed values of sorption rate constants varied from 195.30 to 385.46 $cm^3/min.g$, while deactivation rate constants altered from 0.569 to 1.121 min^{-1}.

Table 7.1.2 Rate parameters obtained by the analysis of CO_2 breakthrough curves on hydrotalcite (dry) using deactivation model

Temperature (^oC)	k_oW/Q	k_o ($cm^3/min.g$)	k_d (min^{-1})	χ^2
400	6.828	385.46	1.121	0.0280
424	5.544	314.35	0.894	0.0421
452	4.053	248.05	0.729	0.0368
475	2.759	169.65	0.569	0.0535
500	5.097	330.54	1.047	0.0256
527	2.842	195.30	0.684	0.0483

Chi-square analysis technique was a powerful method to justify the validity of the parameters obtained from the experimental breakthrough data. Similar to R^2 approach, χ^2 follows the residuals from each points and LevenbergMarquardt method was applied to experimental raw data for nonlinear regression analysis. Since model used was straightforward and simple, departure of model from breakthrough data essentially arose from the experimental errors. In other words, breakthrough experiments were not quite reasonable or oscillated too much for some reasons.

Numerical integration of breakthrough curves (Chp. 5.1.1) up to break point (0.05 of inlet concentration) gives breakthrough capacities and total integration of breakthrough curves gives saturation capacity (or total capacity). Table 7.1.3 shows usable (breakthrough) capacities and total adsorption capacities for the hydrotalcite in the absence of steam. Some unexpected variation within the sorption capacity is due to composition change within the feed conditions, 15-16 % mole carbon dioxide inlet conditions were observed (App. C) for this set of experiments. Change of both temperature and composition might not give an accurate capacity for the sorbent but this phenomenon at least gives an idea about the ranges of sorption. On the other hand, usable capacities are more realistic to predict the real sorption characteristics of the sorbent. Comparable decrease of breakthrough capacity with respect to total capacity was observed for the reaction temperatures.

Table 7.1.3 Adsorption properties of hydrotalcite (dry) samples

Temperature (^oC)	Breakthrough Capacity (min)	Total Capacity (min)	Total Capacity (mol/kg)
400	4.23	6.95	1.18
424	3.23	6.72	1.06
452	3.73	6.22	1.16
475	2.29	5.39	0.88
500	3.72	5.42	0.97
527	1.55	4.52	0.80

In Figure 7.1.7, temperature dependencies of sorption and deactivation rate constants are shown for the temperature range 400-527 ^oC. Arhenius plots of the sorbent showed almost straight line for both deactivation and sorption rate constants.

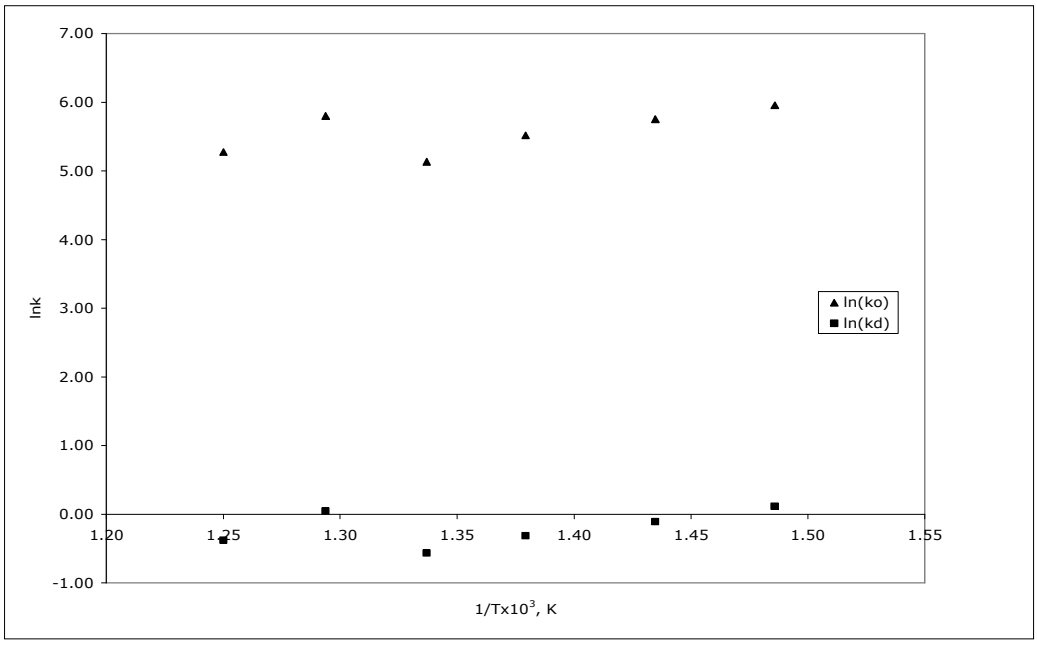

Figure 7.1.7 Temperature dependence of sorption and deactivation rate constants for CO_2 sorption on activated hydrotalcite sorbent in the absence of steam

7.1.2 Hydrotalcite (wet)

It was important to know sorption characteristics of the novel sorbent hydrotalcite in the presence of steam. For this purpose, steam was sent in excess with respect to carbon dioxide so that it was possible to see the response of adsorption of carbon dioxide for wet conditions. This was particularly important in terms of reforming conditions since off-gas from conventional

reformers include steam besides carbon dioxide. Figure 7.1.8 shows the breakthrough curves for hydrotalcite in the presence of steam (flow rate for steam was ca. 7-10 cm^3/min for experimental runs).

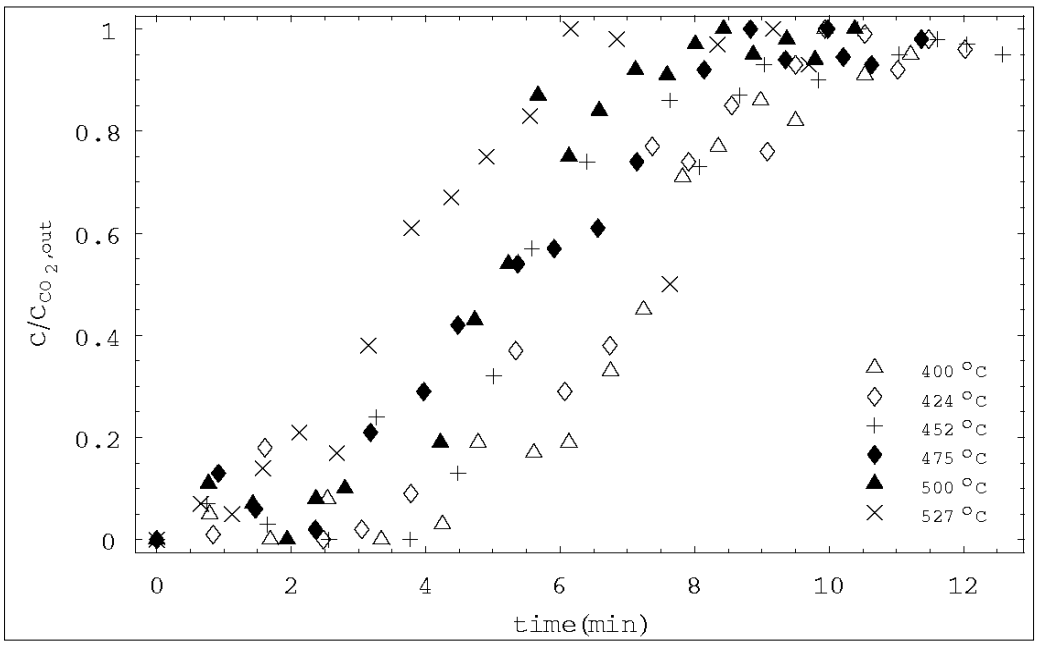

Figure 7.1.8 Experimental CO_2 breakthrough curves obtained with hydrotalcite sorbent in the presence of steam for different temperatures (App C.3.1-C.3.6)

When this behavior is compared with the steam-free conditions, it is observed that the experimental data fluctuated in a wide range. This is probably due to excess steam (steam instabilizes the system). That is, it was not always easy to handle steam flow rate sent to the tubular reactor due to bad control of water bath temperature and possibly large amounts of steam might cause to a scattered breakthrough data (departure from breakthrough).

Figure 7.1.9 shows the predictions of two-parameter deactivation model for activated hydrotalcite in the presence of steam for three temperatures, 400 °C, 452 °C, 500 °C. For some regions of experimental breakthrough curves, model fit was in a tolerable error range and for the most part prediction was poor. This was probably due to experimental errors encountered within the adsorption system.

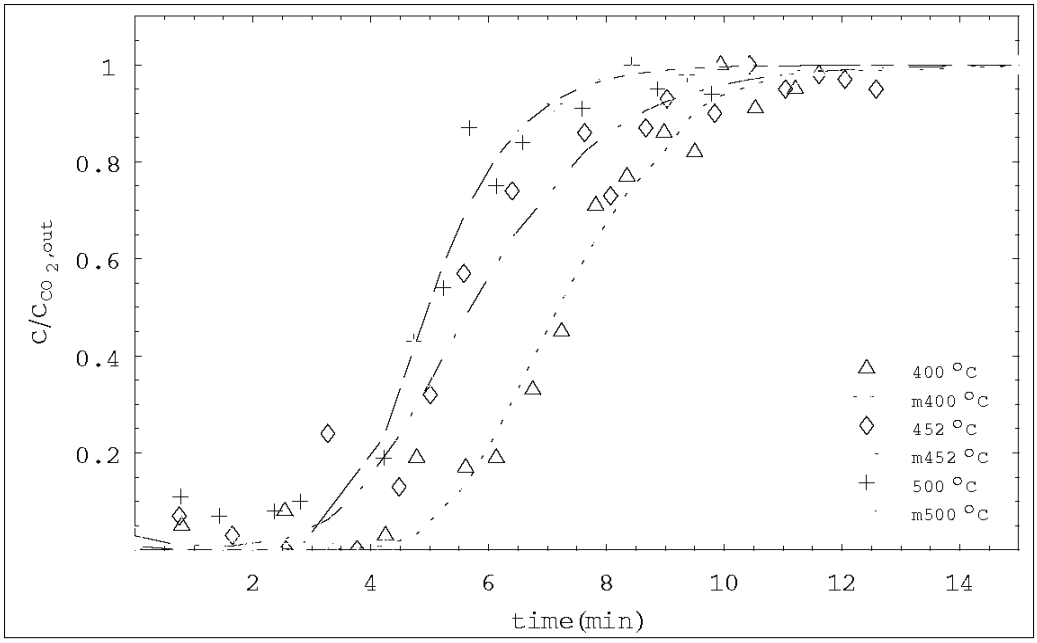

Figure 7.1.9 Comparison of experimental breakthrough curves obtained with hydrotalcite sorbent in the presence of steam with the two-parameter deactivation model for different temperatures (400 °C, 452 °C, 500 °C)

Table 7.1.4 Rate parameters obtained by the analysis of CO_2 breakthrough curves on hydrotalcite (wet) using deactivation model

Temperature (°C)	k_oW/Q	k_o (cm^3/min.g)	k_d (min^{-1})	χ^2
400	4.758	261.21	0.709	0.0662
424	3.630	212.17	0.598	0.1228
452	3.532	211.39	0.670	0.1078
475	2.727	173.57	0.559	0.0499
500	4.795	310.96	1.033	0.0733
527	2.610	171.61	0.762	0.2583

In Table 7.1.4 rate parameters, obtained from the sorption of carbon dioxide in the presence of steam, are shown. Compared to dry sorption conditions, a lowered sorption rate parameters were observed and deactivation rate constants were somewhat similar in the temperature range. Another reason in the change of sorption rate constants is due to total volumetric flow rate. Although it was fixed at around 50 cm^3/min, it showed departure from its set value and this affected the sorption rate constants.

Total sorption capacity of the sorbent varied from 1.07 mol/kg to 0.66 mol/kg as the temperature was increased from 400 to 527 °C (Table 7.1.5). Low breakthrough capacities were observed at higher temperatures (around 1 minute). That is, in order to achieve 0.05 of the inlet concentration 1 minute

was sufficient. In order to follow this breakthrough, too many injections were performed manually in a short time, which caused signal errors from the chromatograph and sensitivity of the analysis somehow changed.

Table 7.1.5 Adsorption properties of hydrotalcite (wet) samples

Temperature (^{o}C)	Breakthrough Capacity (min)	Total Capacity (min)	Total Capacity (mol/kg)
400	2.47	7.12	1.07
424	2.30	6.49	1.17
452	2.46	5.81	1.10
475	2.19	5.27	0.98
500	1.80	4.98	0.87
527	1.06	4.01	0.66

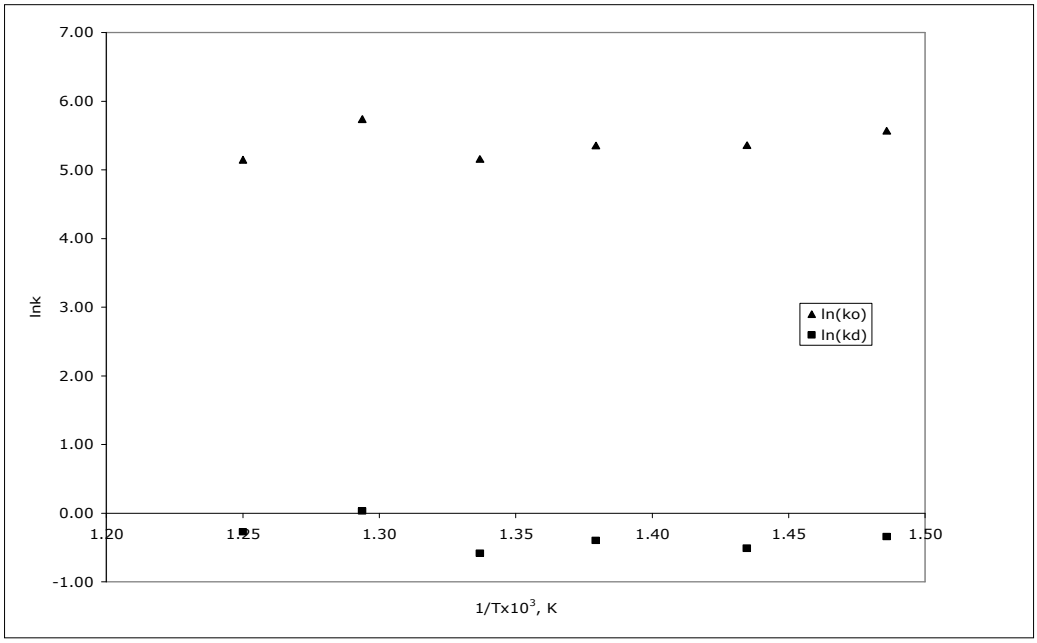

Figure 7.1.10 Temperature dependence of sorption and deactivation rate constants for CO_2 sorption on activated hydrotalcite sorbent in the presence of steam

Temperature dependencies of the hydrotalcite in the presence of steam are shown in Figure 7.1.10 for the temperatures of interest. Small slopes for both sorption and deactivation rate constants indicate small activation energies for the two model parameters.

7.2 Trona

Activated soda is a good sorbent for carbon dioxide removal at lowered temperatures. One source for activated soda is trona. Trona obtained from Beypazarı was used in this study for carbon dioxide removal. Calcination of the samples were achieved at 200 ^{o}C under the flow of helium. Table 7.2.1 shows the physical properties of trona and activated soda evaluated from the analysis of B.E.T and Hg porosimetry results. Activated trona samples have an average pore diameter of 59.78 A^{o} with a porosity of 0.75. Trona used in this study has a low surface area but its structure is highly porous. Moreover, surface area results obtained from B.E.T was not reasonable and this might be an instrumental error encountered during nitrogen adsorption. Regarding to low surface area results, one can conclude that this structure has no micropores but exhibits a macroporous structure.

Table 7.2.1 Physical properties of trona samples

Physical Property	**Trona**	**Activated Trona**
Porosity	0.75	0.75
Surface Area (Hg porosimeter) (m^2/g)	2.64	8.92
B.E.T Surface Area (N_2 adsorption) (m^2/g)	5.26	4.89
Solid Density (g/cm^3)	2.84	2.12
Apparent Density (g/cm^3)	0.71	0.53
Average Pore Diameter (by B.E.T) (A^{o})	40.79	59.78

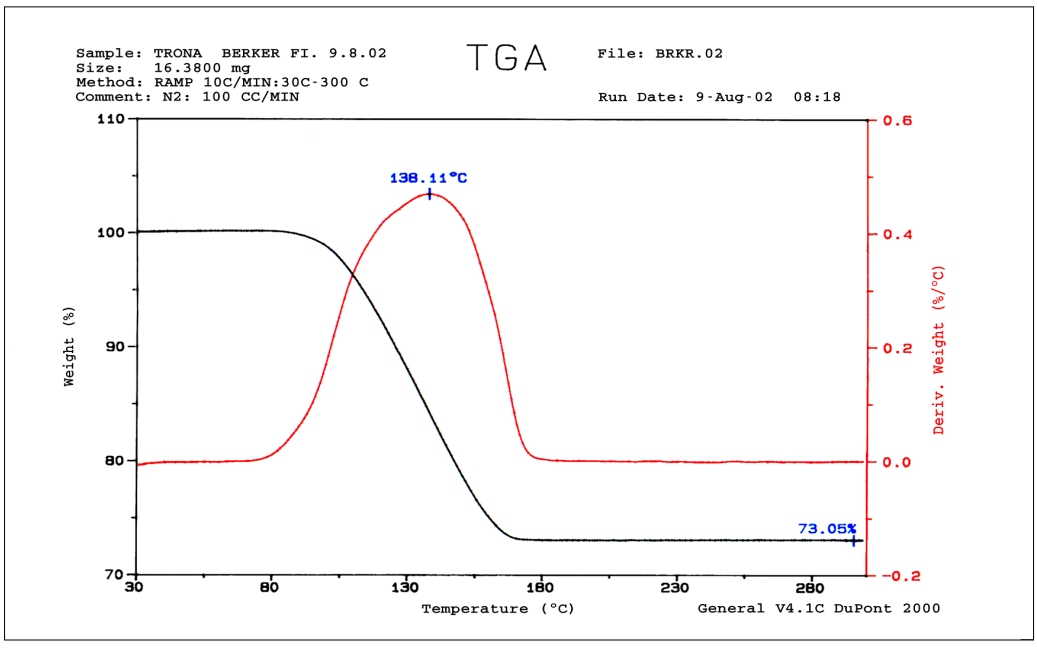

Figure 7.2.1 Thermal Gravimetric Analysis (TGA) results for trona sample

It could be observed from the TGA results (Figure 7.2.1) for trona that the crystalline water was given off at a temperature about 138 ^{o}C and desorption of steam and carbon dioxide was completed around 200 ^{o}C. For this purpose, calcination temperature was set at 200 ^{o}C to ensure activation without deactivating the structure of soda. Besides these, it would be convenient to mention the difference between carbon dioxide desorption temperatures for trona and hydrotalcite. For trona desorption of CO_2 was completed around 200 ^{o}C, whereas for hydrotalcite carbon dioxide desorption was started at ca. 350 ^{o}C. The diffrence between these two TGA results depend on the chemical structures of both sorbents [31,40]. Hydrotalcite contains carbonate molecules between two layers (hydroxide layers) and therefore has a different orientation compared to trona. For this reason, a higher temperature is necessary for HT to desorp carbon dioxide.

Pore size distributions of trona samples were almost coupled for untreated and calcined samples. This behavior could be seen in Figure 7.2.2 and also physical properties listed in Table 7.2.1 justify this overlapping. As the sample was activated at 200 ^{o}C, slight increase of pore size distributions to larger pores were observed.

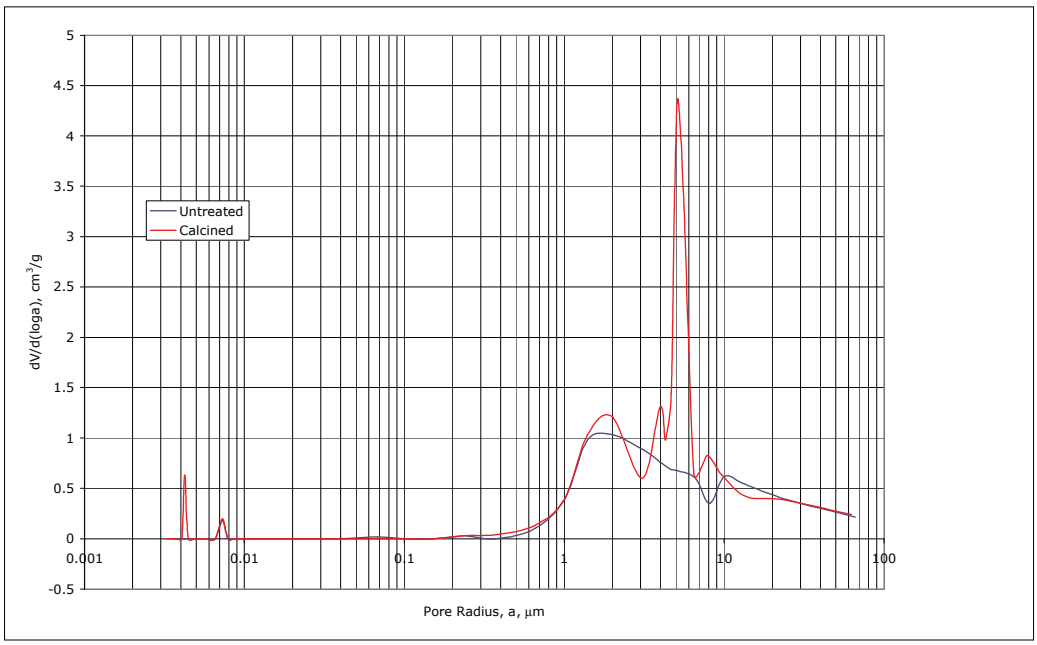

Figure 7.2.2 Pore size distributions of untreated and calcined trona samples

In Figure 7.2.3, the distinction between trona and activated soda could be seen after a pore diameter of 10 μm. Maximum intrusion of mercury was around 1.5 cm^3/g for calcined samples, whereas trona in pure form permits a maximum intrusion of ca. 1.2 cm^3/g.

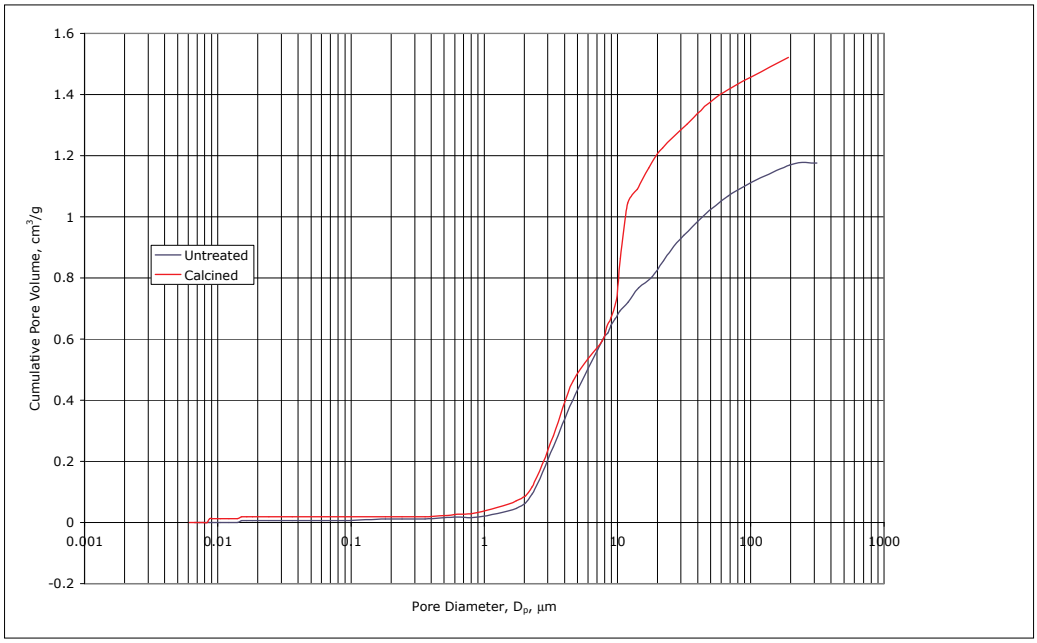

Figure 7.2.3 Cumulative pore volume distributions of untreated and calcined trona samples

Typical calcination curve obtained for trona samples are shown in Figure 7.2.4. Calcination temperature of reactor started at room temperature and it was altered upto 200 ^oC with a maximum ramp within the heating medium. Calcination of samples (2g trona in powder form) were completed at 200 ^oC (furnace was heated up with maximum heating rate ca. 70 ^oC/min) and in almost 20 minutes effluent gas mixture's carbon dioxide content reduced to nondetectable limits. To ensure complete calcination system was settled for further calcination at 200 ^oC (response of desorption temperature w.r.t. to time were shown App.D.3).

Breakthrough data for activated trona were observed for the temperature range from 80 ^oC to 152 ^oC in the presence of steam. Results of the S-shaped curves are shown in Figure 7.2.5. Rather short breakthrough time was observed for the activated trona in powder form. Mass transfer zone was elongated from the breakthrough time to infinite time or equilibrium conditions for fixed temperature. This sudden change in sorption might be due to pore mouth

closure within pores of activated soda. Another reason might be calcination temperature for trona. In other words, lowering calcination temperature slightly could probably enhance usable capacity of the sorbent. This rather high calcination temperature might cause sintering or closure of pores and causing pores to become inactive.

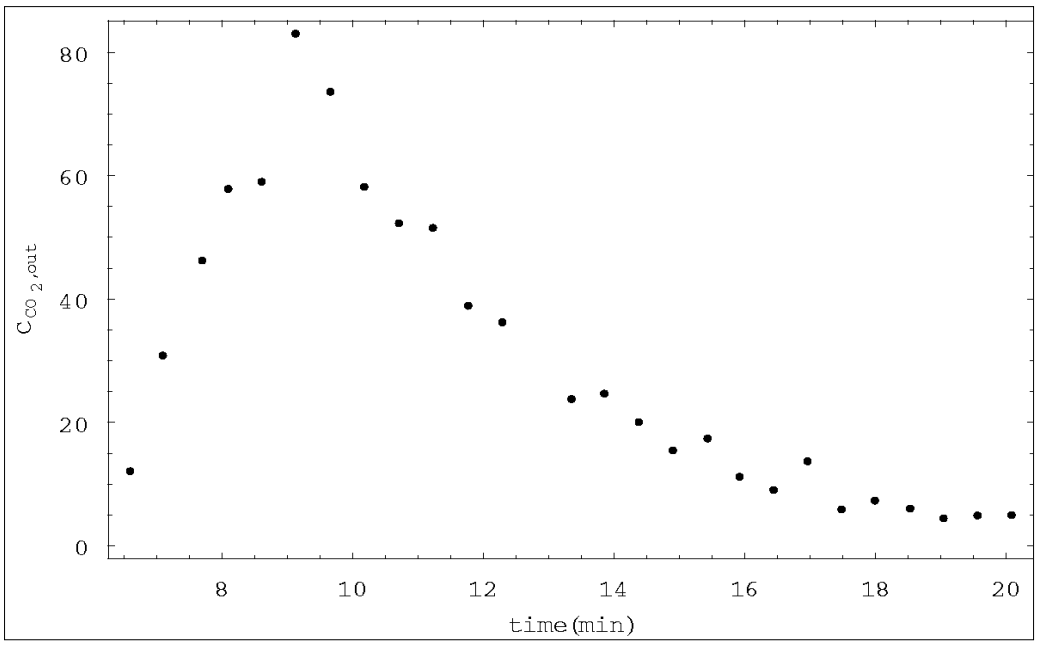

Figure 7.2.4 Temperature variant CO_2 desorption curve for trona sample calcined at 200 °C (He flow at 30 ml/min, 2g sorbent)

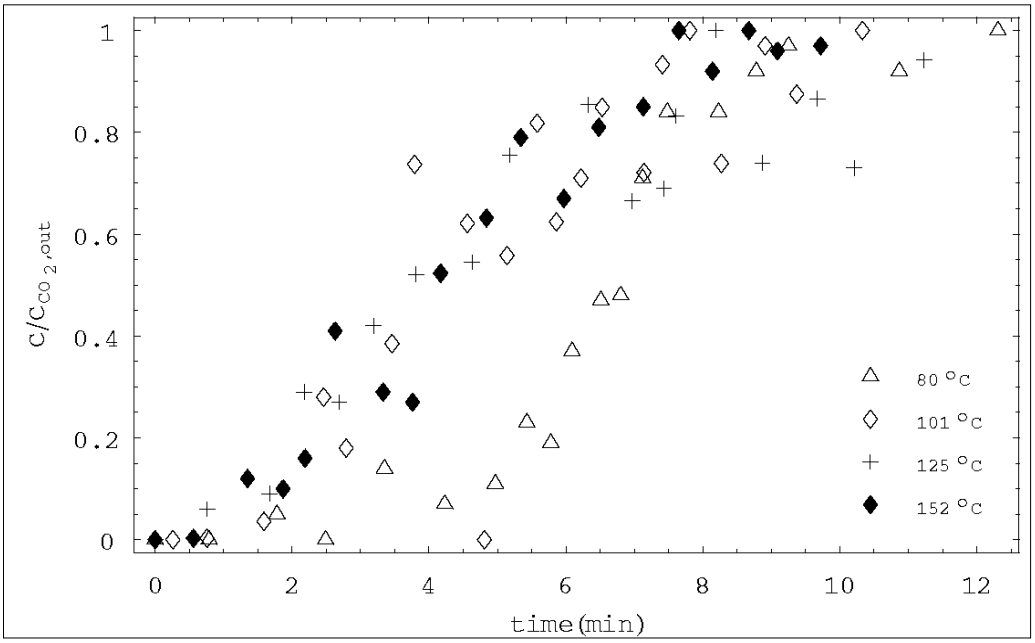

Figure 7.2.5 Experimental CO_2 breakthrough curves obtained with activated trona sorbent in the presence of steam for different temperatures (App C.4.1-C.4.4)

For an increase in the temperature, a shift of curve to left was observed, which indicates lowered sorption for activated trona at elevated temperatures. This was reasonable since adsorption is an exothermic process and indeed sharpened breakthrough curves are extremely desirable for high sorption of carbon dioxide. A sharp interface between the breakpoint and mass transfer region would lead to efficient use of bed. However, for activated trona this was not the case. Diffusional limitations cause significant response changes in the particle. Trona was used as in powder form within the tubular reactor and excess steam might cause samples to stick reactor walls and cause lowering of conversions for the temperature range. Decreasing particle size was good for eliminating diffusional purposes but this caused an increase in pressure drop in the bed and this lead to oscillating flow rates at the inlet and outlet of the reactor.

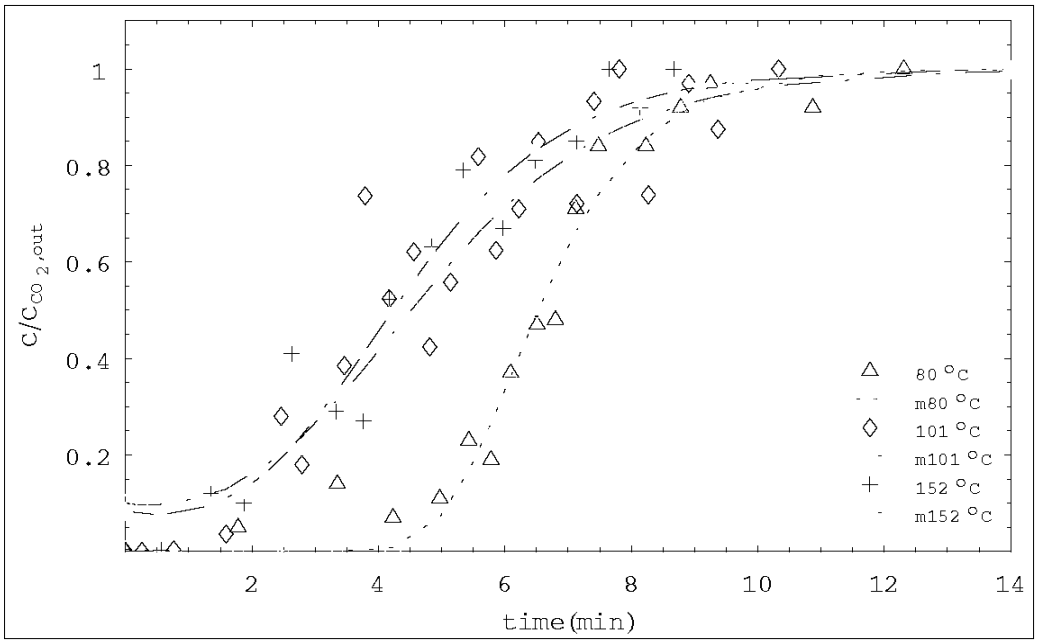

Figure 7.2.6 Comparison of experimental breakthrough curves obtained with activated trona sorbent in the presence of steam with the two-parameter deactivation model for different temperatures (80 °C, 101 °C, 152 °C)

Figure 7.2.6 shows the predictions of deactivation model for activated trona for 80 °C, 101 °C, and 152 °C in the presence of steam (around 8cm^3/min). Unexpected predictions might be due to excess steam sent into flow reactor. Activated trona placed into the reactor was in powder form and excess steam might cause trona to stick on the walls of stainless steel reactor. If this

were the case, some of the sorbent was unable to adsorb carbon dioxide and this might be one reason for the observed scattered experimental data.

Table 7.2.2 Rate parameters obtained by the analysis of CO_2 breakthrough curves on activated trona using deactivation model

Temperature (^oC)	k_oW/Q	k_o ($cm^3/min.g$)	k_d (min^{-1})	χ^2
80	5.427	156.84	0.885	0.0655
101	2.308	73.16	0.538	0.6003
125	1.936	64.66	0.456	0.2233
152	2.485	87.60	0.626	0.1068

Table 7.2.2 shows rate parameters obtained from the analysis of breakthrough data for activated soda at different temperatures. For an inlet composition change from 16.1 to 17.3% carbon dioxide, sorption rate constant was changed from 156.84 to 87.60 $cm^3/min.g$.

For same temperature and composition range deactivation rate constant was varied from 0.885 to 0.626 min^{-1}. Rather lowered chi-squares indicate a better fit for the sample. Table 7.2.3 shows sorption properties of the activated trona samples and a decrease of capacity from 1.15 mol/kg to 0.82 mol/kg was observed as the temperature was increased from 80 to 152 ^oC.

Table 7.2.3 Adsorption properties of activated trona samples

Temperature (^oC)	Breakthrough Capacity (min)	Total Capacity (min)	Total Capacity (mol/kg)
80	2.44	6.55	1.15
101	1.58	4.71	0.84
125	1.57	4.72	0.79
152	1.31	4.32	0.82

Arhenius plots for activated trona samples are shown in Figure 7.2.7 and straight line behavior for some temperature indicates small activation. In fact, somewhat higher activation energies were expected for both trona and sodium bicarbonate. This lowered activation energies resulted from the serious experimental errors encountered in the course of reaction.

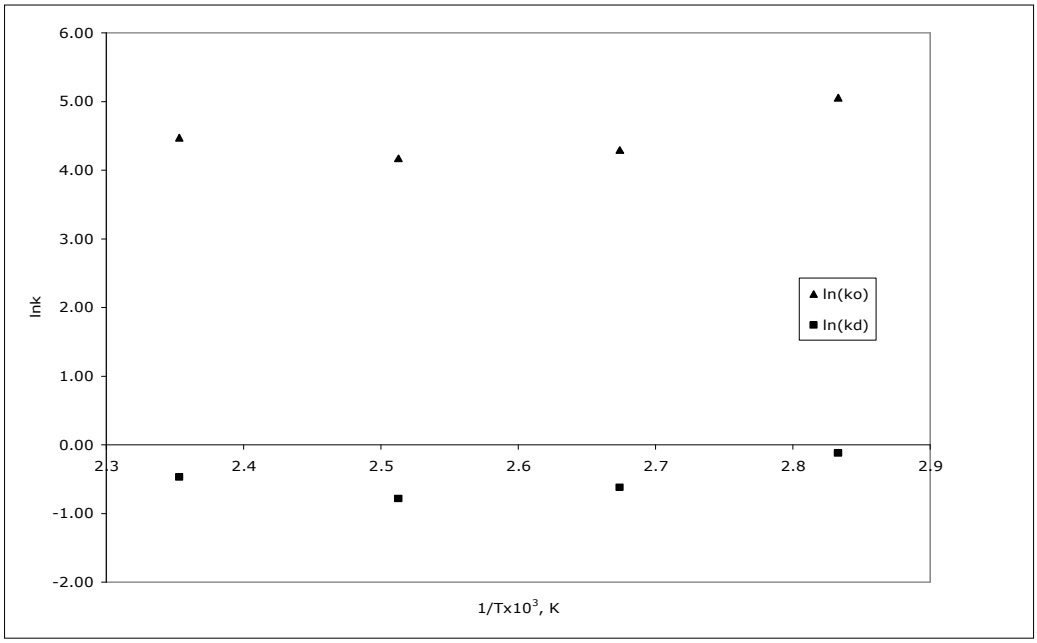

Figure 7.2.7 Temperature dependence of sorption and deactivation rate constants for CO_2 sorption on activated trona sorbent in the presence of steam

7.3 Sodium bicarbonate ($NaHCO_3$)

Another well known source for activated soda is sodium bicarbonate. In order to compare the activities of trona and $NaHCO_3$ based sorbents, $NaHCO_3$ was studied for carbon dioxide removal.

Table 7.3.1 Physical properties of $NaHCO_3$ samples

Physical Property	**$NaHCO_3$**	**Activated $NaHCO_3$**
Porosity	0.03	0.44
Surface Area (Hg porosimeter) (m^2/g)	0.06	4.27
B.E.T Surface Area (N_2 adsorption) (m^2/g)	7.86	4.86
Solid Density (g/cm^3)	0.96	1.02
Apparent Density (g/cm^3)	0.93	0.57
Average Pore Diameter (by B.E.T) (A^o)	29.22	85.79

In Table 7.3.1, some physical properties of $NaHCO_3$ and activated soda are listed. Probably because of high water content within the structure, porosity of $NaHCO_3$ increased from 0.03 to 0.44 as the sample was calcined at 200 ^oC. In addition, surface area of activated sodium bicarbonate was found to be 4.27 m^2/g for Hg porosimetry and 4.86 m^2/g for B.E.T. These similar and low surface area possibly results from the macroporous structure of sodium bicarbonate.

Decrease in surface area with activation for B.E.T adsorption might be due to closure of small pores with continous calcination (e.g. like sintering) or it could be an instrumental error resulting from B.E.T apparatus. Besides these, activated soda sample's average pore diameter were observed to increase from ca. 29 A^{o} to ca. 86 A^{o}.

TGA results of sodium carbonate was rather different than trona. In Figure 7.3.1, it could be seen that there is a slight weight loss at around 110 ^{o}C. During this weight loss, probably, water was desorbed from the structure and further heating of sorbent showed that complete desorption of water and carbon dioxide was accomplished at around 216 ^{o}C. Pore size and cumulative pore volume distributions of sodium bicarbonate samples are shown in Figure 7.3.2 and Figure 7.3.3.

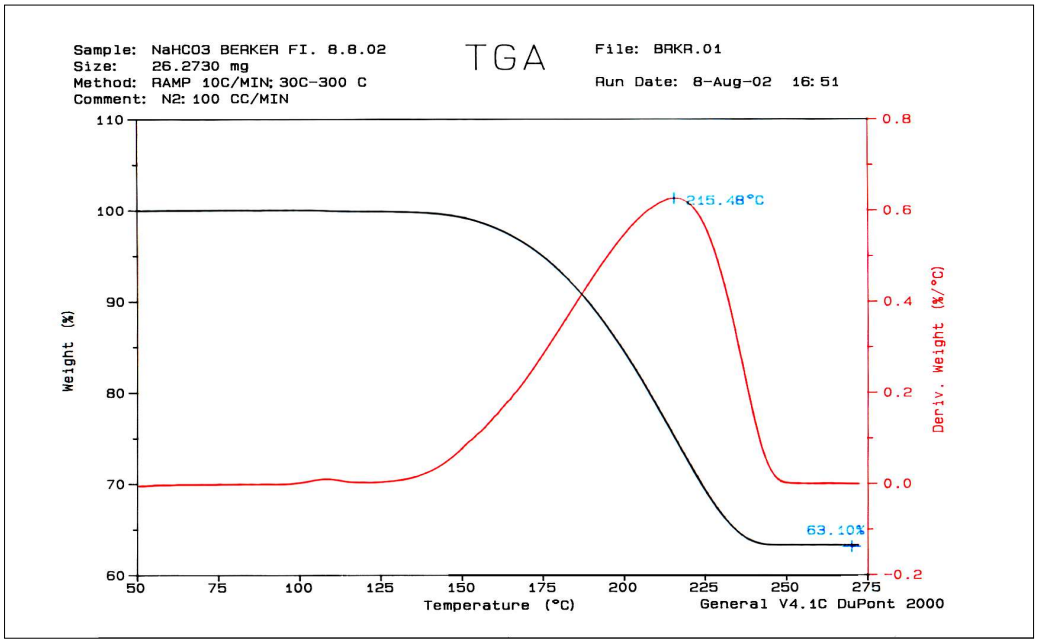

Figure 7.3.1 Thermal Gravimetric Analysis (TGA) results for $NaHCO_3$ sample

An observed distribution for calcined samples were around pore radius 0.1 μm and for pore radius larger than 10 μm pore size distribution curve shifted upwards for a small region. For cumulative pore volume distributions, an interesting tendency was investigated for calcined sample. That is, a step wise intrusion of mercury within the pores was seen and this might be due to impurities within the structure or this might arise from overcalcining of the

sodium bicarbonate samples. In addition, for pore diameter larger than 100 μm sudden increase in penetration was detected for activated sodium bicarbonate samples.

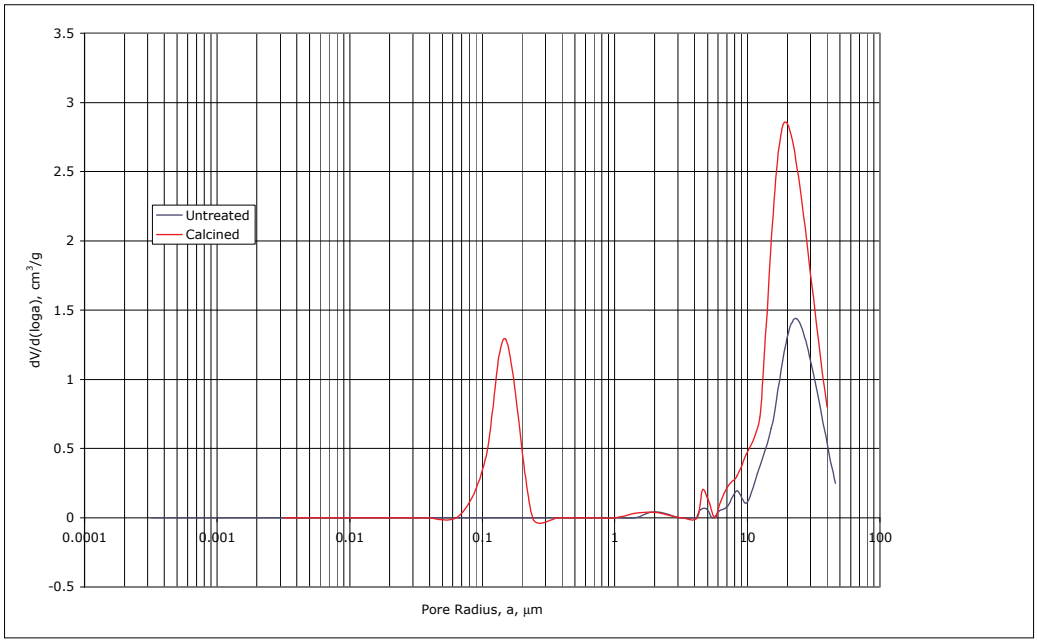

Figure 7.3.2 Pore size distributions of untreated and calcined $NaHCO_3$ samples

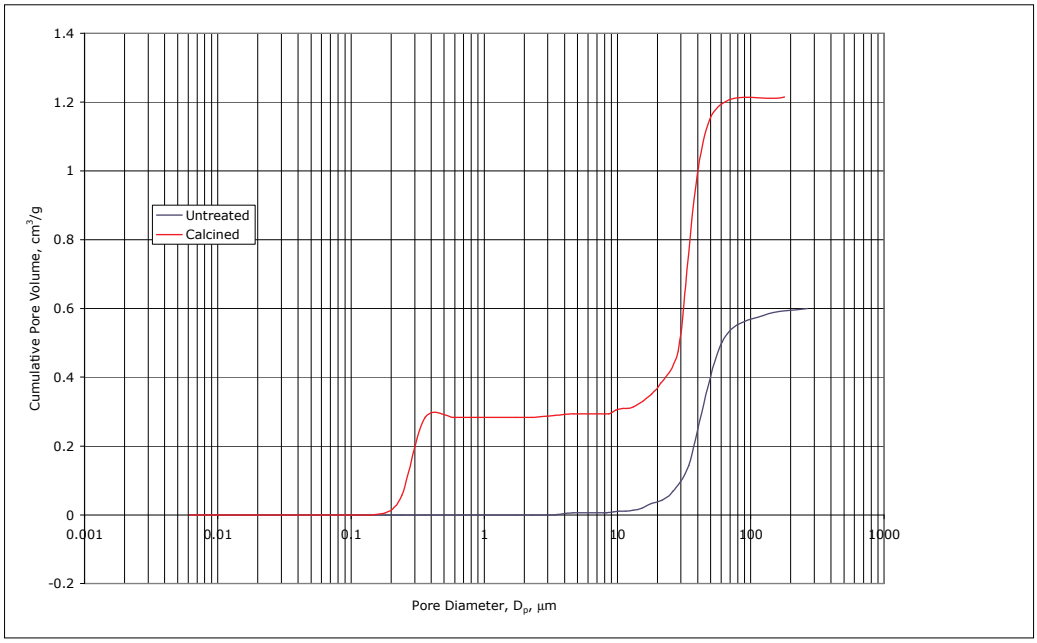

Figure 7.3.3 Cumulative pore volume distributions of untreated and calcined $NaHCO_3$ samples

Calcination of sodium bicarbonate samples were conducted at 200 °C and at about 20 minutes the complete desorption of carbon dioxide was seen (Figure 7.3.4). After 5 minutes of calcination a sudden desorption of carbon dioxide was

monitored and this behavior was consistent with the TGA result for $NaHCO_3$ shown in Figure 7.3.1.

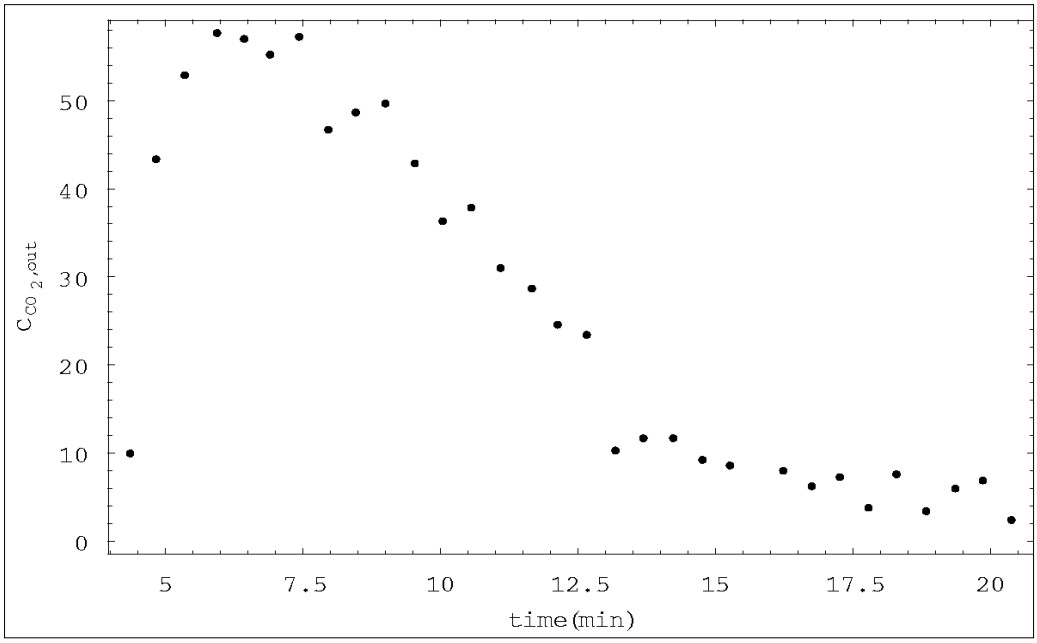

Figure 7.3.4 Temperature variant CO_2 desorption curve for $NaHCO_3$ sample calcined at 200 °C (He flow at 30 ml/min, 2g sorbent)

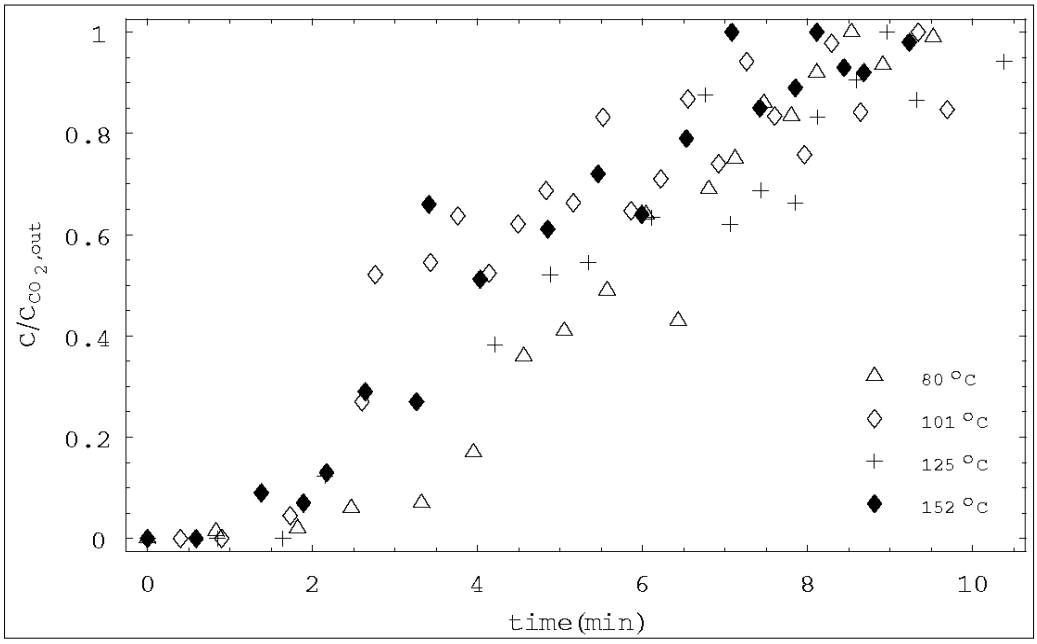

Figure 7.3.5 Experimental CO_2 breakthrough curves obtained with activated $NaHCO_3$ sorbent in the presence of steam for different temperatures (App C.5.1-C.5.4)

Breakthrough curves for activated sodium bicarbonate (calcined at 200 °C) samples are shown in Figure 7.3.5. At lower temperatures resistance of sorbent through carbon dioxide capture was low or sorbent was capable of capturing carbon dioxide for 5-6 minutes of total sorption time. Sodium bicarbonate samples exhibited short breakthrough times within the packed bed, which was not good. Activated sodium bicarbonate particles were rather observed to have sticky structure and excess loading of steam might hinder the sorption of carbon dioxide by forming a circular resistance around the particle.

Figure 7.3.6 shows the predictions of deactivation model for activated sodium bicarbonate in the presence of steam for three temperatures. Poor predictions could be resulted from both experimental errors and diffusional effects (neglecting diffusion around the particles and within the particles). A diffusion model with an optimized (i.e. a better control of steam rate with qualified signals from chromatograph) experimental conditions might solve this unexpected predictions.

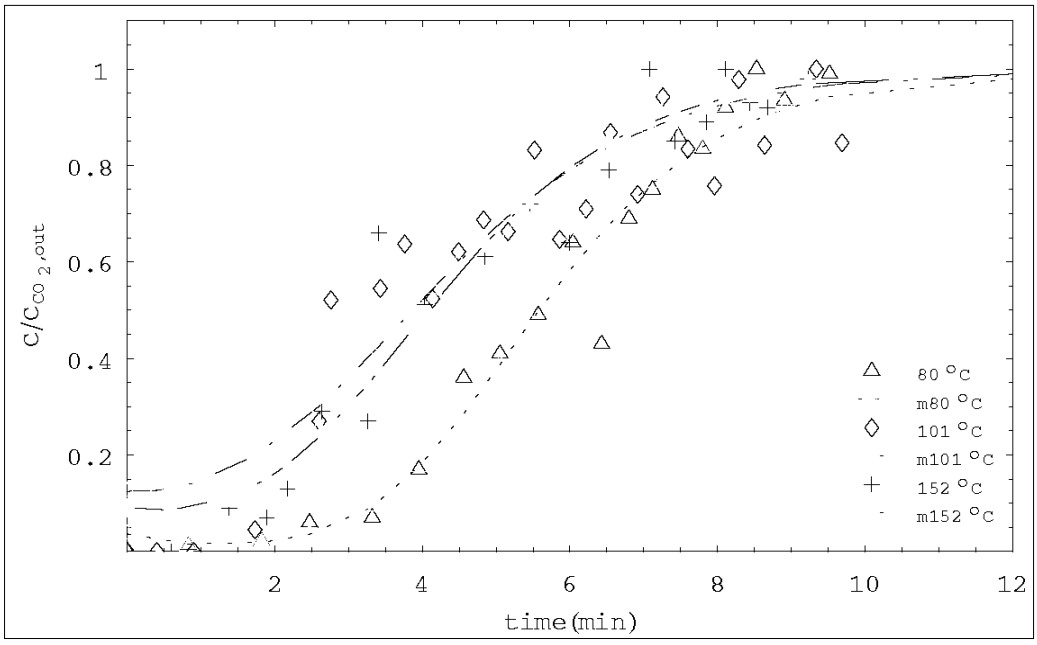

Figure 7.3.6 Comparison of experimental breakthrough curves obtained with activated $NaHCO_3$ sorbent in the presence of steam with the two-parameter deactivation model for different temperatures (80 °C, 101 °C, 152 °C)

Rate parameters obtained from the analysis of breakthrough curves on activated sodium bicarbonate samples are tabulated in Table 7.3.2. Sorption

rate constants vary from 95.64 to 82.16 cm^3/min.g, whereas deactivation alters between 0.641 to 0.624 min^{-1} for a temperature change from 80 °C to 152 °C.

Table 7.3.2 Rate parameters obtained by the analysis of CO_2 breakthrough curves on activated $NaHCO_3$ using deactivation model

Temperature (°C)	k_oW/Q	k_o (cm^3/min.g)	k_d (min^{-1})	χ^2
80	3.315	95.64	0.641	0.0850
101	2.082	65.37	0.558	0.2722
125	2.478	85.37	0.509	0.1225
152	2.399	82.16	0.624	0.1665

Activated sodium bicarbonate sorption properties are shown in Table 7.3.3. Saturation capacity of the packed bed decreased from 0.85 mol/kg to 0.68 mol/kg as the temperature was increased from 80 °C to 152 °C. On the other hand, breakthrough capacity was changing from 1.44 min to 2.08 min for the same temperature region. However, these sorption capacities are well below the theoretical sorption capacity of the activated soda obtained from sodium bicarbonate. In addition, sudden loading of adsorbate onto sorbent first causes a fast breakthrough than this curve was enlarged for the rest of adsorption.

Table 7.3.3 Adsorption properties of activated $NaHCO_3$ samples

Temperature (°C)	Breakthrough Capacity (min)	Total Capacity (min)	Total Capacity (mol/kg)
80	1.44	4.64	0.85
101	1.72	4.46	0.76
125	2.12	5.32	0.94
152	2.08	4.18	0.68

Response to change in temperature effects for sorption and deactivation rate parameters were plotted and shown in Figure 7.3.7. Similar activation energies were observed for sodium bicarbonate samples. However, for sodium carbonate carbonation, one would expect a higher activation energy. If the sorption of carbon dioxide was hindered due to excess steam or for some reason within the reactor, this would lower the sorption and consequently activation energies of both sorption and deactivation rate parameters. Low activation energies indicate physisorption and this is rather questionable for sodium carbonate carbonation (chemisorption was expected due to well known sodium bicarbonate formation reaction).

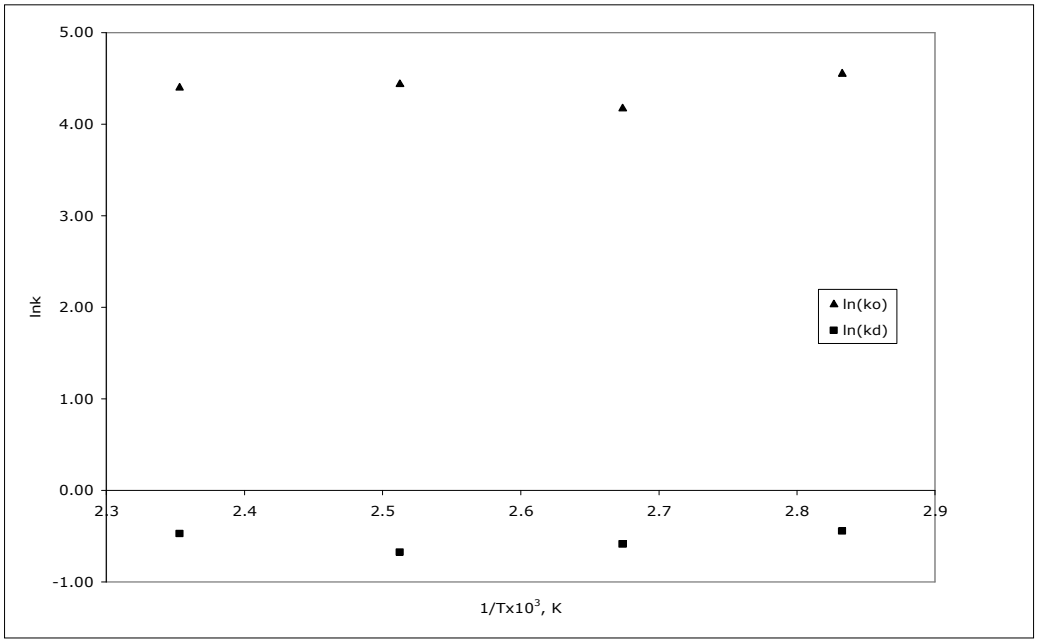

Figure 7.3.7 Temperature dependence of sorption and deactivation rate constants for CO_2 sorption on activated $NaHCO_3$ sorbent in the presence of steam

After all, it would be convenient to highlight the possible experimental and instrumental errors encountered. Multiplication of these complexities decreased the accuracy of the system and lead to unexpected or unreasonable results for some parts of the experiments. Troubleshooting of these pitfalls is listed as follows:

- All in all, the major experimental errors were resulted from gas chromatograph. The linearity of the chromatograph, somehow, was not good enough to response sudden changes in the signals. That is, sensitivity of detector was changing from time to time (change in current was observed). Continuous manual control of chromatograph settings helped a lot to minimize errors.

- Experiments, which were carried out in the presence of steam, exhibited an unexpected deviation. This might be due to the temperature controller of the water bath used to produce steam as a feed to reactor. Inefficient control of temperature probably caused fluctuations within the reactor and this affected elution profiles at the bed outlet.

- It was possible to adjust inlet feed composition by using a three-way valve. However, the desired composition was adjusted at the bed outlet by following the peaks from gas chromatograph. Although CO_2 composition was considered to be a fixed parameter throughout the experiments, for same set of conditions (e.g. loading, flow rate) adjusted composition altered slightly for almost every run. This might be due to the change in head pressures of the cylinders (He and CO_2) and/or the sweeping of the gaseous mixture within the reactor. In other words, sorbent might stick on the walls of the reactor (e.g. in case of excess steam) and adsorption of carbon dioxide might exhibit variations with respect to temperature.

- Another possible error might be due to the temperature controller of the tubular furnace. During the course of reaction sudden and little changes in reaction temperature was observed for sluggish response of controller. This would probably affect the shape of breakthrough curves especially when the temperature was elevated (high loss of heat to the surrounding even for sufficient insulation).

One or more of the cases listed above probably lowered the sensitivity of the experimental results obtained from the gas chromatograph. No matter which error was dominant in the experiments, reasonable results were obtained and evaluated at the end.

CHAPTER 8

CONCLUSIONS AND RECOMMENDATIONS

Adsorption of carbon dioxide onto hydrotalcite, sodium bicarbonate, and trona were studied at different temperature ranges. As a result of the experiments conducted, concluding remarks observed are as follows:

1. Hydrotalcite like materials could adsorb carbon dioxide efficiently in the temperature range 400-527 ^{o}C. Therefore, it is possible to use hydrotalcite as a carbon dioxide removing agent (adsorbent) within the steam methane reformer. Separation of carbon dioxide and production of hydrogen will occur at the same time within the reformer (SERP). Furthermore, reformer temperature will be lowered and production of hydrogen will be cost effective. In addition, coke formation possibilities could also be reduced due to the lowered temperature conditions.

2. Breakthrough curves for hydrotalcite became sharpened as the temperature was increased from 400 ^{o}C to 527 ^{o}C. This indicates that mass transfer zone shrinks as the temperature increases. However, since adsorption is exothermic in nature, breakthrough capacity of the material reduced from 1.18 mol/kg for 400 ^{o}C to 0.80 mol/kg for 527 ^{o}C. For this reason, an optimum temperature could be selected to optimize adsorption capacity of adsorbent when it is to be used within the reformer.

3. In the analysis of experimental data, two-parameter deactivation model was used. Model was in acceptable agreement with the experimental data. As a result of nonlinear regression analysis, sorption rate constant for hydrotalcite was found to change from 261.21 to 195.30 cm^3/min.g as

temperature was increased from 400 to 527 ^{o}C. On the other hand, deactivation rate constant was found to change from 0.709 to 0.762 min^{-1} within the same temperature range. In addition, using arhenius plots of these parameters for the temperature range studied, activation energies for the two rate parameters were evaluated. For hydrotalcite, activation energy for sorption rate constant was found to be 65.0 kj/mol, whereas the activation energy for deactivation rate constant was calculated as 35.4 kj/mol. These activation energies might imply that chemisorption is dominant for the reaction.

4. Experiments carried out with hydrotalcite indicated that when steam was used in the feed, adsorption capacity of the material was enhanced slightly. For instance, at temperature 475 ^{o}C, adsorption capacity of the material was altered from 0.88 to 0.98 mol/kg in the presence of steam. Since reformer effluent gas also includes steam besides carbon dioxide, adsorption of CO_2 will be enhanced when SERP concept is considered.

5. Layered double hydroxides (hydrotalcite) could be improved for carbon dioxide capture by modifying their structure with the use of K_2CO_3 or Na_2CO_3. Promoting with these chemicals will probably increase active sites for adsorption and the breakthrough capacity of the material will be enhanced for this temperature range. Using chemically modified hydrotalcite, adsorption experiments should be performed so as to compare the sorption capacities of the novel sorbent.

6. Adsorption of carbon dioxide onto trona and $NaHCO_3$ was studied within the temperature range of 80 to 152 ^{o}C. These similar structures exhibited similar adsorption characteristics. Due to very small equilibrium constants at temperatures above 200 ^{o}C, it is not possible to adsorb CO_2 onto these adsorbents at elevated temperatures (i.e. almost no conversion could be observed at reforming temperatures). Thus, it is not possible to use these adsorbents within the steam methane reformer as adsorbent. However, reformer off-gas could be cooled down to lower temperatures and trona or sodium bicarbonate could be activated for the adsorption of carbon dioxide within the multiple adsorber beds.

7. Breakthrough capacities for trona decreased slightly as the temperature was increased from 80°C to 152°C. For some temperature, sluggish response of breakthrough curve was observed probably because of the diffusional limitations encountered within the structure. Breakthrough capacity of activated trona reduced from 1.15 mol/kg for 80 °C to 0.82 mol/kg for 152 °C. Moreover, sorption rate constant for activated trona was found to change from 156.84 to 87.60 cm^3/min.g as temperature was increased from 80 to 152°C. On the other hand, deactivation rate constant was found to change from 0.885 to 0.626 min^{-1} within the same temperature range. Activation energy for sorption rate constant was found to be 4.7 kj/mol, whereas the activation energy for deactivation rate constant was calculated as 3.9 kj/mol.

8. Similar response of breakthrough curves with respect to trona was observed for $NaHCO_3$. Although deactivation model predicted experimental data in good agreement, a model considering diffusional effects within the sorbent could explain the behavior of mass transfer zone for breakthrough curves more accurately. Total adsorption capacity of activated $NaHCO_3$ decreased from 0.85 mol/kg for 80 °C to 0.68 mol/kg for 152 °C. Sorption rate constant for $NaHCO_3$ was found to change from 95.64 to 82.16 cm^3/min.g, as temperature was increased from 80 to 152°C. In addition, deactivation rate constant was found to change from 0.641 to 0.624 min^{-1} within the same temperature range. Also, activation energy for sorption rate constant was found to be 13.8 kj/mol, whereas the activation energy for deactivation rate constant was calculated as 2.9 kj/mol.

9. To sum up, for high temperature removal of CO_2, HT like materials could be used and their chemically promoted forms exhibit even better sorption properties. Besides these, in the presence of steam carbon dioxide sorption capacity was increased slightly (probably steam activates adsorption sites by maintaining hydroxyl concentration of the surface and/or preventing site poisoning) for hydrotalcite. On the contrary, for low temperature carbon dioxide removal, activated soda could be considered as a good sorbent. Activated soda obtained from trona was found to show rather improved sorption characteristics compared to sodium bicarbonate based activated soda due to its high Na_2CO_3 content within the chemical structure.

REFERENCES

1. Hoffmann P., (2001), "Tomorrow's Energy: Hydrogen, Fuel Cells, and the Prospects for a Cleaner Planet", 1st edition, MIT Press
2. Blier A. (Ed.), (1993), "Hydrogen", Kirk-Othmer Encyclopedia of Chemical Technology, 4th edition, Vol. 13, p 852-885
3. HydrogenWorks LLC, "Hydrogen.com",http://www.hydrogen.com/faq.asp/, USA, 2004
4. Thomas G., (2000), "Overview of Storage Development DOE Hydrogen Program",http://www.eere.energy.gov/hydrogenandfuelcells/pdf/storage.pdf , 2004
5. Wang M., (2004), "Freedom Car and Vehicle Technologies Program", http://www.eere.energy.gov/vehiclesandfuels/pdfs/success/greet.pdf, 2004
6. D. S. Newsome, B. G. Mandelik, (1981), Kirk-Othmer Encyclopedia of Chemical Technology, 3rd edition, Vol. 12, p 938
7. Hufton J. R., Mayorga S., Sircar S., (1999), "Sorption-Enhanced Reaction Process for Hydrogen Production", AIChE Journal, Vol. 45(2), p 248-256
8. Van Hook J. P., (1980), "Methane-Steam Reforming", Catal. Rev. Sci. Eng., Vol. 21(1), p 1-51
9. Trimm D. L., (1999), "Catalysts for the Control of Coking During Steam Reforming", Catalysis today, Vol. 49, p 3-10
10. Armor J. N., (1999), "Review- The Multiple Roles for Catalysis in the Production of H_2", Applied Catalysis A: General, Vol. 176, p 159-176
11. Newsome D. S., (1980), "The Water-Gas Shift Reaction", Catal. Rev. Sci. Eng., Vol. 21(2), p 275-318
12. Jarosch K., De Lasa H. I., (1999), "Novel Riser Simulator for Methane Reforming Using High Temperature Membranes", Chemical Engineering Science, Vol. 54, p 1455-1460

13. Adris A. M., Lim C. J., Grace J. R., (1997), "The Fluidized-bed Membrane Reactor for Steam Methane Reforming: Model Verification and Parametric Study", Chemical Engineering Science, Vol. 52(10), p 1609-1622

14. Barbieri G., Violante V., Di Maio F. P., Criscuoli A., Drioli E., (1997), "Methane Steam Reforming Analysis in a Palladium-Based Catalytic Membrane Reactor" , Ind. Eng. Chem. Res., Vol. 36, p 3369-3374

15. Barbieri G., Di Maio F. P., (1997), "Simulation of the Methane Steam Reforming Process in a Catalytic Pd-Membrane Reactor", Ind. Eng. Chem. Res., Vol. 36, p 2121-2127

16. Balasubramanian B., Ortiz A. L., Kaytakoğlu S., Harrison D. P., (1999), "Hydrogen from Methane in a Single-Step Process", Chemical Engineering Science, Vol. 54, p 3543-3552

17. Carvill B. T., Hufton J. R., Anand M., Sircar S., (1996), "Sorption-Enhanced Reaction Process", AIChE Journal, Vol. 42(10), p 2765-2772

18. Vaporciyan G. G., Kadlec R. H., (1989), "Periodic Separating Reactors: Experiments and Theory", AIChE Journal, Vol. 35, p 831

19. Ding Y., Alpay E., (2000), "Adsorption-enhanced Steam-methane Reforming", Chemical Engineering Science, Vol. 55, p 3929-3940

20. Han C., Harrison D. P., (1997), "Multicycle Performance of a Single-Step Process for H_2 Production", Separation Science and Technology, Vol. 32(1-4), p 681-697

21. Hufton J., Waldron W., Weigel S., Rao M., Nataraj S., Sircar S., (2000), "Sorption Enhanced Reaction Process(SERP) for the Production of Hydrogen", Proceedings of the 2000 Hydrogen Program Review, p 1-11

22. Han C., Harrison D. P., (1994), "Simultaneous Shift Reaction and Carbon dioxide Separation for the Direct Production of Hydrogen", Chemical Engineering Science, Vol. 49, p 5875-5883

23. Ding Y., Alpay E., (2000), "Equilibria and Kinetics of CO_2 adsorption on Hydrotalcite Adsorbent", Chemical Engineering Science, Vol. 55, p 3461-3474

24. Pena M. A., Gomez J. P., Fierro J. L. G., (1996), "Review- New Catalytic Routes for Syngas and Hydrogen Production", Applied Catalysis A: General, Vol. 144, p 7-57

25. McKetta J. J., (1994), "Carbon dioxide Removal", Encyclopedia of Chemical Processing and Design, Vol. 6, p 292-310, Marcel Dekker

26. Haussinger P., Lohmuller R., Watson A. M., (1989), "Hydrogen", Ullmann's Encyclopedia of Industrial Chemistry, Vol. A(13), p 297-443, Wiley-VCH

27. Schweitzer P. A., (1997), "Handbook of Separation Techniques for Chemical Engineers", 3rd ed., McGraw Hill

28. Yong Z., Rodrigues A. E., (2002), "Hydrotalcite-like Compounds as adsorbents for Carbon dioxide", Energy Conversion and Management, Vol. 43, p 1865-1876

29. Space Science Outreach and Research, SSOAR, http://www.ssoar.org/ research/space-suits/ucb/suzuki, Berkeley, 2004

30. Güldür Ç., Doğu G., Doğu T., (2001), "Kinetics of trona sulfur dioxide reaction", Chemical Engineering and Processing, Vol. 40, p 13-18

31. Uçar F. Ç., (1990), "Trona based scrubbing of sulfur dioxide in a spray dryer", M.S. Thesis, METU

32. Vaccari A., (1999), "Clays and catalysis: a promising future", Applied Clay Science, Vol. 14, p 161-198

33. Labajos F. M., Sanchez-Montero M. J., Holgado M. J., Rives V., (2001), "Thermal evolution of V(III)-containing layered double hydroxides", Thermochimica Acta, Vol. 370, p 99-104

34. David Barthelmy, "Mineralogy Database", http://webmineral.com/data/ Hydrotalcite.shtml, 2004

35. Yong Z., Mata V., Rodrigues A. E., (2002), "Adsorption of Carbon dioxide at High Temperature- a Review", Separation and Purification Technology, Vol. 26, p 195-205

36. Vaccari A., (1998), "Preparation and catalytic properties of cationic and anionic clays", Catalysis Today, Vol. 41, p 53-71

37. Lazaridis N. K., Asouhidou D. D., (2003), "Kinetics of sorptive removal of chromium(VI) from aqueous solutions by calcined Mg-Al-CO_3 hydrotalcite", Water Research, Vol. 37, p 2875-2882

38. Marquevich M., Medina F., Montane D., (2001), "Hydrogen production via steam reforming of sunflower oil over Ni/Al catalysts from hydrotalcite materials", Catalysis Communications, Vol. 2, p 119-124

39. Jiratova K., Cuba P., Kovanda F., Hilaire L., Pitchon V., (2002), "Preparation and characterisation of activated Ni(Mn)/Mg/Al hydrotalcites for combustion catalysis", Catalysis Today, Vol. 76, p 43-53

40. Yang W., Kim Y., Liu P. K. T., Sahimi M., Tsotsis T. T., (2002), "A study by in situ techniques of the thermal evolution of the structure of a Mg-Al-CO_3 layered double hydroxide", Chemical Engineering Science, Vol. 57, p 2945-2953

41. Frost R. L., Weier M. L., Clissold M. E., Williams P. A., Kloprogge J. T., (2003), "Thermal decomposition of the natural hydrotalcites carrboydite and hydrohonessite", Thermochimica Acta, Vol. 407 p 1-9

42. Kisuma Chemicals, "Unique products through unique technologies", http://www.kisuma.com/new/dht4a_files/image002.jpg, Netherlands April 2002

43. Zhao R., Yin C., Zhao H., Liu C., (2003), "Synthesis, characterization, and application of hydrotalcites in hydrodesulfurization of FCC gasoline", Fuel Processing Technology, Vol. 81, p 201-209

44. NIRE, "National Institute for Resources and Environment", http://www.aist.go.jp/NIRE/~silica/si/talcite/topic.htm/, Japan, 2004

45. Smith J. M., (1970), "Chemical Engineering Kinetics", 2nd edition, McGrawHill

46. Mersmann A., (1989), "Adsorption", Ullmann's Encyclopedia of Industrial Chemistry, Vol. B(3), Chapter 9, Wiley-VCH

47. Levine I. N., (1995), "Physical Chemistry", 4th ed., p 363-368, McGraw Hill

48. Levenspiel O., (1999), "Chemical Reaction Engineering", 3rd edition, p 570, John Wiley&Sons

49. Stephen Wolfram, "Wolfram Research", http://www.wolfram.com, 2004

50. Ramachandran P. A., Smith J. M., (1977), "Effect of Sintering and Porosity Changes on Rates of Gas-Solid Reactions", The Chemical Engineering Journal, Vol. 14, p 137-146

51. Ramachandran P. A., Smith J. M., (1977), "A Single-Pore Model for Gas-Solid Noncatalytic Reactions", AIChE Journal, Vol. 23(3), p 353-361

52. Doğu T., (1984), "Effect of Pore Structure on the Mechanism of SO_2 Sorption on Activated Soda", Frontiers in Chemical Reaction Engineering, p 152-161

53. Orbey N., Doğu G., Doğu T., (1982), "Breakthrough Analysis of NonCatalytic Solid-Gas Reactions: Reaction of SO_2 with Calcined Limestone", Canadian Journal of Chemical Engineering, Vol. 60, p 314-318

54. Doğu T., (1981), "The Importance of Pore Structure and Diffusion in the Kinetics of Gas-Solid Non-catalytic Reactions: Reaction of Calcined Limestone with SO_2", Chemical Engineering Journal, Vol. 21, p 213-222

55. Sohn H. Y., Szekely J., (1974), "The Effect of Intragrain Diffusion on the Reaction between a Porous Solid and a Gas", Chemical Engineering Science, Vol. 29, p 630-634

56. Yaşyerli S., Doğu G., Ar İ., Doğu T., (2001), "Activities of Copper Oxide and Cu-V and Cu-Mo Mixed Oxides for H_2S Removal in the Presence and Absence of Hydrogen and Predictions of a Deactivation Model ", Ind. Eng. Chem. Res., Vol. 40, p 5206-5214

57. Yaşyerli S., Doğu G., Ar İ., Doğu T., (2002), "Removal of Hydrogen Sulfide by Clinoptilolite in a Fixed Bed Adsorber", Chemical Engineering and Processing, Vol. 41, p 785-792

58. Yaşyerli N., Doğu T., Doğu G., Ar İ., (1996), "Deactivation Model for Textural Effects on Kinetics of Gas-Solid Noncatalytic Reactions: Char Gasification with CO_2", Chemical Engineering Science, Vol. 51(11), 2523-2528

59. Yaşyerli S., Doğu G., Ar İ., Doğu T., (2003), "Breakthrough Analysis of H_2S Removal on Cu-V-Mo, Cu-V, and Cu-Mo Mixed Oxides", Chem. Eng. Comm., Vol. 190, p 1055-1072

60. Kopaç T., Kocabaş S., (2003), "Sulfur dioxide Adsorption Isotherms and Breakthrough Analysis on Molecular Sieve 5A Zeolite", Chem. Eng. Comm., Vol. 190, p 1041-1054

61. Bird R. B., Stewart W. E., Lightfoot E. N., (1960), "Transport Phenomena", p 554-591, John Wiley&Sons

62. Geankoplis C. J., (1993), "Transport Processes and Unit Operations", 3rd edition, p 701-706, Prentice Hall

63. Ball M. C., Snelling C. M., Strachan A. N., Strachan R. M., (1992), "Thermal Decomposition of Solid Sodium Sesquicarbonate, $Na_2CO_3.NaHCO_3.2H_2O$", J. Chem. Soc. Faraday Trans., Vol. 88(4), p 631-636

64. Ball M. C., Snelling C. M., Strachan A. N., Strachan R. M., (1986), "Thermal Decomposition of Solid Sodium Bicarbonate", J. Chem. Soc. Faraday Trans., Vol. 82, p 3709-3715

65. Hu W., Smith J. M., Doğu T., Doğu G., (1986), "Kinetics of Sodium Bicarbonate Decomposition", AIChE Journal, Vol. 32, p 1483-2490

66. Perry, R. H.,Green, D. W., (1998), "Perry's Chemical Engineers' Handbook", 7th ed., McGraw Hill International Editions, Australia

67. Sandler S. I., (1989), "Chemical and Engineering Thermodynamics", 2nd edition, John Wiley and Sons

68. Çengel Y. A., (1998), "Heat Transfer: A Practical Approach", 1st edition, McGrawHill

APPENDIX A

GAS CHROMATOGRAPH

A.1 Carbon dioxide Calibration

Analysis of outlet stream from the reactor was achieved by means of a Varian 1400 Gas Chromatograph. Table A.1.1 shows the calibration data for the calculation of carbon dioxide concentrations at the exit of the reactor.

Table A.1.1 Carbon dioxide calibration data for bypass condition

Peak Area	CO_2 Mole (%)
0	0
83.97	13.18
121.86	16.76
222.23	21.77
309.42	28.58
528.22	35.62
660.11	42.54
789.16	49.7
1069.41	61.87
1304.14	77.46
1435.90	100

In order to calculate all carbon dioxide concentrations from the reaction zone the following equation was fitted using the data tabulated in Table A.1.1.

For $V_i \equiv CO_2$ volume%, and $A_i \equiv$ Peak Area

$$V_i = 7\times10^{-12} A_i^4 + 5\times10^{-8} A_i^3 - 0.0001 A_i^2 + 0.1151 A_i + 2.2607 \qquad \text{(A.1.1)}$$

Assuming ideal gas law for the species, it can be shown that volume % is almost equal to mole % for carbon dioxide for constant temperature and pressure conditions. For this purpose, writing ideal gas law for carbon dioxide and for total composition yields the following equality:

$$\frac{PV_{CO_2}}{PV_T} = \frac{n_{CO_2}RT}{n_T RT} \qquad \text{(A.1.2)} \qquad \Rightarrow \qquad \frac{V_{CO_2}}{V_T} = \frac{n_{CO_2}}{n_T} \qquad \text{(A.1.3)}$$

Equation A.1.3 was used in sample calculations for the derivation of breakthrough data from the experimental results.

A.2 Gas Chromatograph Settings

In order to differentiate peaks from noises, it was necessary to optimize peak resolution in the monitor for better results. After several trials, the following fixed parameters were used during the experiments.

Table A.2.1 Gas Chromatograph (Varian 1400) settings for the experiments

Parameter	**Value**
TCD Temperature	170 ^{o}C
Column Temperature	120 ^{o}C
Column Flow Rate	32 cm^3/min
Reference Flow Rate	67.5 cm^3/min
Current	200 mA
Attenuation	32

Thermal conductivity detector temperature was set to 170 ^{o}C. However, it was oscillating slightly between 160-170 ^{o}C. In addition, current was adjusted to 200 mA to obtain sharp peaks. Due to the malfunction in the linearity of the chromatograph, current exhibited a tendency to decrease during the

experiments. Therefore, it was crucial to check these two parameters all the time to have correct peaks from Varian 1400.

Table A.2.2 Thermal conductivities of some gases at different temperatures [68]

Temperature	**Thermal Conductivity (W/m.^{o}C)**			
(K)	He	CO_2	H_2O	N_2
350	0.1650	0.0205	0.0222	0.0294
400	0.1800	0.0244	0.0264	0.0325
450	0.2950	0.0283	0.0307	0.0356

TCD detector analyzes the gas composition with respect to the thermal conductivities of the individual gases used in the experiments. Table A.2.2 [68] shows thermal conductivities of some gases at different temperatures. First, nitrogen was used as carrier gas for the experiments. Since thermal conductivity [66] of nitrogen was very close to H_2O and CO_2 for the temperature of interest, output from the chromatograph was not sufficient to observe peaks rather than noises. Hence, it was necessary to use a better carrier gas such as helium or argon. Helium was suitable for TCD analysis to differentiate peaks precisely. Thus, He was selected as the carrier gas.

APPENDIX B

PROPERTIES OF CHEMICALS

Table B.1.1 shows the chemicals used in the experiments. Densities of carbon dioxide and helium are at 300 ^{o}C and other chemicals densities are from the Hg penetrometer instrument analysis.

Table B.1.1 Properties of chemicals used in the adsorption experiments

Chemical	**Chemical Formula**	**Molecular Weight (g/mol)**	**Density (kg/m^3)**	**Firm**
Carbon dioxide	CO_2	44.012	1.789	Air Products
Helium	He	4.003	0.163	Oksan
Hydrotalcite	$Mg_6Al_2CO_3(OH)_{16}.4H_2O$	603.974	2810	Sigma Aldrich
Sodium bicarbonate	$NaHCO_3$	84.006	2110	Merck
Trona	$Na_2CO_3.NaHCO_3.2H_2O$	226.024	4150	Beypazarı
Sodium carbonate	Na_2CO_3	105.988	2540	Merck

APPENDIX C

EXPERIMENTAL DATA

C.1 Experimental Data for Calcination of Adsorbents

Adsorbents were activated before the adsorption studies so as to remove carbon dioxide and water molecules within the structure. Each sample were activated before each run and below three table shows sample calcination data for the adsorbents used in this study.

Calcination temperatures for hydrotalcite, trona, and sodium bicarbonate were 550 ^{o}C, 200 ^{o}C, and 200 ^{o}C respectively. 2 g of sorbent was activated in each run under the flow of 30 cm^3/min helium.

Table C.1.1 Calcination of hydrotalcite (magnesium aluminum hydroxy carbonate) under the flow of Helium at 550 °C

He Flow Rate (cm^3/min): 30 Loading (g): 2 Calcination Temperature (°C): 550 Adsorbent : Hydrotalcite (pellet, ASTM 14)			
Injection #	Time (sec)	Area (mV.sec)	$C_{CO2,out}$ (%)
1	207.1	32.24	7.64
2	390.0	27.81	7.12
3	414.3	30.00	7.38
4	432.0	38.61	8.35
5	450.6	42.16	8.73
6	492.0	116.55	15.14
7	510.1	320.66	27.37
8	533.9	707.22	45.35
9	552.0	827.46	50.66
10	569.8	1012.44	59.08
11	588.0	1068.34	61.76
12	612.2	955.06	56.41
13	642.4	1097.55	63.20
14	672.1	993.70	58.20
15	707.8	944.16	55.91
16	792.2	928.60	55.20
17	810.1	974.35	57.30
18	828.5	838.26	51.14
19	852.0	1015.83	59.24
20	887.9	693.17	44.73
21	912.3	647.48	42.71
22	930.0	505.30	36.31
23	948.1	229.57	22.41
24	960.0	441.64	33.34
25	990.2	306.46	26.63
26	1014.0	300.57	26.32
27	1032.2	177.76	19.29
28	1056.0	29.83	7.36
29	1086.1	1.53	2.72

Table C.1.2 Calcination of trona under the flow of Helium at 200 ^{o}C

He Flow Rate (cm^3/min): 30 Loading (g): 2 Calcination Temperature (^{o}C): 200 Adsorbent : Trona (powder)			
Injection #	Time (sec)	Area (mV.sec)	$C_{CO2,out}$ (%)
1	395.8	77.99	12.10
2	425.8	389.90	30.85
3	462.2	727.41	46.24
4	485.8	986.19	57.85
5	516.8	1010.95	59.01
6	547.8	1409.80	83.02
7	579.4	1286.03	73.61
8	611.0	993.05	58.17
9	642.4	863.83	52.28
10	673.8	847.25	51.54
11	706.4	562.19	38.90
12	737.6	503.78	36.24
13	801.0	253.73	23.78
14	831.2	270.03	24.68
15	863.0	189.95	20.05
16	893.8	120.79	15.45
17	925.6	148.58	17.39
18	955.0	67.57	11.19
19	986.4	45.33	9.06
20	1017.4	97.71	13.71
21	1048.8	18.26	5.91
22	1079.2	29.49	7.32
23	1111.6	19.39	6.06
24	1142.4	8.35	4.47
25	1173.6	11.27	4.92
26	1204.6	11.61	4.97

Table C.1.3 Calcination of sodium bicarbonate under the flow of Helium at 200 ^{o}C

He Flow Rate (cm^3/min): 30 Loading (g): 2 Calcination Temperature (^{o}C): 200 Adsorbent : $NaHCO_3$ (powder)			
Injection #	Time (sec)	Area (mV.sec)	$C_{CO2,out}$ (%)
1	261.4	54.45	9.97
2	289.8	661.93	43.35
3	321.0	877.01	52.87
4	356.2	982.11	57.66
5	385.6	967.87	57.00
6	413.8	928.82	55.21
7	445.8	972.62	57.22
8	477.6	737.40	46.68
9	507.6	781.83	48.64
10	539.8	804.90	49.66
11	571.8	651.09	42.87
12	602.6	505.30	36.31
13	633.4	539.21	37.86
14	665.4	393.17	31.01
15	699.6	346.06	28.67
16	728.0	267.84	24.56
17	759.8	247.48	23.43
18	790.8	58.01	10.31
19	821.6	73.23	11.69
20	853.8	73.34	11.70
21	885.8	47.09	9.24
22	915.8	41.03	8.61
23	973.8	35.42	8.00
24	1005.2	20.83	6.25
25	1035.8	29.23	7.29
26	1067.0	4.40	3.82
27	1097.6	31.98	7.61
28	1129.8	3.76	3.42
29	1161.6	18.86	5.99
30	1191.8	25.99	6.90
31	1223.0	2.97	2.42

C.2 Experimental Data for Hydrotalcite (dry)

In this study adsorption experiments with hydrotalcite were carried out both in the presence and absence of steam. Below experimental data shows the carbon dioxide outlet concentration at the exit of the reactor.

Table C.2.1 Experimental data for hydrotalcite in the absence of steam at 400 ^{o}C

Total Flow Rate (cm^3/min): 50.0 Composition: 15.3% CO_2, 84.7% He Loading (g): 2 Adsorption Temperature (^{o}C): 400 Adsorbent : Activated Hydrotalcite (pellet, ASTM 14)			
Injection #	Time (sec)	Area (mV.sec)	$C_{CO2,out}$ (%)
1	0.00006	0.000	0.00
2	51	0.000	0.00
3	105	0.000	0.00
4	156	0.000	0.00
5	199.8	0.000	0.00
6	253.8	0.078	0.01
7	304.2	3.782	1.68
8	325.8	7.337	2.45
9	346.2	8.327	2.91
10	364.8	16.435	5.66
11	387	23.405	6.58
12	408	60.641	10.56
13	427.2	70.775	11.48
14	448.2	90.766	13.16
15	468	86.998	12.85
16	489	100.437	13.92
17	517.8	112.508	14.84
18	537	106.410	14.38
19	658.8	104.405	14.23
20	750	118.730	15.30

Table C.2.2 Experimental data for hydrotalcite in the absence of steam at 424 °C

Total Flow Rate (cm^3/min): 48.5 Composition: 14.6% CO_2, 85.4% He Loading (g): 2 Adsorption Temperature (°C): 424 Adsorbent : Activated Hydrotalcite (pellet, ASTM 14)			
Injection #	Time (sec)	Area (mV.sec)	$C_{CO2,out}$ (%)
1	0.0	0.000	0.00
2	51.0	0.000	0.00
3	98.4	0.000	0.00
4	153.0	0.000	0.00
5	194.4	0.023	0.58
6	292.8	0.079	1.31
7	320.4	0.233	3.07
8	366.6	10.596	4.82
9	405.6	18.830	5.99
10	423.6	45.249	9.05
11	446.4	61.729	10.66
12	469.8	81.659	12.41
13	488.4	88.739	12.99
14	515.4	94.188	13.43
15	538.8	99.755	13.87
16	560.4	109.290	14.60
17	589.2	103.531	14.16
18	627.6	101.637	14.02
19	664.2	105.438	14.31
20	698.4	109.290	14.60

Table C.2.3 Experimental data for hydrotalcite in the absence of steam at 452 °C

Total Flow Rate (cm^3/min): 50.3 Composition: 16.7% CO_2, 83.3% He Loading (g): 2 Adsorption Temperature (°C): 452 Adsorbent : Activated Hydrotalcite (pellet, ASTM 14)			
Injection #	Time (sec)	Area (mV.sec)	$C_{CO2,out}$ (%)
1	0.0	0.000	0.00
2	45.0	0.000	0.00
3	97.8	0.000	0.00
4	154.2	0.000	0.00
5	196.2	0.000	0.00
6	223.8	0.031	0.01
7	280.2	6.233	2.17
8	301.8	13.016	5.18
9	367.2	48.194	9.35
10	411.0	83.036	12.53
11	475.8	108.349	14.53
12	498.0	81.039	12.36
13	520.2	108.349	14.53
14	541.8	124.224	15.70
15	586.8	117.323	15.20
16	631.2	128.905	16.03
17	652.8	126.556	15.87
18	675.0	136.043	16.53
19	697.2	133.648	16.37
20	724.2	138.454	16.70

Table C.2.4 Experimental data for hydrotalcite in the absence of steam at 475 °C

Total Flow Rate (cm^3/min): 49.0 Composition: 15.0% CO_2, 85.0% He Loading (g): 2 Adsorption Temperature (°C): 475 Adsorbent : Activated Hydrotalcite (pellet, ASTM 14)			
Injection #	Time (sec)	Area (mV.sec)	$C_{CO2,out}$ (%)
1	0.0	0.000	0.00
2	56.4	0.000	0.00
3	87.0	2.678	1.50
4	144.0	1.338	0.75
5	190.2	5.461	2.85
6	243.0	10.477	4.80
7	262.8	22.388	6.45
8	327.0	33.642	7.80
9	354.6	43.302	8.85
10	395.4	46.204	9.15
11	448.8	71.627	11.55
12	488.4	114.650	15.00
13	532.2	96.944	13.65
14	568.8	100.784	13.95
15	598.8	112.629	14.85
16	616.8	114.650	15.00
17	669.0	108.627	14.55
18	700.2	113.638	14.93
19	740.4	111.423	14.76
20	765.6	112.629	14.85

Table C.2.5 Experimental data for hydrotalcite in the absence of steam at 500 °C

Total Flow Rate (cm^3/min): 50.0 Composition: 16.1% CO_2, 83.9% He Loading (g): 2 Adsorption Temperature (°C): 500 Adsorbent : Activated Hydrotalcite (pellet, ASTM 14)			
Injection #	Time (sec)	Area (mV.sec)	$C_{CO2,out}$ (%)
1	0.0	0.000	0.00
2	46.2	0.000	0.00
3	88.2	0.000	0.00
4	160.8	0.000	0.00
5	204.0	0.000	0.00
6	223.8	0.023	0.01
7	256.2	10.052	2.90
8	289.8	21.058	6.28
9	325.8	41.817	8.69
10	358.8	95.348	13.52
11	376.2	77.695	12.08
12	409.8	91.312	13.20
13	427.2	112.119	14.81
14	460.8	116.466	15.13
15	495.0	123.099	15.62
16	529.2	127.595	15.94
17	546.0	118.662	15.30
18	562.8	125.339	15.78
19	580.2	118.662	15.30
20	598.2	129.865	16.10

Table C.2.6 Experimental data for hydrotalcite in the absence of steam at 527 °C

Total Flow Rate (cm^3/min): 51.2 Composition: 15.5% CO_2, 84.5% He Loading (g): 2 Adsorption Temperature (°C): 527 Adsorbent : Activated Hydrotalcite (pellet, ASTM 14)			
Injection #	Time (sec)	Area (mV.sec)	$C_{CO2,out}$ (%)
1	0	0.000	0.00
2	33.6	0.000	0.00
3	67.2	0.184	0.08
4	94.8	1.135	2.17
5	124.2	2.128	2.95
6	202.8	2.937	3.57
7	237.6	14.746	5.43
8	285.6	49.219	9.46
9	328.8	53.938	9.92
10	367.8	77.871	12.09
11	418.8	87.157	12.87
12	432.6	121.480	15.50
13	467.4	110.955	14.73
14	502.8	115.123	15.04
15	537.6	120.411	15.42

C.3 Experimental Data for Hydrotalcite (wet)

The following experimental data were obtained in the presence of steam at different temperatures. Temperature was varied from 400 to 527 °C and total flow rate was fixed around 50 cm^3/min.

Table C.3.1 Experimental data for hydrotalcite in the presence of steam at 400 °C

Total Flow Rate (cm^3/min): 48.6 Composition: 13.8% CO_2, in H_2O+He Loading (g): 2 Adsorption Temperature (°C): 400 Adsorbent : Activated Hydrotalcite (pellet, ASTM 14) at 550 °C			
Injection #	Time (sec)	Area (mV.sec)	$C_{CO2,out}$ (%)
1	0.0	0.000	0.00
2	47.4	0.897	0.69
3	101.4	0.000	0.00
4	152.4	1.518	1.10
5	200.4	0.000	0.00
6	255.0	0.614	0.41
7	286.8	4.781	2.62
8	336.6	4.220	2.40
9	367.8	4.781	2.62
10	405.0	8.880	4.55
11	434.4	20.528	6.21
12	469.2	52.686	9.80
13	501.0	61.383	10.63
14	538.8	75.281	11.87
15	570.0	68.980	11.32
16	596.4	98.858	13.80
17	631.8	83.433	12.56
18	672.6	90.171	13.11

Table C.3.2 Experimental data for hydrotalcite in the presence of steam at 424 °C

Total Flow Rate (cm^3/min): 50.0 Composition: 16.2% CO_2, in H_2O+He Loading (g): 2 Adsorption Temperature (°C): 424 Adsorbent : Activated Hydrotalcite (pellet, ASTM 14) at 550 °C			
Injection #	Time (sec)	Area (mV.sec)	$C_{CO2,out}$ (%)
1	0.0	0.000	0.00
2	50.4	0.339	0.16
3	96.6	9.493	2.92
4	148.8	0.000	0.00
5	183.0	0.901	0.32
6	226.8	4.748	1.46
7	320.4	18.890	5.99
8	364.2	9.809	4.70
9	404.4	20.115	6.16
10	442.2	82.425	12.47
11	474.6	76.677	11.99
12	513.0	98.474	13.77
13	544.8	80.492	12.31
14	570.0	115.543	15.07
15	596.4	131.283	16.20
16	631.8	128.989	16.04
17	661.2	113.355	14.90
18	688.8	126.711	15.88
19	721.2	122.198	15.55

Table C.3.3 Experimental data for hydrotalcite in the presence of steam at 452 °C

Total Flow Rate (cm^3/min): 49.2 Composition: 17.3% CO_2, in H_2O+He Loading (g): 2 Adsorption Temperature (°C): 452 Adsorbent : Activated Hydrotalcite (pellet, ASTM 14) at 550 °C			
Injection #	Time (sec)	Area (mV.sec)	$C_{CO2,out}$ (%)
1	0.0	0.000	0.00
2	45.0	3.301	1.21
3	99.0	1.682	0.52
4	153.6	0.000	0.00
5	196.2	12.791	4.15
6	226.2	0.028	0.01
7	268.8	6.873	2.25
8	300.6	15.535	5.54
9	334.8	53.331	9.86
10	384.0	86.388	12.80
11	457.8	113.005	14.88
12	484.2	84.289	12.63
13	520.2	115.340	15.05
14	541.8	129.710	16.09
15	590.4	122.447	15.57
16	625.8	147.241	17.30
17	662.4	134.636	16.44
18	696.6	142.150	16.95
19	723.0	139.629	16.78
20	754.8	134.636	16.44

Table C.3.4 Experimental data for hydrotalcite in the presence of steam at 475 °C

Total Flow Rate (cm^3/min): 50.7 Composition: 16.4% CO_2, in H_2O+He Loading (g): 2 Adsorption Temperature (°C): 475 Adsorbent : Activated Hydrotalcite (pellet, ASTM 14) at 550 °C			
Injection #	Time (sec)	Area (mV.sec)	$C_{CO2,out}$ (%)
1	0.0	0.000	0.00
2	55.2	1.487	2.13
3	88.2	0.675	0.98
4	141.6	0.223	0.33
5	190.8	2.263	3.44
6	238.2	10.188	4.76
7	268.8	25.893	6.89
8	322.2	43.359	8.86
9	354.6	48.154	9.35
10	393.6	54.806	10.00
11	428.4	78.412	12.14
12	488.4	115.841	15.09
13	529.8	134.134	16.40
14	561.0	120.322	15.42
15	598.8	134.134	16.40
16	612.6	121.452	15.50
17	637.8	118.074	15.25
18	682.2	129.469	16.07

Table C.3.5 Experimental data for hydrotalcite in the presence of steam at 500 ^{o}C

Total Flow Rate (cm^3/min): 50.0 Composition: 15.7% CO_2, in H_2O+He Loading (g): 2 Adsorption Temperature (^{o}C): 500 Adsorbent : Activated Hydrotalcite (pellet, ASTM 14) at 550 ^{o}C			
Injection #	Time (sec)	Area (mV.sec)	$C_{CO2,out}$ (%)
1	0.0	0.000	0.00
2	46.2	5.552	1.73
3	85.8	4.621	1.10
4	116.4	0.000	0.00
5	142.2	4.897	1.26
6	168.0	5.118	1.57
7	253.2	10.013	2.98
8	283.8	24.781	6.75
9	313.8	39.790	8.48
10	340.2	97.059	13.66
11	367.8	74.206	11.78
12	394.8	91.138	13.19
13	427.2	107.226	14.44
14	455.4	105.163	14.29
15	480.6	117.760	15.23
16	505.8	124.252	15.70
17	532.2	113.503	14.92
18	562.2	119.910	15.39
19	587.4	111.396	14.76
20	622.8	124.252	15.70

Table C.3.6 Experimental data for hydrotalcite in the presence of steam at 527 ^{o}C

Total Flow Rate (cm^3/min): 49.0 Composition: 15.1% CO_2, in H_2O+He Loading (g): 2 Adsorption Temperature (^{o}C): 527 Adsorbent : Activated Hydrotalcite (pellet, ASTM 14) at 550 ^{o}C			
Injection #	Time (sec)	Area (mV.sec)	$C_{CO2,out}$ (%)
1	0.0	0.000	0.00
2	39.6	3.216	1.06
3	67.2	3.015	0.76
4	94.8	7.087	2.11
5	127.2	8.351	3.17
6	160.8	7.325	2.57
7	189.0	16.995	5.74
8	227.4	46.802	9.21
9	262.8	55.982	10.12
10	294.6	69.081	11.33
11	333.0	83.133	12.53
12	369.6	116.004	15.10
13	410.4	111.931	14.80
14	457.8	31.458	7.55
15	500.4	109.915	14.65
16	550.2	116.004	15.10
17	582.0	101.986	14.04

C.4 Experimental Data for Trona

The following experimental data were obtained in the presence of steam at different temperatures. Temperature was varied from 80 to 152 °C and total flow rate was fixed around 50 cm^3/min.

Table C.4.1 Experimental data for trona in the presence of steam at 80 °C

Total Flow Rate (cm^3/min): 48.8 Composition: 16.1% CO_2, in H_2O+He Loading (g): 2 Adsorption Temperature (°C): 80 Adsorbent : Activated Trona (powder) at 200 °C			
Injection #	Time (sec)	Area (mV.sec)	$C_{CO2,out}$ (%)
1	0.0	0.000	0.00
2	47.4	0.062	0.06
3	106.8	0.851	0.81
4	149.4	0.027	0.03
5	201.0	2.141	2.25
6	253.8	1.069	1.13
7	298.2	1.859	1.77
8	325.8	3.720	3.70
9	346.8	18.613	5.96
10	365.4	31.605	7.57
11	390.6	33.008	7.73
12	408.0	70.276	11.43
13	427.2	95.959	13.57
14	448.8	95.348	13.52
15	493.8	112.119	14.81
16	526.8	123.099	15.62
17	555.0	115.373	15.05
18	652.2	111.042	14.73
19	738.6	129.865	16.10

Table C.4.2 Experimental data for trona in the presence of steam at 101 °C

Total Flow Rate (cm^3/min): 50.5 Composition: 15.8% CO_2, in H_2O+He Loading (g): 2 Adsorption Temperature (°C): 101 Adsorbent : Activated Trona (powder) at 200 °C			
Injection #	Time (sec)	Area (mV.sec)	$C_{CO2,out}$ (%)
1	0.0	0.000	0.00
2	15.6	0.000	0.00
3	45.6	0.054	0.05
4	95.4	0.059	0.57
5	147.6	8.055	4.42
6	167.4	4.651	2.84
7	207.6	19.561	6.08
8	227.4	72.707	11.64
9	250.2	37.954	8.28
10	273.6	52.827	9.81
11	288.6	24.365	6.70
12	308.4	42.981	8.82
13	334.8	87.884	12.92
14	351.6	53.313	9.86
15	373.2	67.882	11.22
16	391.8	93.964	13.41
17	428.4	69.834	11.39
18	444.6	111.174	14.74
19	468.6	125.647	15.80
20	496.2	73.070	11.68
21	534.6	119.086	15.33
22	562.2	99.178	13.83
23	619.8	125.647	15.80

Table C.4.3 Experimental data for trona in the presence of steam at 125 °C

Total Flow Rate (cm^3/min): 50.0 Composition: 15.0% CO_2, in H_2O+He Loading (g): 2 Adsorption Temperature (°C): 125 Adsorbent : Activated Trona (powder) at 200 °C			
Injection #	Time (sec)	Area (mV.sec)	$C_{CO2,out}$ (%)
1	0.0	0.000	0.00
2	45.6	1.038	0.90
3	100.2	1.457	1.35
4	130.8	7.591	4.35
5	161.4	5.755	4.05
6	191.4	21.220	6.30
7	228.6	33.774	7.82
8	277.8	37.002	8.18
9	310.8	69.081	11.33
10	379.8	86.485	12.81
11	418.2	54.506	9.98
12	445.8	58.433	10.35
13	456.6	82.497	12.48
14	491.4	114.650	15.00
15	532.2	66.568	11.10
16	580.2	88.690	12.99
17	612.6	64.911	10.95
18	673.8	103.115	14.13

Table C.4.4 Experimental data for trona in the presence of steam at 152 °C

Total Flow Rate (cm^3/min): 49.4 Composition: 17.3% CO_2, in H_2O+He Loading (g): 2 Adsorption Temperature (°C): 152 Adsorbent : Activated Trona (powder) at 200 °C			
Injection #	Time (sec)	Area (mV.sec)	$C_{CO2,out}$ (%)
1	0.0	0.000	0.00
2	33.6	0.054	0.05
3	81.0	1.978	2.08
4	112.2	1.534	1.73
5	131.4	2.453	2.77
6	157.8	27.582	7.09
7	199.8	11.925	5.02
8	225.6	9.634	4.67
9	250.2	45.210	9.05
10	290.4	64.731	10.93
11	320.4	97.161	13.67
12	358.2	72.095	11.59
13	388.8	101.598	14.01
14	427.8	110.688	14.71
15	459.0	147.241	17.30
16	488.4	127.272	15.92
17	520.2	147.241	17.30
18	545.4	137.124	16.61
19	583.2	139.629	16.78

C.5 Experimental Data for Sodium bicarbonate

The following experimental data were obtained in the presence of steam at different temperatures. Temperature was varied from 80 to 152 °C and total flow rate was fixed around 50 cm^3/min.

Table C.5.1 Experimental data for sodium bicarbonate in the presence of steam at 80 °C

Total Flow Rate (cm^3/min): 48.7 Composition: 16.9% CO_2, in H_2O+He Loading (g): 2 Adsorption Temperature (°C): 80 Adsorbent : Activated $NaHCO_3$ (powder) at 200 °C			
Injection #	Time (sec)	Area (mV.sec)	$C_{CO2,out}$ (%)
1	0.0	0.000	0.00
2	49.8	0.952	0.24
3	109.2	1.112	0.34
4	148.2	3.218	1.01
5	199.2	3.451	1.18
6	237.0	9.652	2.87
7	273.6	19.568	6.08
8	303.0	26.228	6.93
9	334.2	37.970	8.28
10	362.4	63.444	10.82
11	385.8	29.040	7.27
12	408.0	72.895	11.66
13	427.2	84.845	12.68
14	448.2	108.415	14.53
15	468.0	102.874	14.11
16	486.6	122.143	15.55
17	511.8	141.361	16.90
18	534.6	125.668	15.80
19	571.2	138.903	16.73

Table C.5.2 Experimental data for sodium bicarbonate in the presence of steam at 101 °C

Total Flow Rate (cm^3/min): 50.0 Composition: 15.2% CO_2, in H_2O+He Loading (g): 2 Adsorption Temperature (°C): 101 Adsorbent : Activated $NaHCO_3$ (powder) at 200 °C			
Injection #	Time (sec)	Area (mV.sec)	$C_{CO2,out}$ (%)
1	0.0	0.000	0.00
2	24.0	0.000	0.00
3	54.0	0.000	0.00
4	103.8	0.897	0.68
5	156.0	6.080	4.10
6	165.6	34.699	7.92
7	205.8	37.998	8.28
8	225.6	51.508	9.68
9	248.4	35.106	7.96
10	269.4	49.061	9.44
11	289.8	59.415	10.44
12	309.6	55.571	10.08
13	331.2	84.499	12.65
14	351.6	53.058	9.83
15	373.2	63.182	10.79
16	393.0	91.208	13.19
17	415.2	68.217	11.25
18	435.6	105.574	14.32
19	456.0	84.867	12.68
20	477.6	71.304	11.52
21	497.4	112.838	14.87
22	518.4	86.344	12.80
23	560.4	117.364	15.20
24	581.4	87.272	12.87

Table C.5.3 Experimental data for sodium bicarbonate in the presence of steam at 125 °C

Total Flow Rate (cm^3/min): 51.6 Composition: 15.3% CO_2, in H_2O+He Loading (g): 2 Adsorption Temperature (°C): 125 Adsorbent : Activated $NaHCO_3$ (powder) at 200 °C			
Injection #	Time (sec)	Area (mV.sec)	$C_{CO2,out}$ (%)
1	0.0	0.000	0.00
2	51.0	0.000	0.00
3	98.4	0.000	0.00
4	129.0	3.012	1.88
5	195.6	6.244	4.13
6	252.6	17.892	5.86
7	292.8	35.164	7.97
8	320.4	38.498	8.34
9	366.6	51.689	9.70
10	405.6	93.821	13.40
11	423.6	49.682	9.50
12	445.8	60.149	10.51
13	471.0	56.263	10.14
14	487.2	85.507	12.73
15	515.4	99.453	13.85
16	537.6	118.730	15.30
17	559.2	91.907	13.25
18	590.4	67.335	11.17
19	622.8	106.812	14.41

Table C.5.4 Experimental data for sodium bicarbonate in the presence of steam at 152 °C

Total Flow Rate (cm^3/min): 48.0 Composition: 15.1% CO_2, in H_2O+He Loading (g): 2 Adsorption Temperature (°C): 152 Adsorbent : Activated $NaHCO_3$ (powder) at 200 °C			
Injection #	Time (sec)	Area (mV.sec)	$C_{CO2,out}$ (%)
1	0.0	0.000	0.00
2	35.4	0.000	0.00
3	82.8	1.767	1.36
4	113.4	1.482	1.06
5	130.2	3.128	1.96
6	158.4	7.772	4.38
7	195.6	5.917	4.08
8	204.6	54.413	9.97
9	241.8	33.036	7.73
10	291.0	46.951	9.23
11	327.6	64.056	10.87
12	359.4	51.322	9.66
13	391.8	75.990	11.93
14	424.8	116.004	15.10
15	445.2	86.790	12.84
16	471.0	94.276	13.44
17	486.6	116.004	15.10
18	506.4	101.986	14.04
19	520.8	100.038	13.89
20	553.8	111.931	14.80

APPENDIX D

CALIBRATION

D.1 Calibration of Water Bath

Steam was produced in a water bath by bubbling gas mixture into water tank placed inside a water bath. Figure D.1.1 shows the calibration of water bath used in the experiments.

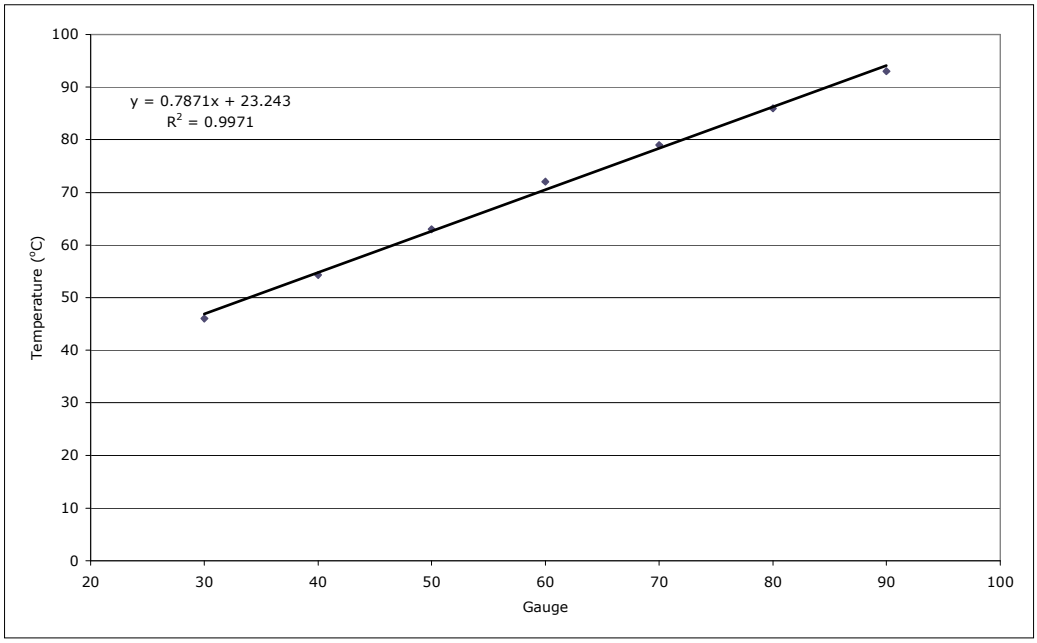

Figure D.1.1 Calibration of water bath used in the experiments

D.2 Calibration of Reactor Temperature

Figure D.2.1 is the calibration curve for thermocouple placed on top of reactor (thermocouple positioned in the middle) for different tubular furnace set temperatures.

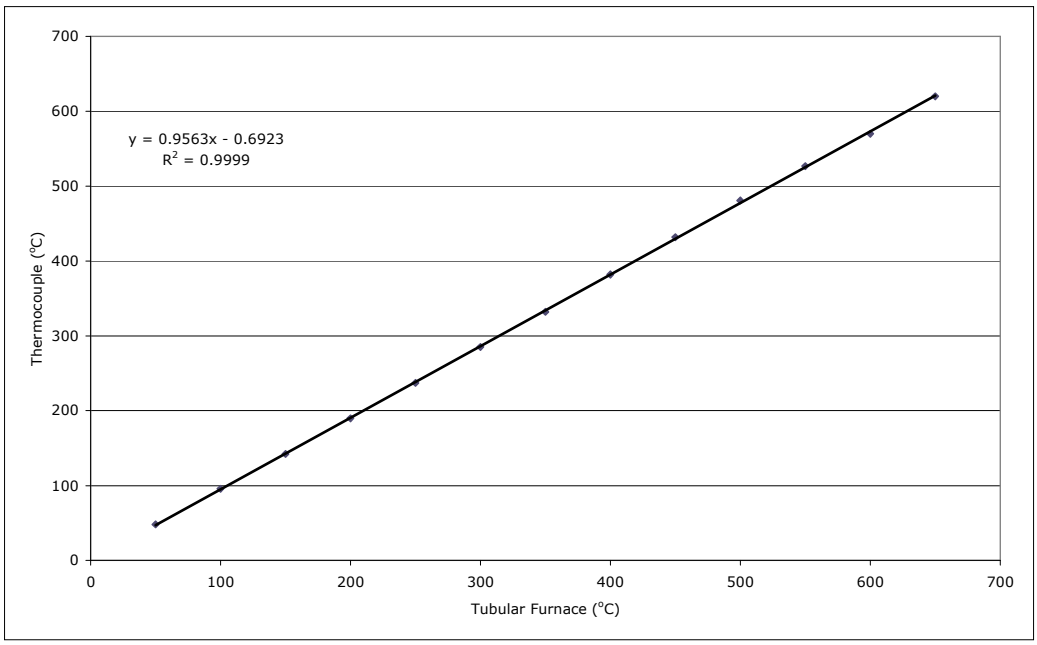

Figure D.2.1 Calibration of thermocouple used in the experiments

D.3 Response Curve for Thermocouple and Tubular Furnace

It is important to know the time required for thermocouple to reach its set point. Temperature difference between furnace and thermocouple essentially depends on the insulation that is made to obtain uniform temperature for the reactor.

Figure D.3.1 shows the response curves for both tubular furnace and thermocouple for 240 ^{o}C (set point). Response time is not very critical for adsorption part of the experiments due to the fact that the experiments do not start till the reaction temperature is fixed at the desired temperature. However, rate of calcination depends on temperature since samples were not put at the calcination temperature but they were replaced into furnace before the heating was started.

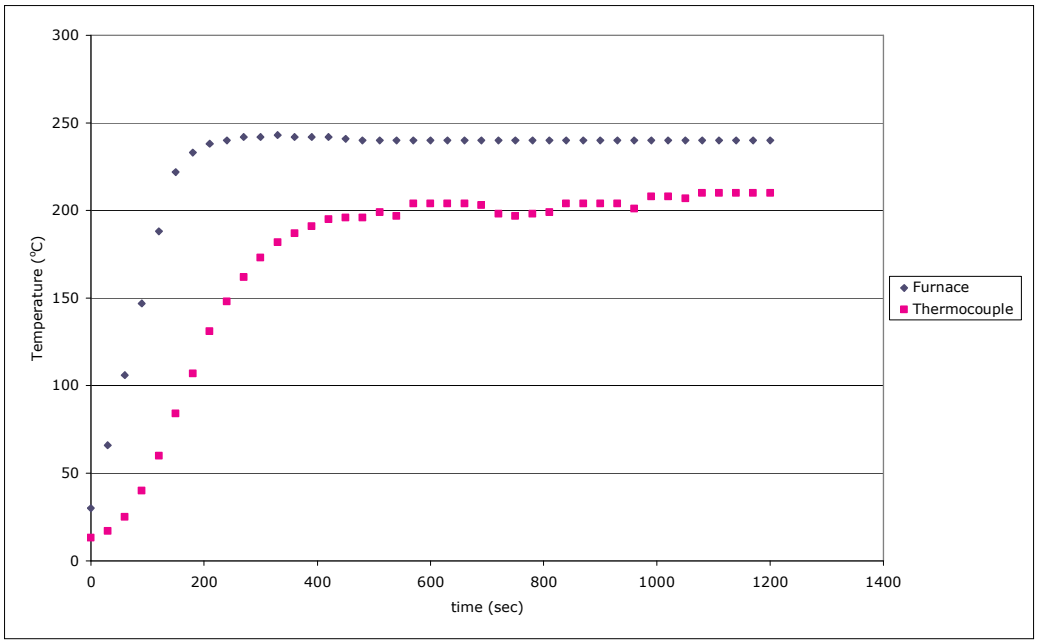

Figure D.3.1 Temperature response curves for tubular furnace and thermocouple

APPENDIX E

SAMPLE CALCULATION

Analysis of experimental data could be considered in three parts. First of all, calcination peak areas are calculated and converted into desorption concentration of carbon dioxide. In the second part, peak areas for adsorption experiments were calculated and derived breakthrough curves for this part were reported in the result section. Finally, deactivation model was applied to experimental data so as to compare experimental data and model. Using the model, some parameters and adsorption properties were also obtained. In all these calculations Mathematica 4.2 was used for the sake of simplicity and accuracy.

E.1 Calcination of Adsorbents

The first step in peak area calculation was to transfer experimental data couples (time-milivolt array) from a text file to a list in Mathematica. The following command line reads the file htk550.txt and transfers experimental data to an array named "data".

```
data=ReadList["C:\Documents and
Settings\Administrator\Desktop\htk550.txt", {Number,Number}];
```

Data stores the array as follows: data={{0., 4.3741}, {0.1, 12.2070}, …, {1., 312.3820},…, {1200., 12.2070}}. First element in array shows time (unit for time is second) and second element is the signal from chromatograph (unit for signal is milivolts). To visualize the calcination (desorption) peaks, the following command line was used in Mathematica. Figure E.1.1 shows calcination chromatogram for the time range of [510-630] seconds.

```
ListPlot[data, PlotJoined->True, PlotRange-
>{{510,630},{300,950}}, AxesLabel->{"Time(sec)","Voltage(mV)"}]
```

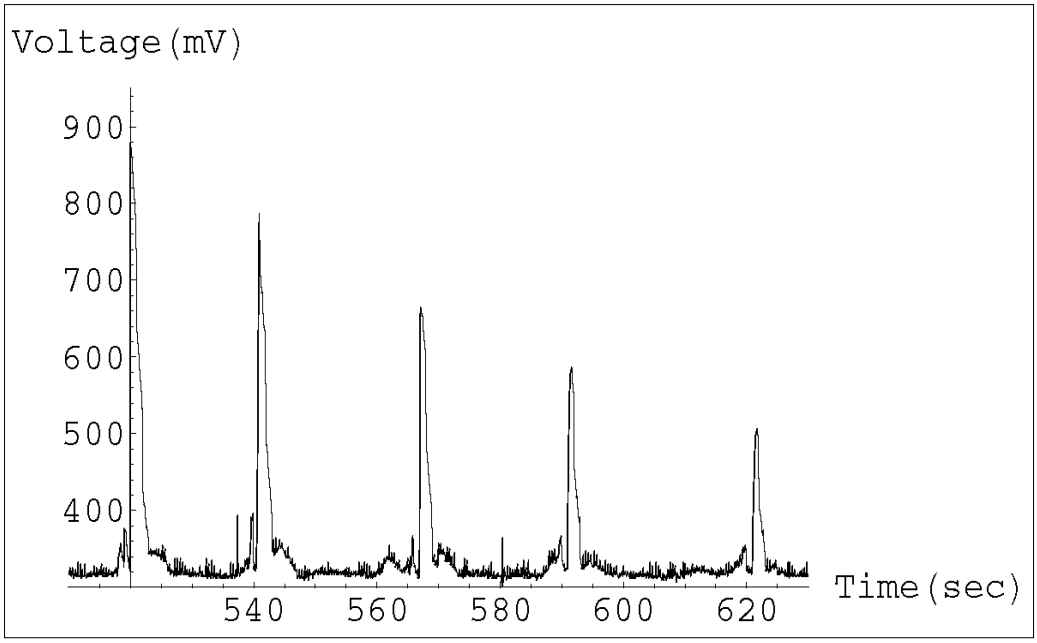

Figure E.1.1 Calcination chromatogram for hydrotalcite at 550 °C

It is possible to zoom into each peak so that one could understand whether it is peak or a noise. The following command was used for storing a single peak data into a variable called "peak".

```
Peak=Take[data, {5403,5434}]
```

In order to integrate the data couples stored in "peak" for a single peak, it is required to load NumericalMath package in Mathematica. For numerical integration of data "ListIntegrate" command was used, which uses "roots and weights" in calculation.

```
<<NumericalMath'ListIntegrate'

ListIntegrate[peak]

451.787
```

This peak area is then converted into carbon dioxide volume% (equivalent to mole% for ideal conditions). The following calibration equation was used to obtain effluent concentrations from the differential tubular reactor.

```
co2mol%=f[peak]=7*10^12*(peak^4)+5*10^-8*(peak^3)-
0.0001*(peak^2)+0.1151*peak+2.2607

f[451.787]    38.753
```

For a peak area of 451.787 carbon dioxide volume% was found to be 38.753. Similar analysis was performed for each peak and calcination curves reported in result section were obtained. Since calcination was a desorption run, it was unnecessary to normalize the elution curve and results were reported in the original form (volume %).

E.2 Adsorption of Carbon dioxide

For the adsorption part of the experiments, similar analysis (described in part E.1) was carried out to obtain breakthrough curves for each run. The only difference with respect to calcination runs was that the breakthrough curve was normalized according to the initial carbon dioxide concentration. Figure E.2.1 shows a typical adsorption chromatogram for a time range of [50-120] seconds.

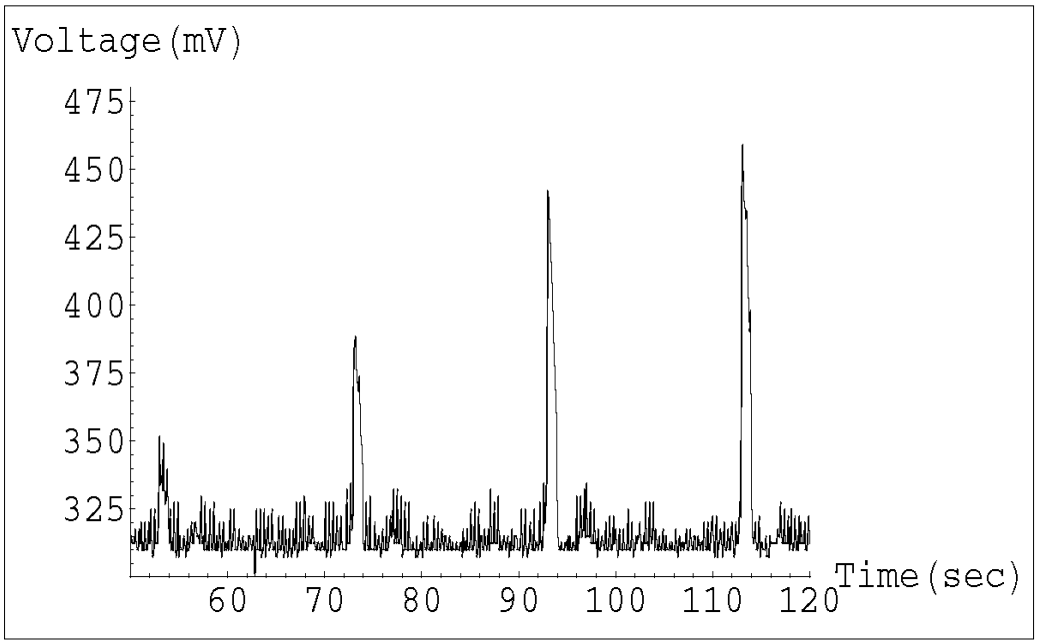

Figure E.2.1 Chromatogram for breakthrough data obtained from the adsorption of hydrotalcite at 475 ^{o}C

Having obtained each peak area and corresponding concentration, breakthrough curves were derived and reported in result section in a normalized form.

E.3 Application of Deactivation Model

The following "deactivation model analysis" was applied to breakthrough data obtained from the adsorption of carbon dioxide onto hydrotalcite at 500 °C. Breakthrough data was transferred into a variable, named "data" as follows:

```
data={{0.000001,0},{0.77,0},{1.47,0},{2.68,0},{3.4,0.0001},{3.7
3,0.0007},{4.27,0.18},{4.83,0.39},{5.43,0.54},{5.98,0.84},{6.27,0.75
},{6.83,0.82},{7.12,0.92},{7.68,0.94},{8.25,0.97},{8.82,0.99},{9.1,0
.95},{9.38,0.98},{9.67,0.95},{9.97,0.999}};
```

Breakthrough curve could be plotted in Mathematica for the region of interest by using the below command line.

```
ListPlot[data, PlotRange->{{0,10},{0,1}}, AxesLabel->
{"time(sec)","Cout/Cin"}]
```

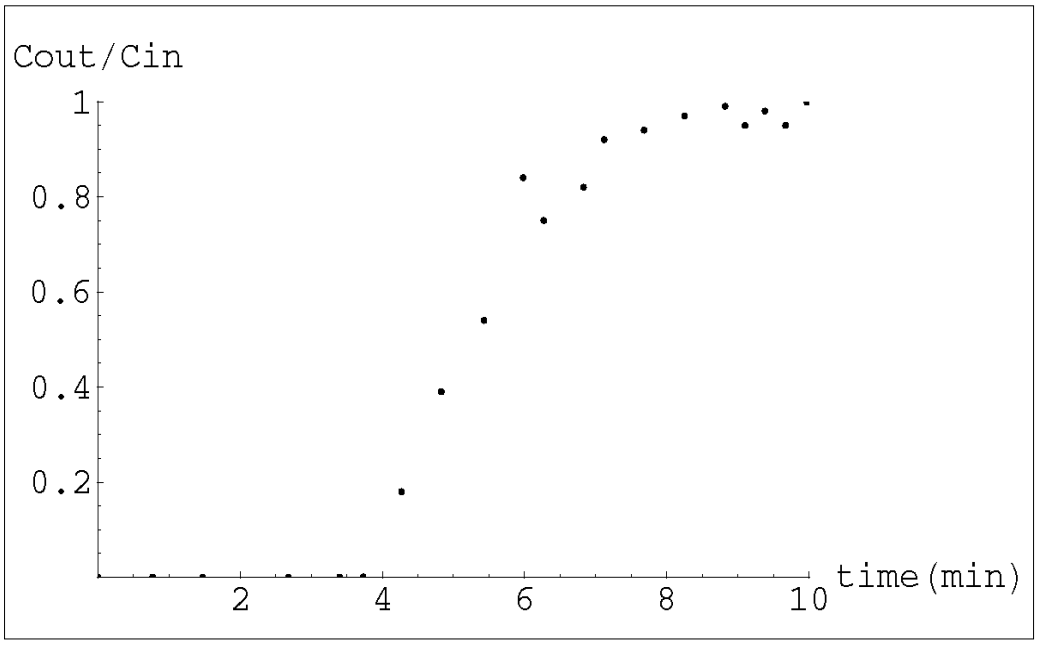

Figure E.3.1 Breakthrough curve for activated hydrotalcite at 500 °C

For the rest of calculations another Mathematica package was required to perform nonlinear regression analysis. Final form of deactivation model used in calculations is shown below.

$$\frac{C_A}{C_{Ao}} = \exp\left\{\frac{\left[1-\exp(k_o W/Q((1-\exp(-k_d t)))\right]\exp(-k_d t)}{\left[1-\exp(-k_d t)\right]}\right\} \qquad (5.2.3.6)$$

Instead of $k_o W/Q$ "dummy" variable used in Mathematica. For statistical analysis NonlinearFit package was loaded as follows:

```
<<Statistics'NonlinearFit'
```

Although there are several ways to perform nonlinear regression analysis in Mathematica, the following "NonlinearRegress" command returns with the best results by minimizing the errors. For the calculation of rate parameters (sorption rate constant and deactivation rate constant), breakthrough data together with equation (5.2.3.4) was supplied to program:

```
BestFitParameters/NonlinearRegress[data,Exp[(1-Exp[dummy*(1-
Exp[-kd*t])]*Exp[-kd*t])//1-Exp[-
kd*t])],{t},{dummy,kd},RegressionReport->BestFitParameters]
```

Output from the nonlinear regression analysis returned the variables "dummy" and k_d.

```
BestFitParameters->{dummy->2.5141,kd->0.253398}
```

Loading and volumetric flow rate (Using ideal gas law, volumetric flow rates were corrected for temperatures higher than room temperature) was supplied to program to obtain sorption rate constant at 500 ^oC.

```
w=2;

q=50;

dummy=2.5141;

ko=q*dummy/w;

ko->62.8525
```

Thus, sorption and deactivation rate constants were found to be 62.8525 cm^3/min.g and 0.253398 min^{-1} respectively. Once model rate parameters were calculated, it was required to reload "NumericalMath" to find adsorption properties of the adsorbent.

```
<<NumericalMath'ListIntegrate'
```

Whole range of data gives the total capacity of the adsorbent. Integrating the variable "data" and subtracting from the rectangular region defined by breakthrough curve leads to total capacity.

```
Totalcapacity=ListIntegrate[data]

4.54791
```

Total capacity was calculated as 5.42209 min (9.97-4.54791, subtraction from the rectangular region) for hydrotalcite at 500 ^oC. Similarly, one could integrate variable "data" to obtain breakthrough capacity. As a rule of thumb, taking 0.05% of initial concentration as break point, it is possible to evaluate the breakthrough capacity for the sample. Considering data beginning from the break point (variable named as "breakcapacity") and integrating yields the following:

```
Breakcapacity=Take[data,{7,20}]

ListIntegrate[breakcapacity]

5.73805
```

Subtracting from the rectangular region (9.97-5.73805), breakthrough capacity was calculated as 4.23195 min. Having supplied total flow rate, ideal gas constant, molecular weight of carbon dioxide, and carbon dioxide mole percent in the feed, amount of carbon dioxide adsorbed was calculated as follows:

```
vn=22400;

tf=50;

mwco2=44.012;
```

co2=0.15;

Multiplication of total capacity and mass flow rate yields the amount of carbon dioxide adsorbed:

massflowrate=tf*co2/vn*mwco2;

gcarbondioxide=massflowrate*totalcapacity;

0.0670188

Hydrotalcite was capable of adsorbing around 0.067 g carbon dioxide at 500 ^{o}C. It is best to report this amount on the basis adsorbent loading:

loading=2;

satgram=gcarbondioxide/loading

0.0335094 g/g is the adsorption capacity of hydrotalcite at 500 ^{o}C. This value could be converted into "mol/kg" units to visualize the adsorption characteristics of the adsorbent.

satmolkg=satgram*1000/mwco2

0.761369

Finally, it could be concluded that ≈0.76 mol/kg is the working capacity of hydrotalcite at 500 ^{o}C.

Simplified set of calculations for calcination and adsorption is described in parts E.1 to E.3. These analyses were performed for each run for hydrotalcite, trona, and sodium bicarbonate. Having calculated the rate parameters from the deactivation model, activation energies of the sorption and deactivation rate were calculated from the arhenius plots.

E.4 Chi Square Analysis for Error Minimization

Chi square analysis is a powerful method for error minimization in regression analysis. For this reason, using Mathematica 4.2 with LevenbergMarquardt method predicts the model parameters in an adjustable confidence level. The following command line lets mathematica regress a list of experimental data to find out the model parameters dummy (k_oW/Q) and k_d. Chi square values should approach zero for a better fit to data and one can adjust tolerance or precision goal depending on the accuracy level desired from the experimental data.

```
NonlinearRegress[d5,
Exp[(1 - Exp[dummy * (1 - Exp[-kd * t])] * Exp[-kd * t]) / (1 - Exp[-kd * t])], {t},
 {{dummy, 1, 4}, {kd, 0, 0.5}}]
```

Some kind of a regression report is obtained from the nonlinear regression and to show accuracy of the fit, chi square values are reported in the rate parameter tables. Below Table E.4.1 shows a typical regression report obtained from nonlinear regression analysis.

Table E.4.1 Typical regression report of deactivation model

```
{BestFitParameters → {dummy → 2.51426, kd → 0.253441},

                              Estimate     Asymptotic SE     CI
ParameterCITable → dummy      2.51426      0.185548          {2.12444, 2.90408}  ,
                   kd         0.253441     0.0293499         {0.191779, 0.315103}

                                                    DF     SumOfSq      MeanSq
                                   Model            2      9.04176      4.52088
EstimatedVariance → 0.0439576, ANOVATable → Error   18     0.791238     0.0439576,
                                   Uncorrected Total 20    9.833
                                   Corrected Total   19    3.53768

AsymptoticCorrelationMatrix → {{1., 0.942949}, {0.942949, 1.}},

                                        Curvature
FitCurvatureTable → Max Intrinsic       0.0807766}
                    Max Parameter-Effects 0.188225
                    95. % Confidence Region 0.530405
```

APPENDIX F

GAS CHROMATOGRAPH PROGRAM

F.1 GC Program for Monitoring Peaks

In order to obtain adsorption/desorption peaks, it was necessary to write a data acquisition program for monitoring and analyzing the experimental data. Following program is written in Quickbasic and it is capable of scanning 10 signals in a second. Scanning time and gain are adjustable parameters, that is, it is possible to enlarge or shrink peaks so as to observe the accuracy of peaks (necessary to differentiate from the noises). Experimental data were stored in time-milivolt arrays and they were further analyzed for peak area analysis in Mathematica 4.2. Below program is written for PCL-711 data acquisition card and some parameters should be changed when it is necessary to use some other data cards (e.g. PCL-711S).

```
'*********************************************************************
'**
'*  Description : Program for PCL-711 pacer trigger A/D conversion
'*
'* with software data transfer.Output peaks are written to a file
'*
'*
'*
'*  Version     : 1.00
'*
'*  Date        : 15/10/2002         Berker Fıçıcılar,   Che/METU
'*
'*********************************************************************
'***
'
'VARIABLES
'
'yt: measurement at time t
'ydt: measurement at t+dt
'xc: x multiplier
```

```
'yc: y multiplier
'va: reference voltage
'vb: reference voltage
'olcum: number of measurement
'x: x pozition
'y: y position
'xx:second x position
'
'
DIM PARAM%(60)                  ' If two boards installed, need to
'declare
                                ' the second parameter array
DIM dat%(24000)                 ' Conversion data buffer
PARAM%(0) = 0                   ' Board number
PARAM%(1) = &H220               ' Base I/O address
PARAM%(5) = 250                 ' Pacer rate = 2M / (50 * 100) = 400
'Hz
PARAM%(6) = 200
PARAM%(7) = 0                   ' Trigger mode, 0 : pacer trigger
PARAM%(10) = VARPTR(dat%(0))    ' Offset of A/D data buffer A
PARAM%(11) = VARSEG(dat%(0))    ' Segment of A/D data buffer A
PARAM%(12) = 0                  ' Data buffer B address, if not used,
PARAM%(13) = 0                  ' must set to 0.
PARAM%(14) = 39                 ' A/D conversion number
PARAM%(15) = 0                  ' A/D conversion start channel
PARAM%(16) = 0                  ' A/D conversion stop channel
PARAM%(17) = 0                  ' Overall gain code, 0 : +/- 5V
'param%(45) : Error Code
'param%(46) : Return Value 0
'param%(47) : Return Value 1
'
FUN% = 3                        ' FUNCTION 3
'CALL PCL711(FUN%, SEG PARAM%(0))   ' Func 3 : Hardware
'initialization
'IF PARAM%(45) <> 0 THEN PRINT "DRIVER INITIALIZATION FAILED !":
STOP
'
FUN% = 4                        ' FUNCTION 4
'CALL PCL711(FUN%, SEG PARAM%(0))   ' Func 4 : A/D initialization
'IF PARAM%(45) <> 0 THEN PRINT "A/D INITIALIZATION FAILED !": STOP
FUN% = 5                        ' FUNCTION 5

' PROGRAM NAME IS WRITTEN
CLS
RNK1 = 11: RNK2 = 13: SAY = 6: SAY2 = 1: SEC = 0
ZEMIN$ = STRING$(80, CHR$(219))
FOR i = 1 TO 24
LOCATE i, 1: PRINT ZEMIN$
NEXT i
COLOR 7, 7
1 TUSAL$ = INKEY$
x = 8
y = 24
ADET = 7
ICER$(1) = "                                      "
ICER$(2) = "          GC-DETECT V1.1              "
ICER$(3) = "  Gas Chromatography Monitoring       "
ICER$(4) = "              Program                 "
ICER$(5) = "  Chemical Engineering Department     "
```

```
ICER$(6) = "      METU/TURKEY      2002          "
GEN = LEN(ICER$(1))
COLOR RNK1, RNK2
LOCATE x, y: PRINT CHR$(218) + STRING$(GEN, CHR$(196)) + CHR$(191)
FOR I1 = x + 1 TO ADET + x + 1
LOCATE I1, y: PRINT CHR$(179) + STRING$(GEN, " ") + CHR$(179)
NEXT I1
LOCATE x + ADET + 1, y: PRINT CHR$(192) + STRING$(GEN, CHR$(196)) +
CHR$(217)
LOCATE x + 1, y + 1: PRINT ICER$(SAYAC)
COLOR RNK1, RNK2
FOR I1 = x + 2 TO ADET + x
SAYAC = SAYAC + 1
LOCATE I1, y + 1: PRINT ICER$(SAYAC)
NEXT I1
COLOR 11, 13
LOCATE 23, 44: PRINT " Press Any Key to Continue ...."
354 TUSAL$ = INKEY$: IF LEN(TUSAL$) = 0 THEN 354

CLS
LOCATE 3, 10: PRINT "Input File Name:"
LOCATE 3, 47: INPUT a$
LOCATE 5, 10: PRINT "Enter max. time for analysis(sec):"
LOCATE 5, 47: INPUT olcum
LOCATE 7, 10: PRINT "Detector Temperature(oC):"
LOCATE 7, 47: INPUT det
LOCATE 9, 10: PRINT "Column Oven Temperature(oC):"
LOCATE 9, 47: INPUT cot
LOCATE 11, 10: PRINT "Current(mA):"
LOCATE 11, 47: INPUT cu
LOCATE 13, 10: PRINT "Attenuation:"
LOCATE 13, 47: INPUT att
LOCATE 15, 10: PRINT "Coarse:"
LOCATE 15, 47: INPUT coa


WIDTH 80, 43
SCREEN 9
WINDOW (0, 0)-(350, 640)
COLOR 11, 13

LINE (33, 105)-(33, 588)
LINE (33, 105)-(305, 105)
LINE (33, 588)-(305, 588)
LINE (305, 588)-(305, 105)
LOCATE 8, 74: PRINT "mV"
LOCATE 3, 73: PRINT "Time"


LOCATE 2, 2: PRINT "(mV)"
LOCATE 2, 12: PRINT "Dosya:"
LOCATE 2, 18: PRINT a$
LOCATE 41, 32: PRINT " Time (Sec)"

FOR VERT = 105 TO 588 STEP (588 - 105) / 11
LINE (22, VERT)-(33, VERT)
LINE (33, VERT)-(305, VERT), , , &H999
NEXT VERT
```

```
FOR HOR = 33 TO 305 STEP (305 - 33) / 10
LINE (HOR, 95)-(HOR, 105)
LINE (HOR, 105)-(HOR, 588), , , &H999
NEXT HOR

'location of vertical labels
LOCATE 34, 3: PRINT "0"
LOCATE 37, 2: PRINT "-1"
FOR VL = 1 TO 10
LOCATE (VL * 3 + 1), 2: PRINT (11 - VL)
NEXT VL

'location of horizontal labels
FOR i = 1 TO 60
LOCATE 3, i: PRINT " "
LOCATE 39, i + 6: PRINT " "
NEXT i
sc = olcum / 10
FOR HL = 1 TO 11
LOCATE 39, (HL * 6 + 1): PRINT (HL - 1) * sc
NEXT HL

c$ = ".txt": d$ = a$ + c$: a1$ = "i": B$ = a$ + a1$ + c$

OPEN B$ FOR OUTPUT AS #4
PRINT #4, "File:", d$
PRINT #4,
PRINT #4, "Detector Temperature(oC)", det
PRINT #4, "Column Oven Temperature(oC)", cot
PRINT #4, "Current(mA)", cu
PRINT #4, "Attenuation", att
PRINT #4, "Coarse", coa
CLOSE #4
OPEN d$ FOR OUTPUT AS #3
PRINT #3, "time(sec)", "  peak(mV)"
tt = 0: yc = 120: top = 0
FOR j = 0 TO 1: SLEEP 1
'CALL PCL711(FUN%, SEG PARAM%(0))   ' Func 5 :"N" times of A/D
trigger
'IF PARAM%(45) <> 0 THEN PRINT "A/D SOFTWARE DATA TRANSFER FAILED
!": STOP
dat%(0) = 2150
dat%(19) = 2150
aa = dat%(0)
bb = dat%(19)
yt = (10 * (aa / 4096) + (-5))
ydt = (10 * (bb / 4096) + (-5))
top = top + (yt + ydt)
NEXT
dc = top / 4
vb = dc
tt = 0
xc = 272 / (olcum - .1) / 10: dt = .1: xb = 33: yb = 149
DIM pe(100)
nn = 0
yk = 1
yl = 1
ym = 1
yn = 1
```

```
yo = 1
FOR j = 0 TO olcum: SLEEP 1
'CALL PCL711(FUN%, SEG PARAM%(0))   ' Func 5 :"N" times of A/D
trigger
'IF PARAM%(45) <> 0 THEN PRINT "A/D SOFTWARE DATA TRANSFER FAILED
!": STOP
DIM y(11), tt(11)
FOR i = 0 TO 39 STEP 4
dat%(i) = 2150 + RND(1) * 100
IF j = 5 THEN dat%(i) = 2150 + RND(1) * (350 + i * 2)
NEXT i

tt(0) = tt
FOR i = 0 TO 9
a = dat%(4 * i)
y(i) = (10 * (a / 4096) + (-5))
tt(i + 1) = tt + dt
NEXT i

IF j = olcum THEN GOTO 10

FOR i = 1 TO 10
PRINT #3, USING " ###.##       #####.####"; tt(i); y(i) * 1000
NEXT i

LOCATE 5, 73: PRINT tt
LOCATE 10, 72: PRINT USING "#####.#"; y(1) * 1000
LOCATE 10, 72: PRINT USING "#####.#"; y(10) * 1000

yd = 40 / dc
ye = 400 / dc
yc = yd
IF (j = 0) THEN x1 = xb + j * 10 * xc
IF (j = 0) THEN y1 = yb + (y(0) - dc) * yc
son = 9
IF j = (olcum - 1) THEN son = 8
FOR i = 0 TO son
x2 = x1 + xc
yy = (y(i) - dc)
IF yy < dc / 1.25 THEN yy = 0
o5 = (yk + yl + ym + yn + yo) / 5 + .1
o3 = (yk + yl + ym) / 3 + .1
IF (o3 / o5) > 1.5 THEN pv = 1: yc = ye
IF (o3 / o5) < .4 THEN pv = 0: yc = yd: LOCATE 15 + nn, 69: PRINT
USING "#####.##"; pe(nn): nn = nn + 1
IF pv = 1 THEN pe(nn) = pe(nn) + dt * y(i)
y2 = yb + (EXP(((yy + (y1 - yb) / yc) / 2) / 2) - 1) * yc
LINE (x1, y1)-(x2, y2), 1
x1 = x2
y1 = y2
yo = yn
yn = ym
ym = yl
yl = yk
yk = yy

NEXT i

tt = tt + 1
```

```
NEXT
10 CLOSE #3
END
```

F.2 Program Output

Output for gcpeak3d.bas program was written into two different files. One of these files stores gas chromatograph setting information like current, detector temperature etc. and the other file stores the experimental data (time-milivolt array). Typical program outputs are as follows:

For a calcination run at 550 ^{o}C, chromatograph settings were stored in file kih550.txt.

```
File: kiht550.txt

Detector Temperature(oC) 150
Column Oven Temperature(oC) 120
Current(mA) 200
Attenuation 32
Coarse 1
```

For the same calcination experiment, hydrotalcite desorption data was stored in the file kht550.txt.

```
File: kht550.txt

  time(sec)      peak(mV)
   0.00          12.2070
   0.10          12.2070
   0.20          14.6484
   0.30          26.8555
   0.40          12.2070
   0.50           7.3242
   0.60           9.7656
   0.70          26.8555
   0.80          12.2070
   0.90          12.2070
   1.00         317.3828
   1.10         310.0586
   1.20         310.0586
   1.30         310.0586
   1.40         314.9414
   1.50         310.0586
   1.60         312.5000
   1.70         310.0586
   1.80         317.3828
```

1.90	312.5000
2.00	324.7070
2.10	312.5000
2.20	310.0586
2.30	312.5000
2.40	324.7070
2.50	310.0586
2.60	310.0586
2.70	310.0586
2.80	322.2656
2.90	310.0586
3.00	317.3828
.	.
.	.
3.80	317.3828
3.90	312.5000
4.00	312.5000
4.10	310.0586
4.20	310.0586
4.30	322.2656
4.40	310.0586
4.50	310.0586
4.60	314.9414
4.70	327.1484
4.80	307.6172
4.90	312.5000
5.00	312.5000
.	.
.	.
.	.

These experimental data is stored in the specific files. Since scanning time could alter between 30 min. to 75 min., all experimental data was not shown in the above output. This large range of data requires a sophisticated analysis tool to calculate both peak areas and model the experimental data. For this purpose, Mathematica 4.2 was used in the rest of calculations. Sample calculations and typical chromatograms were shown in Appendix E.

APPENDIX G

EQUILIBRIUM CONSTANTS

G.1 Sodium bicarbonate Decomposition

It was important to estimate the temperature of adsorption for activated soda. However, when hydrogen production is taken into account, adsorption temperature range should be optimized to obtain the maximum yield from the coupled reactions. Equilibrium constants for the following reaction could give an idea to select the temperature range.

$$2NaHCO_3 \leftrightarrow Na_2CO_3 + CO_2 + H_2O \qquad (G.1.1)$$

Chemeq.bas program [67], written in quickbasic, was used to find the thermodynamic properties for the temperature range 323-523 K. The following data is supplied to program.

REACTION DATA

Name	Stoichiometric coefficient
CO2	-1.0000
H2O(g)	-1.0000
NaHCO3	2.0000
Na2CO3	-1.0000

G.2 Output from Chemeq.bas for $NaHCO_3$ Decomposition

Output of the program gives equilibrium constants, enthalpy of reaction, and gibbs free energy for the relevant temperature range.

GRXN[T=25C] kJ	HRXN[T=25C] kJ	K	LN(K[T=25C])	LOG10(K[T=25C])
-2.8600E+01	-1.2520E+02	1.025E+05	11.538	5.011

CPA	CPB	CPC	CPD	CPE
-1.7538D+02	-6.1690D-02	2.444D-05	-3.8710D-09	0.000D+00

T[K]	LN(K)	LOG10(K)	K	GRXN (kJ)	HRXN (kJ)
323.00	0.7580D+01	0.3292E+01	0.1958E+04	-2.0355D+01	-1.2998D+02
333.00	0.6116D+01	0.2656E+01	0.4529E+03	-1.6932D+01	-1.3191D+02
343.00	0.4716D+01	0.2048E+01	0.1118E+03	-1.3450D+01	-1.3385D+02
353.00	0.3377D+01	0.1467E+01	0.2929E+02	-9.9119D+00	-1.3579D+02
363.00	0.2094D+01	0.9093E+00	0.8115E+01	-6.3187D+00	-1.3773D+02
373.00	0.8616D+00	0.3742E+00	0.2367E+01	-2.6720D+00	-1.3968D+02
383.00	-.3226D+00	-.1401E+00	0.7243E+00	1.0272D+00	-1.4164D+02
393.00	-.1462D+01	-.6350E+00	0.2317E+00	4.7774D+00	-1.4359D+02
403.00	-.2560D+01	-.1112E+01	0.7730E-01	8.5775D+00	-1.4556D+02
413.00	-.3619D+01	-.1572E+01	0.2681E-01	1.2426D+01	-1.4752D+02
423.00	-.4641D+01	-.2016E+01	0.9644E-02	1.6323D+01	-1.4950D+02
433.00	-.5630D+01	-.2445E+01	0.3590E-02	2.0266D+01	-1.5147D+02
443.00	-.6586D+01	-.2860E+01	0.1380E-02	2.4255D+01	-1.5345D+02
453.00	-.7511D+01	-.3262E+01	0.5470E-03	2.8289D+01	-1.5544D+02
463.00	-.8408D+01	-.3652E+01	0.2230E-03	3.2366D+01	-1.5743D+02
473.00	-.9278D+01	-.4029E+01	0.9344E-04	3.6487D+01	-1.5942D+02
483.00	-.1012D+02	-.4396E+01	0.4016E-04	4.0650D+01	-1.6142D+02
493.00	-.1094D+02	-.4753E+01	0.1768E-04	4.4854D+01	-1.6342D+02
503.00	-.1174D+02	-.5099E+01	0.7964E-05	4.9098D+01	-1.6542D+02
513.00	-.1252D+02	-.5436E+01	0.3666E-05	5.3383D+01	-1.6743D+02
523.00	-.1327D+02	-.5764E+01	0.1723E-05	5.7707D+01	-1.6944D+02